UNIVERSITA' DEGLI STUDI

DI MODENA E REGGIO EMILIA

PhD Course in:

Models and Methods for Material and Environmental Sciences

Cycle XXXVI

Sedimentary architecture and evolution of the central Po Plain through integrated stratigraphic and petrographic analyses

Candidate: Luca Demurtas

Tutor: Prof. Luigi Bruno

Co-Tutor: Prof. Daniela Fontana

Co-Tutor: Prof. Stefano Lugli

PhD Course Coordinator: Prof. Stefano Lugli

INDEX

ABSTRACT

Integrated stratigraphic-compositional studies can provide valuable insights into the sedimentary evolution of multi-source alluvial basins, in response to different controlling factors. The Po Basin is an alluvial basin fed by two orogens that have different physiography, lithology and structural setting. The Alps, with peaks exceeding 4000 m, bound the Po Plain to the north and to the west and are dominated by metamorphic, granitic and ultramaphic rocks and by Mesozoic carbonates. The Northern Apennines, with highest peaks < 2220 m, bound the plain to the south and are dominated by sedimentary rocks.

In this work, the Middle Pleistocene to Holocene succession of the Po Basin was investigated through the correlation of 44 cores and 168 well data, with the aid of pollen data, and ^{14}C, ESR and IRSL absolute dates. Middle Pleistocene to Holocene stratigraphy of the Po Basin is composed of alluvial, paralic, coastal and shallow-marine facies associations arranged in an overall shallowing-upward trend, that reflects the progressive filling of the basin. A cyclic organization of facies, given by the alternation of paralic, coastal and shallow-marine deposits with alluvial sediments is superposed to this general trend. This rhythmical organization of facies reflects Milankovitch-scale glacio-eustatic oscillations, in the 100 ky band. At proximal locations, far from the marine influence, laterally extensive channel-belt sand bodies alternate with overbank deposits.

Sand from fluvial channel bodies, deposited during glacial periods, show distinct compositions. Petrographic analysis of two 101- and 77.5-m-long cores recovered in the central Po Plain, ca. 20 km south of the Po River, revealed the vertical stacking of three petrofacies, ascribable to the three feeding areas of the Po Basin: the Southern Alps, the Western Alps, and the Northern Apennines. The upward transition from sands delivered from the Southern Alps to sands deposited by the Po River, testify to a northward shift of the Po River of more than ~30 km around ~350 ky, possibly driven by local tectonics. A further northward migration of the Po River is recorded during the Holocene as testified by the upward transition to sand delivered from Apennine rivers. The Holocene northward shift of the Po River is recorded also in three 30-m long cores, recovered close to the modern course of the Po River. Here sands with south-alpine affinity, dated to the last glacial phase, were fed by the Garda fluvio-glacial system. The deactivation of this efficient sediment delivery system after the Last Glacial Maximum, likely favoured the formation of swamp areas during the Holocene and the activation of a northern branch of the Po delta system during the Late Bronze Age.

This study explored the sedimentary response of the Po alluvial and coastal plain to Middle and Late Pleistocene climatic and eustatic perturbations. The outcomes of this research may help in predicting the response of modern alluvial and coastal systems to near future climate scenarios.

CHAPTER 1. INTRODUCTION

Alluvial and coastal plains have been preferentially settled by humans due to the nearly flat morphology, the soil fertility and the presence of watercourses. Today, floodplains are the most densely populated areas on the planet, hosting major industrial hubs and providing most of the cultivated land that supply the world's food needs. Climate change affects and will increasingly impact on the population of alluvial and coastal plains, which could be exposed to an increasing flood hazard (Swain et al., 2020). The study of the Middle Pleistocene-to-Holocene sedimentary record may provide clues on the response of alluvial and coastal plains to climatic and sea-level changes. This period, in fact, is characterized by dramatic climatic and eustatic oscillations (Lisieky & Raymo, 2005), which are recorded in several sedimentary successions worldwide.

Integrated stratigraphic and compositional studies may help in reconstructing the sedimentary evolution of alluvial and coastal plains in response to allogenic (e.g., climate and eustasy) and autogenic (e.g., local subsidence, avulsions) controlling factors. The recent decades recorded an increasing knowledge on the stratigraphy of alluvial and coastal plains. Most studies focused on the Late Pleistocene and Holocene deposits of coastal plains (Allen & Posamentier, 1993; Hori et al., 2002; Li et al., 2002; Amorosi et al., 2004; Busschers et al. 2005; Blum & Aslan, 2006; Chen et al., 2010; Tanabe et al., 2015; Ishihara & Sugai, 2017; He et al., 2020), whereas fewer studies have focused on alluvial systems (Rittenour et al., 2007; Amorosi et al., 2008; Götz et al., 2013; Peeters et al., 2016; Hassan et al., 2017; Panin et al., 2017; Bruno et al., 2021). By contrast, Middle Pleistocene alluvial and coastal deposits are largely unexplored because less preserved in the sedimentary record. Thick Middle Pleistocene deposits accumulated only in high accommodation settings, characterized by high subsidence rates and high sediment supply. The Po Basin (northern Italy) is one of the few worldwide basins with these characteristics.

Compositional studies mainly focused on deep-sea (Critelli et al., 2003; Shroeder et al., 2015; Liu et al., 2016; Van Grinsven et al 2019; Li et al., 2021a; Amorosi et al., 2022; Limonta et al., 2023) and coastal (Goodbred & Kuehl, 2000; Xue et al., 2010; Palamenghi et al., 2011; Ji et al., 2022) sinks, whereas the source areas were investigates through geomorphological studies (Chalov et al., 2017; Li et al., 2021b). Sediment-provenance studies in multi-source alluvial systems, if framed into a well constrained stratigraphic architecture, are an excellent tool to reconstruct the hydrographic history of alluvial plains, because the primary signal of sediments stored in floodplains is more preserved than in coastal and marine sinks (Caracciolo, 2020). However, most of the compositional studies in

alluvial settings deal with compositional variations in modern fluvial sediments (Franzinelli et al., 1983; Arribas et al., 2000; Whitmore et al., 2004; Garzanti et al., 2005, 2010, 2015; Singh et al., 2008; do Nascimento Jr et al., 2015; Schneider et al., 2016; Khan et al., 2019). Few compositional studies focused on the sedimentary record, and mainly characterized Late Pleistocene and Holocene deposits (Sinah et al., 2009; Marsaglia et al. 2010; Agrawal et al., 2013; Singh et al., 2016).

Due to its well-preserved sedimentary record, the Po Basin is an ideal site to study the sedimentary response of alluvial and coastal systems to climate and eustatic perturbation. This could help in predicting the response of these densely populated environments to near future climate and sea-level changes. The Po Basin is fed by sediments deriving from two orogens with significantly different physiography, lithology and structural setting. The Alpine chain, bounding the Po Plain to the north and west, with peaks exceeding 4000 m, is characterised by extensive outcrops of metamorphic, granitic and ultramaphic rocks and by wide outcrops of Mesozoic carbonates in the central-southern sector. The Alps were largely glaciated during Middle and Late Pleistocene cold periods, with implications on sediment production and delivery to the alluvial plain. The Apennine chain, bounding the plain to the south, with highest peaks < 2220 m, is a thin-skinned orogen dominated by sedimentary rocks. Scarce evidence of glaciers activity is recorded close to the watershed of the Northern Apennines.

The Po Basin fill, up to 8000 m thick, records a complete foredeep cycle, from underfilled (deep marine) to overfilled (continental and nearshore) stage (Amadori et al., 2019). Continental and coastal sediments, accumulated during the last 870000 year BP (Muttoni et al., 2003; Gunderson et al., 2014), exhibit a cyclic organization of facies (Amorosi et al., 2004, 2008; Massari et al., 2004, Marcolla et al., 2021a; Campo et al., 2020; Rossi et al., 2021) which reflects the Mid-Late Pleistocene high-amplitude climate oscillations. The evolutionary history of the Po alluvial plain is marked by dramatic reorganizations of the fluvial network as documented by sharp variations in sediment composition (Stefani, 2002; Piovan et al., 2010, Amorosi & Sammartino, 2018; Fontana et al., 2019; Bruno et al., 2021; Marcolla et al.,2021b; Norini et al., 2021; Tentori et al., 2021; Demurtas et al., 2022). However, most of these studies focus on changes occurred over the last 50000 years.

A detailed basin-scale stratigraphic study of Middle Pleistocene deposits of the Po Basin is lacking in the literature for three main reasons: (i) seismic surveys do not have adequate resolution to investigate these deposits; (ii) few cores penetrated Middle-Pleistocene units, which locally are encountered at depths > 100 m; (iii) absolute dating on Middle Pleistocene deposits are not available and age attributions rely upon pollen (Amorosi et al., 1999, 2008b) and

magnetostratigraphic (Muttoni et al., 2003, 2011) data; (iv) tectonic deformation, increasing towards older stratigraphic intervals, hinders stratigraphic correlations based uniquely on geometric criteria. A robust chronological control is provided only by the work of Gunderson et al. (2014), which is based on the integration of several dating methods. However, this work is carried out on the margin of the basin where the sedimentary record is more discontinuous.

This PhD thesis consists in an integrated stratigraphic-petrographic study of Middle-Late Pleistocene and Holocene deposits of the central and eastern Po Plain. The aims of this work are: (i) to provide a stratigraphic architecture of Middle Pleistocene-to-Holocene deposits constrained by absolute IRSL ages; (ii) to reconstruct, through petrographic characterization of core sediments, the paleohydrography of the central Po Plain; (iii) to unravel the sedimentary response of the Po alluvial and coastal plain to climatic and eustatic oscillations; (iv) to discuss the impact of other controlling factors on the sedimentary evolution of the basin.

REFERENCES

Agrawal, S., Sanyal, P., Balakrishnan, S., & Dash, J. K. (2013). Exploring the temporal change in provenance encoded in the late Quaternary deposits of the Ganga Plain. *Sedimentary Geology*, **293**, 1-8.

Allen, G. P., & Posamentier, H. W. (1993). Sequence stratigraphy and facies model of an incised valley fill; the Gironde Estuary, France. *Journal of Sedimentary Research*, **63**(3), 378-391. https://doi.org/10.1306/d4267b09-2b26-11d7-8648000102c1865d

Amadori, C.; Toscani, G.; Di Giulio, A.; Maesano, F.E.; D'Ambrogi, C.; Ghielmi, M.; Fantoni, R. From Cylindrical to Non-Cylindrical Foreland Basin: Pliocene–Pleistocene Evolution of the Po Plain–Northern Adriatic Basin (Italy). *Basin Research,* **2019**, 31, 991–1015. https://doi.org/10.1111/bre.12369

Amorosi, A., Colalongo, M. L., Fiorini, F., Fusco, F., Pasini, G., Vaiani, S. C., & Sarti, G. (2004). Palaeogeographic and palaeoclimatic evolution of the Po Plain from 150-ky core records. *Global and planetary Change*, **40**(1-2), 55-78.

Amorosi, A., Pavesi, M., Ricci Lucchi, M., Sarti, G. & Piccin, A. (2008). Climatic signature of cyclic fluvial architecture from the Quaternary of the central Po Plain, Italy. *Sedimentary Geology*, **209**, 58–68.

Amorosi, A. & Sammartino, I. (2018). Shifts in sediment provenance across a hierarchy of bounding surfaces: A sequence-stratigraphic perspective from bulk-sediment geochemistry. *Sedimentary Geology*, **375**, 145–156.

Amorosi, A., Sammartino, I., Dinelli, E., Campo, B., Guercia, T., Trincardi, F., & Pellegrini, C. (2022). Provenance and sediment dispersal in the Po-Adriatic source-to-sink system unraveled by bulk-sediment geochemistry and its linkage to catchment geology. *Earth-Science Reviews*, **104202**. https://doi.org/10.1016/j.earscirev.2022.104202.

Arribas, J., Critelli, S., Le Pera, E., & Tortosa, A. (2000). Composition of modern stream sand derived from a mixture of sedimentary and metamorphic source rocks (Henares River, Central Spain). *Sedimentary Geology*, **133**(1-2), 27-48.

Blum, M. D., & Aslan, A. (2006). Signatures of climate vs. sea-level change within incised valley-fill successions: Quaternary examples from the Texas Gulf Coast. *Sedimentary Geology*, **190**(1-4), 177-211. https://doi.org/10.1016/j.sedgeo.2006.05.024

Bruno, L., Amorosi, A., Lugli, S., Sammartino, I. & Fontana, D. (2021). Trunk river and tributary interactions recorded in the Pleistocene-Holocene stratigraphy of the Po Plain (northern Italy). *Sedimentology*, **68**, 2918-2943.

Busschers, F. S., Weerts, H. J. T., Wallinga, J., Cleveringa, P., Kasse, C., De Wolf, H., & Cohen, K. M. (2005). Sedimentary architecture and optical dating of Middle and Late Pleistocene Rhine-Meuse deposits-fluvial response to climate change, sea-level fluctuation and glaciation. *Netherlands Journal of Geosciences*, **84**(1), 25-41.

Campo, B., Bruno, L., & Amorosi, A. (2020). Basin-scale stratigraphic correlation of late Pleistocene-Holocene (MIS 5e-MIS 1) strata across the rapidly subsiding Po Basin (northern Italy). *Quaternary Science Reviews*, **237**, 106300.

Caracciolo, L. (2020). Sediment generation and sediment routing systems from a quantitative provenance analysis perspective: Review, application and future development. *Earth-Science Reviews*, **209**, 103226. https://doi.org/10.1016/j.earscirev.2020.103226

Chalov, S., Golosov, V., Tsyplenkov, A., Theuring, P., Zakerinejad, R., Märker, M., & Samokhin, M. (2017). A toolbox for sediment budget research in small catchments. *Geography, Environment, Sustainability*, **10**(4), 43-68.

Chen, H. W., Lee, T. Y., & Wu, L. C. (2010). High-resolution sequence stratigraphic analysis of Late Quaternary deposits of the Changhua Coastal Plain in the frontal arc-continent collision belt of Central Taiwan. *Journal of Asian Earth Sciences*, **39**(3), 192-213. https://doi.org/10.1016/j.jseaes.2010.02.009

Critelli, S., Arribas, J., Le Pera, E., Tortosa, A., Marsaglia, K. M., & Latter, K. K. (2003). The recycled orogenic sand provenance from an uplifted thrust belt, Betic Cordillera, southern Spain. *Journal of Sedimentary Research*, **73**(1), 72-81.

Demurtas, L., Bruno, L., Lugli S., & Fontana, D. (2022). Evolution of the Po Alpine River System during the Last 45 Ky Inferred from Stratigraphic and Compositional Evidence (Ostiglia, Northern Italy). *Geosciences*, **12**, 342.

do Nascimento Jr, D. R., Sawakuchi, A. O., Guedes, C. C., Giannini, P. C., Grohmann, C. H., & Ferreira, M. P. (2015). Provenance of sands from the confluence of the Amazon and Madeira rivers based on detrital heavy minerals and luminescence of quartz and feldspar. *Sedimentary Geology*, **316**, 1-12.

Fontana, D., Amoroso, S., Minarelli, L. and Stefani, M. (2019). Sand liquefaction phenomena induced by a blast test: new insights from composition and texture of sands (late Quaternary, Emilia, Italy). *Journal of Sedimentary Research.*, **89**(1), 13–27.

Franzinelli, E., & Potter, P. E. (1983). Petrology, chemistry, and texture of modern river sands, Amazon River system. *The Journal of Geology*, **91**(1), 23-39.

Garzanti, E., Vezzoli, G., Andò, S., Paparella, P., & Clift, P. D. (2005). Petrology of Indus River sands: a key to interpret erosion history of the Western Himalayan Syntaxis. *Earth and Planetary Science Letters*, **229**(3-4), 287-302.

Garzanti, E., Andò, S., France-Lanord, C., Vezzoli, G., Censi, P., Galy, V., & Najman, Y. (2010). Mineralogical and chemical variability of fluvial sediments: 1. Bedload sand (Ganga–Brahmaputra, Bangladesh). *Earth and Planetary Science Letters*, **299**(3-4), 368-381.

Garzanti, E., Andò, S., Padoan, M., Vezzoli, G., & El Kammar, A. (2015). The modern Nile sediment system: Processes and products. *Quaternary Science Reviews*, **130**, 9-56.

Goodbred Jr, S. L., & Kuehl, S. A. (2000). The significance of large sediment supply, active tectonism, and eustasy on margin sequence development: Late Quaternary stratigraphy and evolution of the Ganges–Brahmaputra delta. *Sedimentary Geology*, **133**(3-4), 227-248. https://doi.org/10.1016/S0037-0738(00)00041-5

Götz, J., Otto, J. C., & Schrott, L. (2013). Postglacial sediment storage and rockwall retreat in a semi-closed inner-Alpine sedimentary basin (Gradenmoos, Hohe Tauern, Austria). *Geografia Fisica e Dinamica Quaternaria*, **36**, 63-80. https://doi.org/10.4461/GFDQ.2013.36.5

Gunderson, K.L., Pazzaglia, F.J., Picotti, V., Anastasio, D.A., Kodama, K.P., Rittenou, R.T., Frankel, K.F., Ponza, A., Berti, C., Negri, A. & Sabbatini, A. (2014). Unraveling tectonic and climatic controls on synorogenic growth strata (Northern Appennines, Italy). *GSA Bulletin*, **126**-3 (4), 532–552.

Hassan, F. A., Hamdan, M. A., Flower, R. J., Shallaly, N. A., & Ebrahem, E. (2017). Holocene alluvial history and archaeological significance of the Nile floodplain in the Saqqara-Memphis region, Egypt. *Quaternary Science Reviews*, **176**, 51-70. https://doi.org/10.1016/j.quascirev.2017.09.016

He, L., Amorosi, A., Ye, S., Xue, C., Yang, S., & Laws, E. A. (2020). River avulsions and sedimentary evolution of the Luanhe fan-delta system (North China) since the late Pleistocene. *Marine Geology*, **425**, 106194. https://doi.org/10.1016/j.margeo.2020.106194

Hori, K., Saito, Y., Zhao, Q., & Wang, P. (2002). Evolution of the coastal depositional systems of the Changjiang (Yangtze) River in response to late Pleistocene-Holocene sea-level changes. *Journal of Sedimentary Research*, **72**(6), 884-897. https://doi.org/10.1306/052002720884

Marsaglia, K. M., DeVaughn, A. M., James, D. E., & Marden, M. (2010). Provenance of fluvial terrace sediments within the Waipaoa sedimentary system and their importance to New Zealand source-to-sink studies. *Marine Geology*, **270**(1-4), 84-93.

Marcolla, A., Miola, A., Mozzi, P., Monegato, G., Asioli, A., Pini, R., & Stefani, C. (2021a). Middle Pleistocene to Holocene palaeoenvironmental evolution of the south-eastern Alpine foreland basin from multi-proxy analysis. *Quaternary Science Reviews,* **259**, 106908. https://doi.org/10.1016/j.quascirev.2021.106908

Marcolla, A., Monegato, G., Mozzi, P., Miola, A., & Stefani, C. (2021b). Seesaw longitudinal–transverse drainage patterns driven by Middle and Late Pleistocene climate cycles in the foreland basin of the south-eastern European Alps. *Sedimentary Geology*, **421**, 105960. https://doi.org/10.1016/j.sedgeo.2021.105960.

Massari, F., Rio, D., Barbero, R. S., Asioli, A., Capraro, L., Fornaciari, E., & Vergerio, P. P. (2004). The environment of Venice area in the past two million years. *Palaeogeography, Palaeoclimatology, Palaeoecology*, **202**(3-4), 273-308.

Muttoni, G., Carcano, C., Garzanti, E., Ghielmi, M., Piccin, A., Pini, R., Rogledi, S. & Sciunnach, D. (2003). Onset of major Pleistocene glaciations in the Alps. *Geology*, **31**, 989–992.

Muttoni, G., Scardia, G., Kent, D.V., Morsiani, E., Tremolada, F., Cremaschi, M. & Peretto, C. (2011) First dated human occupation of Italy at ~0.85 Ma during the late Early Pleistocene climate transition. *Earth and Planetary Science Letters,* **307**(3-4), 241-252.

Norini, G., Aghib, F. S., Di Capua, A., Facciorusso, J., Castaldini, D., Marchetti, M., ... & Piccin, A. (2021). Assessment of liquefaction potential in the central Po plain from integrated geomorphological, stratigraphic and geotechnical analysis. *Engineering Geology*, **282**, 105997. https://doi.org/10.1016/j.enggeo.2021.105997.

Ishihara, T., & Sugai, T. (2017). Eustatic and regional tectonic controls on late Pleistocene paleovalley morphology in the central Kanto Plain, Japan. *Quaternary International*, **456**, 69-84. https://doi.org/10.1016/j.quaint.2017.06.029

Ji, H., Chen, S., Pan, S., Xu, C., Tian, Y., Li, P., ... & Chen, L. (2022). Fluvial sediment source to sink transfer at the Yellow River Delta: Quantifications, causes, and environmental impacts. *Journal of Hydrology*, **608**, 127622. https://doi.org/10.1016/j.jhydrol.2022.127622

Khan, M. H. R., Liu, J., Liu, S., Seddique, A. A., Cao, L., & Rahman, A. (2019). Clay mineral compositions in surface sediments of the Ganges-Brahmaputra-Meghna river system of Bengal Basin, Bangladesh. *Marine Geology*, **412**, 27-36.

Li, C., Wang, P., Sun, H., Zhang, J., Fan, D., & Deng, B. (2002). Late Quaternary incised-valley fill of the Yangtze delta (China): its stratigraphic framework and evolution. *Sedimentary Geology*, **152**(1-2), 133-158. https://doi.org/10.1016/S0037-0738(02)00066-0

Li, J., Shi, X., Liu, S., Qiao, S., Zhang, H., Wu, K., ... & Kornkanitnan, N. (2021a). Frequency of deep-sea turbidity as an important component of the response of a source-to-sink system to climate: A case study in the eastern middle Bengal Fan since 32 ka. *Marine Geology*, **441**, 106603. 3227, https://doi.org/10.1016/j.margeo.2021.106603

Li, Z., Liu, Q., Zhu, H., Zhang, X., Li, M., & Zhao, Q. (2021b). Compositional relationship between the source-to-sink segments and their sedimentary response to diverse geomorphology types in the intrabasinal lower uplift of continental basins. *Marine and Petroleum Geology*, **123**, 104716.

Limonta, M., Garzanti, E., & Resentini, A. (2023). Petrology of Bengal Fan turbidites (IODP Expeditions 353 and 354): provenance versus diagenetic control. *Journal of Sedimentary Research*, **93**(4), 256-272. https://doi.org/10.2110/jsr.2022.071

Liu, Z., Zhao, Y., Colin, C., Stattegger, K., Wiesner, M. G., Huh, C. A., ... & Li, Y. (2016). Source-to-sink transport processes of fluvial sediments in the South China Sea. *Earth-Science Reviews*, **153**, 238-273. https://doi.org/10.1016/j.earscirev.2015.08.005

Lisiecki, L. E., & Raymo, M. E. (2005). A Pliocene-Pleistocene stack of 57 globally distributed benthic δ18O records. *Paleoceanography*, **20**(1). https://doi.org/10.1029/2004PA001071PA1003

Palamenghi, L., Schwenk, T., Spiess, V., & Kudrass, H. R. (2011). Seismostratigraphic analysis with centennial to decadal time resolution of the sediment sink in the Ganges–Brahmaputra subaqueous delta. *Continental Shelf Research*, **31**(6), 712-730. https://doi.org/10.1016/j.csr.2011.01.008

Panin, A., Adamiec, G., Buylaert, J. P., Matlakhova, E., Moska, P., & Novenko, E. (2017). Two Late Pleistocene climate-driven incision/aggradation rhythms in the middle Dnieper River basin, west-central Russian Plain. *Quaternary Science Reviews*, **166**, 266-288. https://doi.org/10.1016/j.quascirev.2016.12.002

Peeters, J., Busschers, F. S., Stouthamer, E., Bosch, J. H. A., Van den Berg, M. W., Wallinga, J., ... & Middelkoop, H. (2016). Sedimentary architecture and chronostratigraphy of a late Quaternary incised-valley fill: a case study of the late Middle and Late Pleistocene Rhine system in the Netherlands. *Quaternary Science Reviews*, **131**, 211-236.

Piovan, S., Mozzi, P., & Stefani, C., (2010). Bronze Age paleohydrography of the southern venetian Plain. *Geoarchaeology An Int. J.*, ***25***, pp. 6-35.

Rittenour, T. M., Blum, M. D., & Goble, R. J. (2007). Fluvial evolution of the lower Mississippi River valley during the last 100 ky glacial cycle: Response to glaciation and sea-level change. *Geological Society of America Bulletin*, **119**(5-6), 586-608. https://doi.org/10.1130/B25934.1

Rossi, V., Amorosi, A., Barbieri, G., Vaiani, S. C., Germano, M., & Campo, B. (2021). A Long-Term Record of Quaternary Facies Patterns and Palaeonvironmental Trends from the Po Plain (NE Italy) as Revealed by Bio-Sedimentary Data. *Geosciences*, **11**(10), 401.

Schneider, S., Hornung, J., Hinderer, M., & Garzanti, E. (2016). Petrography and geochemistry of modern river sediments in an equatorial environment (Rwenzori Mountains and Albertine rift, Uganda)—Implications for weathering and provenance. *Sedimentary Geology*, **336**, 106-119.

Schroeder, A., Wiesner, M. G., & Liu, Z. (2015). Fluxes of clay minerals in the South China Sea. *Earth and Planetary Science Letters*, **430**, 30-42. https://doi.org/10.1016/j.epsl.2015.08.001

Sinha, R., Gibling, M.R., Kettanah, Y., Tandon, S.K., Bhattacharja, P.S., Dasgupta, A.S. & Ghazanfari, P. (2009) Craton-derived alluvium as a major sediment source in the Himalayan Foreland Basin of India. *GSA Bulletin*, **121**(11/12), 1596-1610.

Singh, S. K., Rai, S. K., & Krishnaswami, S. (2008). Sr and Nd isotopes in river sediments from the Ganga Basin: sediment provenance and spatial variability in physical erosion. *Journal of Geophysical Research: Earth Surface*, **113**(F3).

Singh, A., Paul, D., Sinha, R., Thomsen, K. J., & Gupta, S. (2016). Geochemistry of buried river sediments from Ghaggar Plains, NW India: Multi-proxy records of variations in provenance, paleoclimate, and paleovegetation patterns in the Late Quaternary. Palaeogeography, Palaeoclimatology, *Palaeoecology*, **449**, 85-100.

Stefani C., (2002). Variation in terrigenous supplies in the Upper Pliocene to Recent deposits of the Venice area. *Sedimentary Geology*, *153*, Issues 1–2, Pages 43-55. ISSN 0037-0738, https://doi.org/10.1016/S0037-0738(02)00101-X.

Swain, D. L., Wing, O. E., Bates, P. D., Done, J. M., Johnson, K. A., & Cameron, D. R. (2020). Increased flood exposure due to climate change and population growth in the United States. *Earth's Future*, **8**(11), e2020EF001778.

Tanabe, S., Nakanishi, T., Ishihara, Y., & Nakashima, R. (2015). Millennial-scale stratigraphy of a tide-dominated incised valley during the last 14 kyr: Spatial and quantitative reconstruction in the Tokyo Lowland, central Japan. *Sedimentology*, **62**(7), 1837-1872. https://doi.org/10.1111/sed.12204

Tentori, D., Amorosi, A., Milli, S., & Marsaglia, K.M. (2021). Sediment dispersal pathways in the Po coastal plain since the Last Glacial Maximum: Provenance signals of autogenic and eustatic forcing. *Basin Research*, *33*, 1407–1428.

Van Grinsven, M., Marsaglia, K. M., & Romans, B. W. (2019). Sand Provenance from Source to Sink in the Santa Monica Basin, California Borderlands: Significance of Calleguas Creek Input. https://doi.org/10.2110/sepmsp.110.06

Whitmore, G. P., Crook, K. A., & Johnson, D. P. (2004). Grain size control of mineralogy and geochemistry in modern river sediment, New Guinea collision, Papua New Guinea. *Sedimentary Geology*, **171**(1-4), 129-157.

Xue, Z., Liu, J. P., DeMaster, D., Van Nguyen, L., & Ta, T. (2010). Late Holocene evolution of the Mekong subaqueous delta, southern Vietnam. *Marine Geology*, **269**(1-2), 46-60. https://doi.org/10.1016/j.margeo.2009.12.005

CHAPTER 2. THESIS STRUCTURE

This thesis is structured in three manuscripts, corresponding to chapters 3, 4 and 5, and in a final chapter (chapter 6) which summarises the main results of this work. Chapters 3, 4 and 5 investigate the subsurface of the Po Plain at three different spatial and time scales.

Chapter 3 depicts the Middle Pleistocene to Holocene stratigraphy of a ~3500 km^2 wide area of the central and eastern Po Plain (Fig. 1) and discusses the main controlling factors of the sedimentary evolution of the Po-Adriatic system. Stratigraphic reconstructions are based on new core data (184S2 and 184S15 in Fig. 1), retrieved for the realization of sheet 184 of the Geological Map of Italy at 1:50,000 scale, and on the reinterpretation of data from published works and from the dataset of the Geological, Seismic and Soil Survey of Regione Emilia-Romagna. This work benefits of absolute ages from radiocarbon, ESR and IRSL ages, which supported and validated stratigraphic correlations. This chapter includes data which will be published in the sheet 184 of the Geological Map of Italy to scale 1:50.000 - and relative illustrative notes - at the end of October 2024. Until that date, these data are protected by embargo. For this reason, this manuscript will be submitted as a scientific article to the journal *Quaternary Science Reviews* at the end of the embargo.

For this chapter I took part in the sedimentological analyses of the new cores, I realised the stratigraphic sections and most of the figures. I also personally prepared and analyzed the three samples for IRSL dating at Utah State University Luminescence Laboratory (Logan, Utah, US) during my period abroad. The writing was limited to the drafting of the chapter methods.

Chapter 4 and **Chapter 5** are based on integrated stratigraphic-petrographic analyses of core sediments in two areas of the fully alluvial portion of the Po Basin. The composition of core sands was compared to that of sands from the modern Po River and its tributaries, in order to assess sediment provenance.

In **Chapter 4,** the study of two long cores (101 and 77.5 m; MDL and SBP in Fig. 1, respectively) permitted to reconstruct the evolution of the Po fluvial network from the late Middle Pleistocene to the Holocene (last ~500000 years). This chapter corresponds to a scientific article published in *Basin Research*.

The activities carried out for Chapter 4 consisted in collection of samples from cores and modern rivers, and their preparation to obtain thin sections. I personally performed the compositional analyses, realised the figures, and wrote a first draft of the manuscript.

Chapter 5 focuses on the evolution of the Po-Alpine river system during the last 45 ky. The sedimentological and compositional analysis of three 30-m-long cores recovered close to the Po River (OS1, OS2 and OS3 in Fig.1) documented the response of the Po-Alpine fluvial system to the climatic changes occurred at the transition from the last glacial to the present interglacial. This chapter corresponds to a paper published in *Geosciences* (see reference list).

In this work, I conducted sampling, treated the samples, and performed petrographic analysis. I also created the figures and wrote a first draft of the manuscript.

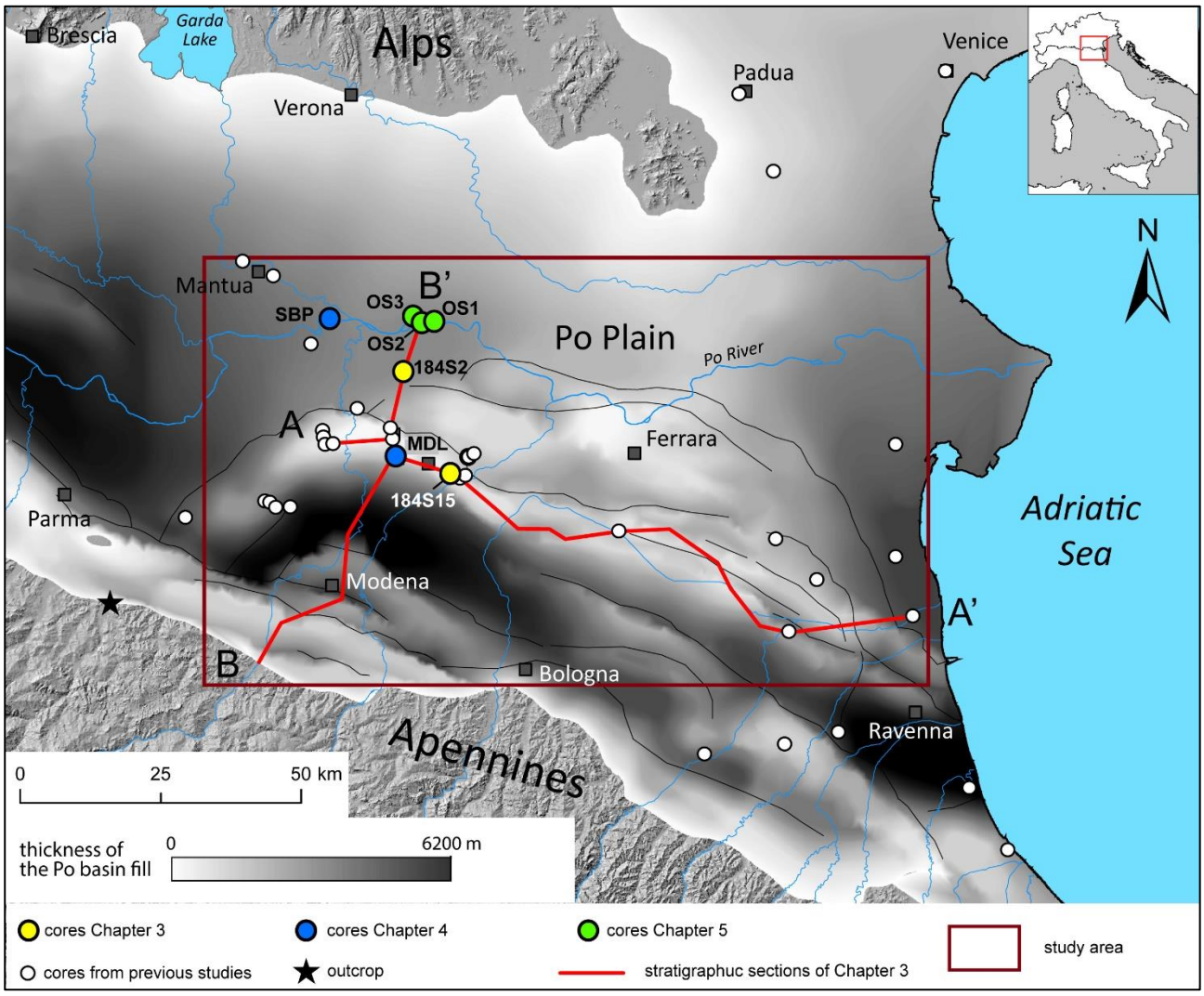

Figure 1. Location of reference cores of Chapters 3, 4 and 5.

CHAPTER 3. Sedimentary response of the Po Basin to Mid-Late Pleistocene glacio-eustatic oscillations

Luigi Bruno[1], Luca Demurtas[1], Tammy Rittenour[2], Wan Hong[3], Alessandro Amorosi[4].

1. Department of Chemical and Geological Sciences, University of Modena and Reggio Emilia, Via Campi 103, 41125, Modena. Corresponding author: luigi.bruno@unimore.it
2. Luminescence Lab, Utah State University, 1770 North Research Parkway Suite 123, North Logan UT 84341.
3. KIGAM Korea Institute of Geoscience and Mineral Resources, 92 Gwahangro, Yuseong-gu, Daejeon Metropolitan City, Korea
4. Department of Biological, Geological and Environmental Sciences, University of Bologna, Via Zamboni 67, 40125, Bologna.

Abstract

The Middle and Late Pleistocene were characterized by high-amplitude climate and sea-level oscillations that deeply influenced the evolution of alluvial and coastal systems worldwide. Through the correlation of 44 cores and 168 well data, with the aid of pollen data, ^{14}C, ESR and IRSL dates, this work provides a detailed reconstruction of the Middle Pleistocene to Holocene stratigraphy and explores the sedimentary response of the Po-Adriatic alluvial-coastal system to glacio-eustatic oscillations and other concomitant forcing factors.

The Middle Pleistocene to Holocene sedimentary succession of the Po Basin is composed of alluvial, paralic, coastal and shallow-marine facies associations arranged in an overall shallowing-upward trend. This general trend is punctuated by the rhythmical alternation of progradationally stacked coastal wedges with thick alluvial deposits. At landward locations, where the coastal facies wedge out, the depositional cyclicity records alternating paralic and alluvial facies associations. Whereas the overall shallowing-upward trend documents the longer-term, progressive filling of the basin driven by high sediment supply which overcame the rate of creation of accommodation induced by subsidence, the cyclic arrangement of facies clearly reflects Milankovitch-scale, glacio-eustatic oscillations in the 100 ky band. Increasing subsidence towards the sea might have enhanced the seaward migration of the coastal wedges.

This study provides clues on the sedimentary response of a low-gradient coastal system to dramatic climatic and eustatic changes. The model of basin evolution presented here may help predict the environmental modifications of coastal areas in the near future scenarios of climate and sea-level change.

Keywords: coastal system, sediment supply, core stratigraphy, Po Plain, Quaternary

Highlights

- The Mid-Late Pleistocene stratigraphy of the Po Basin has a shallowing-upward trend
- Higher-frequency cycles include the rhythmical occurrence of coastal wedges
- Coastal wedges alternate with alluvial units and are progradationally stacked
- The cyclic arrangement of facies reflects glacio-eustatic oscillations
- The progradational stacking of coastal wedges reflects the filling of the basin

3.1. INTRODUCTION

The Middle Pleistocene is marked by high-amplitude climate and sea-level oscillations linked to periodic variations in the Earth's orbital parameters (Lisiecki & Raymo, 2005). Eight glacial cycles with period of ca. 100 ky resulted in eustatic oscillations of ca. 100 m (Rohling et al., 2009; 2013; 2014; Grant et al., 2014). Alluvial systems responded to eustatic drops excavating deep valleys, which were filled with estuarine sediments during the following phases of sea-level rise (Allen and Posamentier, 1993; Blum and Aslan, 2006; Chaumillon et al., 2008; Vis and Kasse 2009; Peeters et al., 2016). Along low-gradient shelves, glacio-eustatic oscillations led to hundreds-km facies shifts (Storms et al., 2008; Neal & Abreu, 2009; Blum et al., 2013), introducing an oscillatory signal in the record of sedimentary basins, superposed to the overall filling trend (Krapez, 1995; Chansong et al., 2004; Yang, 2011; Liu et al., 2023).

A vast literature, produced in the last decades, has documented the effects of Middle and Late Pleistocene glaciations (and related eustatic changes) on sedimentation patterns in the Po-Adriatic Basin. A cyclic organization of facies was documented for the fully alluvial portion of the basin (Amorosi et al., 2001; 2008) and for the coastal plain (Amorosi et al., 2004; Massari et al., 2004; Marcolla et al., 2021; Rossi et al., 2021). These works, however, were limited to relatively small areas

and did not produce a comprehensive stratigraphic and evolutionary picture of the Po-Adriatic Basin. An exception is the work by Campo et al. (2020), who built a general model of Late Pleistocene to Holocene stratigraphy from the alluvial to the coastal realms, providing a detailed paleogeographic reconstruction of the Po coastal plain during MIS 5e. In addition to ^{14}C dates, which constrained stratigraphy in the last 50 ky, this work benefited from ESR ages on Last Interglacial deposits (Ferranti et al., 2006).

In the Po Basin, age attributions older than MIS 5e have relied uniquely on pollen (Amorosi et al., 1999, 2008) and magnetostratigraphic (Muttoni et al., 2003, 2011) data, whereas no absolute ages are available for the buried Middle Pleistocene deposits. Gunderson et al. (2014) provided a detailed chronology of Middle Pleistocene deposits exposed at the basin margin, based on the integration of several dating methods. The dated succession, however, was strongly affected by local tectonics and is rather discontinuous.

In general, the lack of basin-scale studies on the pre-MIS 5e stratigraphy of the Po Basin is attributable to: (i) the poor resolution of industrial seismic profiles in this stratigraphic interval; (ii) the relatively low number of cores penetrating Middle-Pleistocene units, which are typically encountered at depths > 100 m; (iii) the increasing tectonic deformation with depth, which makes stratigraphic correlation uncertain, especially close to the buried tectonic structures. The same limitations affect several other regions worldwide: a rare example of high-resolution investigation of Middle Pleistocene deposits is the one from the Rhine-Meuse system, which is based on a robust, OSL-based chronology (Busschers et al. 2005; Peeters et al., 2016). However, owing to a markedly lower subsidence, Middle Pleistocene deposits in this case were encountered at significantly lower depths.

In this work, we reconstructed the Middle and Late Pleistocene sedimentary evolution of the Po Basin and examined the interaction between high-amplitude climate and sea-level oscillations and the progressive filling of the basin in shaping the Po-Adriatic paleogeography. To this aim, we reconstructed the subsurface stratigraphy through correlation of 44 core data and 6 pollen profiles along two stratigraphic cross-sections, 117 and 67 km long, respectively. The absolute chronology was based on IRSL, ESR and ^{14}C dates. The resulting depositional architecture represents the first chronologically-constrained reconstruction of high-resolution Middle and Late Pleistocene stratigraphy in the area.

3.2. GEOLOGICAL SETTING

The Po Basin represents the foredeep, filled with Plio-Quaternary sediments of the Northern Apennines and of the Southern Alps (Fig. 1). These two mountain belts, showing opposite vergence, developed since the Cretaceous due to the convergence between the European and the Adria plates (Carminati & Doglioni, 2012). The most external portion of the two accretionary wedges is buried beneath the Po Plain and is composed of arcuate systems of thrust-related folds (Fantoni & Franciosi, 2010; Turrini et al., 2014). The Apennine Ferrara folds, tectonically active since the Early Pliocene (Toscani et al., 2009; Boccaletti et al., 2011; DISS Working Group, 2018), include the Mirandola thrust system which was active during the 2012 Emilia earthquake (Bonini et al., 2014). Atop the buried anticlines, the Po Basin fill is a few hundred meters thick, whereas in the depocenters it may attain 6 to 8 km (Fig. 2, Amadori et al., 2018).

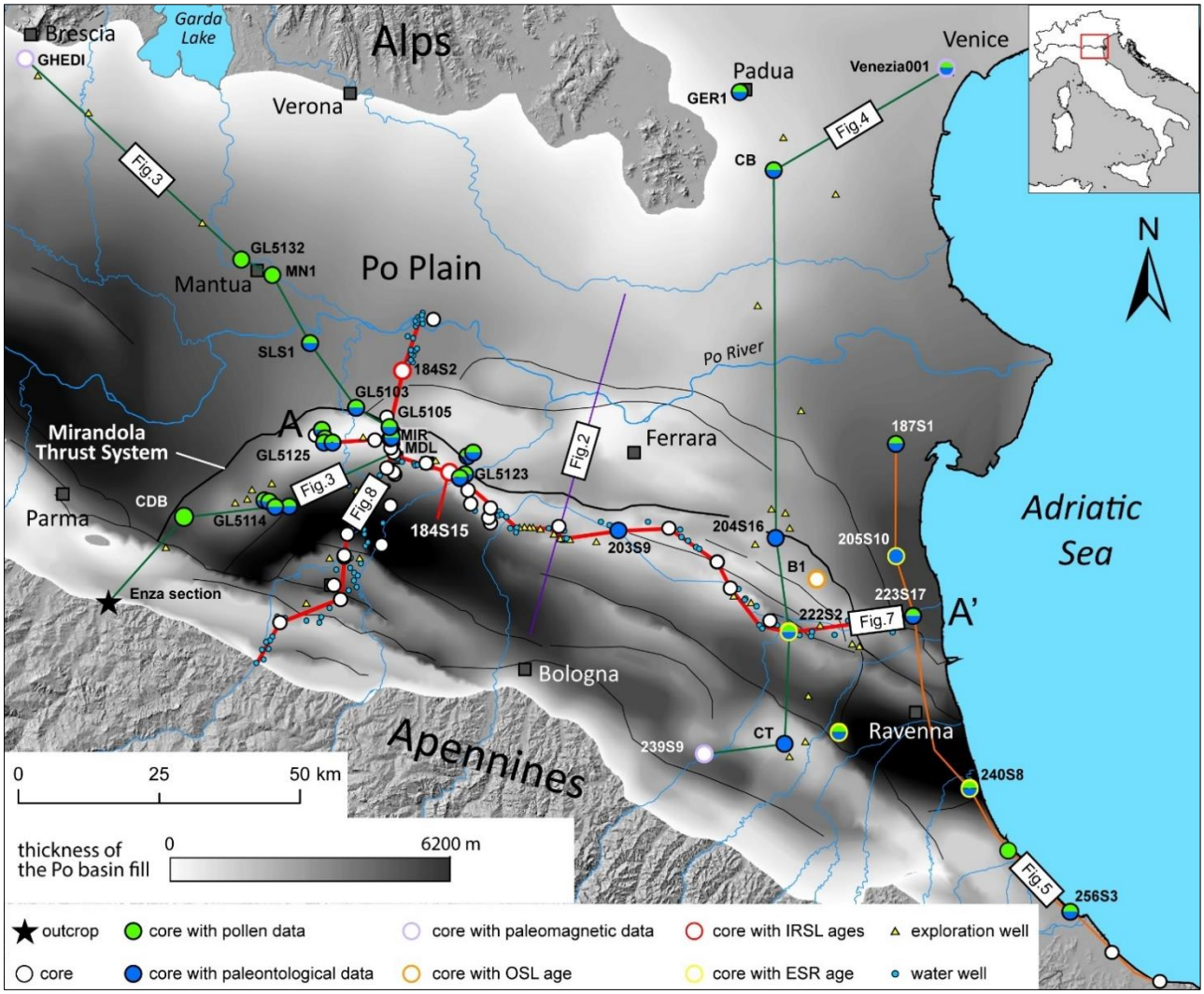

Figure 1. The Po Basin with location of the stratigraphic sections of Figures 2, 3, 4, 5, 7 and 8 and of cores and wells that compose the stratigraphic dataset. The thickness of the Po Basin fill is also indicated (modified after Boccaletti et al., 2011).

The Po Basin fill has been subdivided on a seismic basis in six tectonically-driven stratigraphic units (PL1s, PL2s, PL3s, PS1s, PS2s, PS3s, Ghielmi et al., 2013) bounded at the base by six unconformities (PL1, PL2, PL3, PS1, PS2, PS3 in Fig. 2). Units PL1s to PS2s are deep-water turbidites, whereas unit PS3s records the rapid progradation of the Po delta system, when sediment supply overcame the rates of creation of accommodation space; genetically related turbidites were deposited in the Northern Adriatic Sea (Amadori et al., 2020).

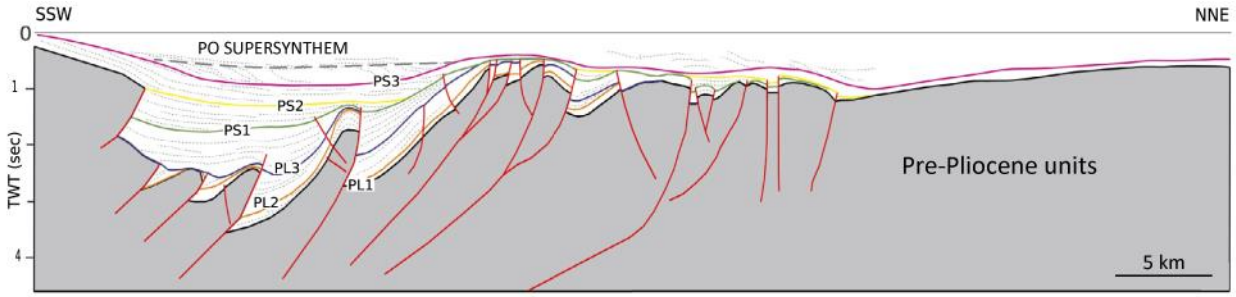

Figure 2. Interpretation of a S-N oriented seismic profile with indication of the main angular unconformities within the Po Basin fill (modified after Amadori et al., 2019). See Fig. 1 for location.

The alluvial units of the Po Basin (Po Supersynthem of Amorosi et al., 2008) constitute the upper portion of unit PS3s and are dated to the last 870 ky (Muttoni et al., 2003; Gunderson et al., 2014). The Po Supersynthem is subdivided into two lower-rank units (Lower and Upper Po Synthem) by a regional unconformity dated to 450 kyr BP (Geomol Team, 2015; Martelli et al., 2017). The Po Supersynthem, poorly resolved in industrial seismic sections (Fig. 2), has been studied through sedimentological, paleontological and palynological analysis on core sediments, which showed a cyclic organization of facies. At the basin margin, mud-prone overbank deposits alternate with fluvial-channel gravels and subordinate sands (Fig. 3A, Gunderson et al., 2014). Here, the gravel-mud ratio increases at the transition from the Lower to the Upper Po Synthem (Figs. 3A, 3I and 4A; Garzanti et al., 2011; Muttoni et al., 2011; Gunderson et al., 2014). In the central Po Plain, beneath the Po River, mud-dominated horizons alternate with sand bodies deposited by the Po River and by its alpine tributaries during glacial periods (Fig. 3D to 3G; Amorosi et al., 2008; Bruno et al., 2021). Mud-prone horizons host pollen from warmth-loving species (broad-leaved trees), typical of interglacial periods, whereas pollen occasionally preserved within predominantly gravel and sand bodies indicates cold-climate associations (*Pinus*, mountain trees and herbs, Figs. 3F, 3G, 3H, ENEL-DCO, 1984, Amorosi et al., 2008; see also Amorosi et al., 2001). The attribution of laterally continuous, coarse-grained sediment bodies to glacial periods is supported by OSL dates from the Enza River section (Gunderson et al., 2014; Fig. 3A).

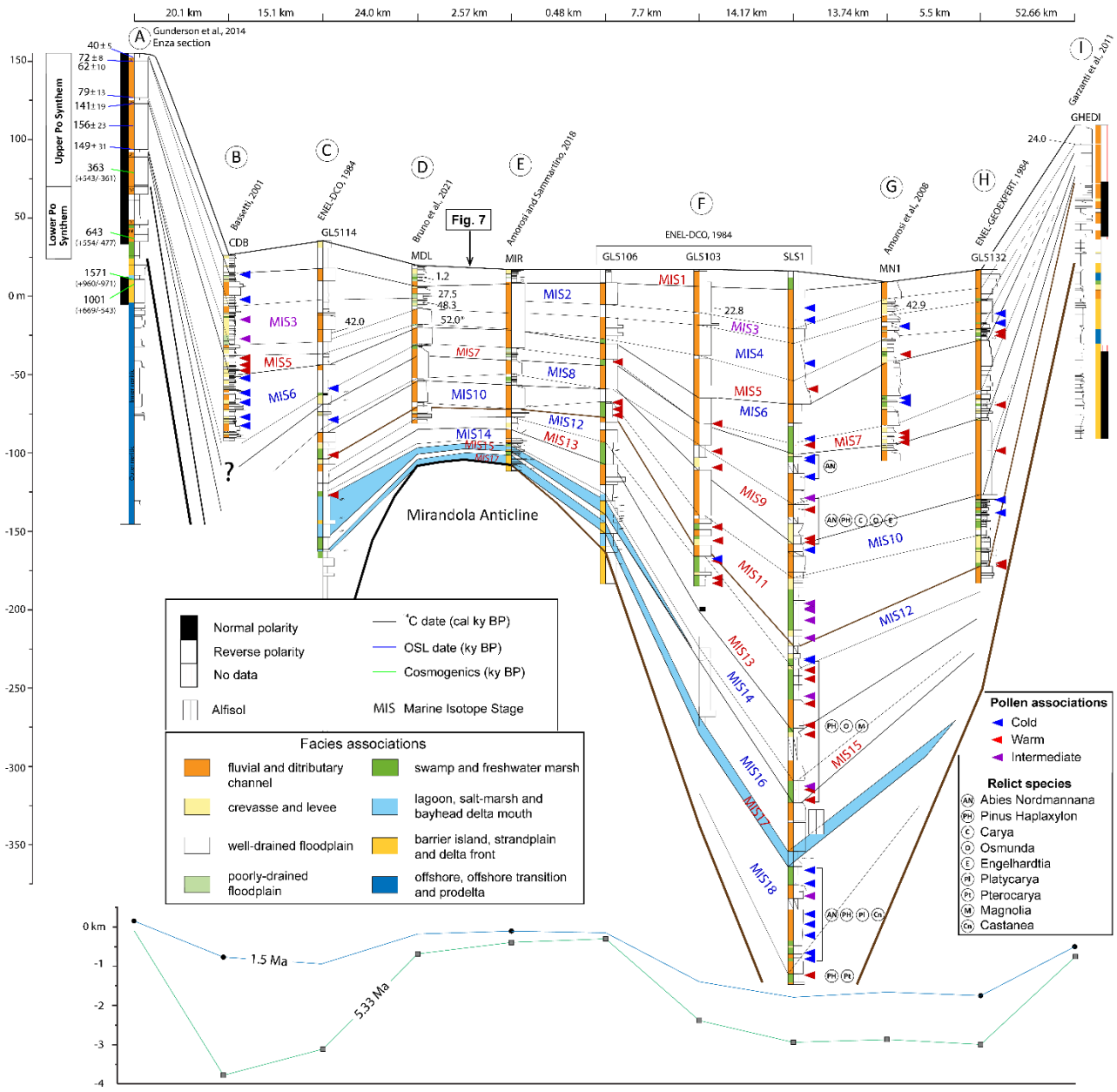

Figure 3. Stratigraphic correlation of cores from previous works which penetrated Middle and Late Pleistocene units of the inner Po Basin. See Fig. 1 for location.

In cores recovered close the Adriatic coastline, alluvial sediments deposited during glacial periods alternate with paralic, coastal and shallow-marine sediments deposited during the interglacials (Figs. 4C to 4G; Amorosi et al., 2004; Massari et al., 2004; Marcolla et al., 2021; Rossi et al., 2021). Coastal sediments assigned to the MISs 5e and 1, studied in detail by Amorosi et al. (2017) and Campo et al. (2020, Fig. 5), are arranged in transgressive-regressive wedges, with a markedly retrogradational stacking pattern of facies (transgressive systems tract, Bruno et al., 2017) overlain by a well-developed progradational parasequence set (highstand systems tract; Amorosi et al.,

2020). The maximum landward position of the Adriatic coastline during MIS1 and MIS5e was about 25 and 35 km inland of the modern coastline (Bruno et al., 2017; Campo et al., 2020), respectively.

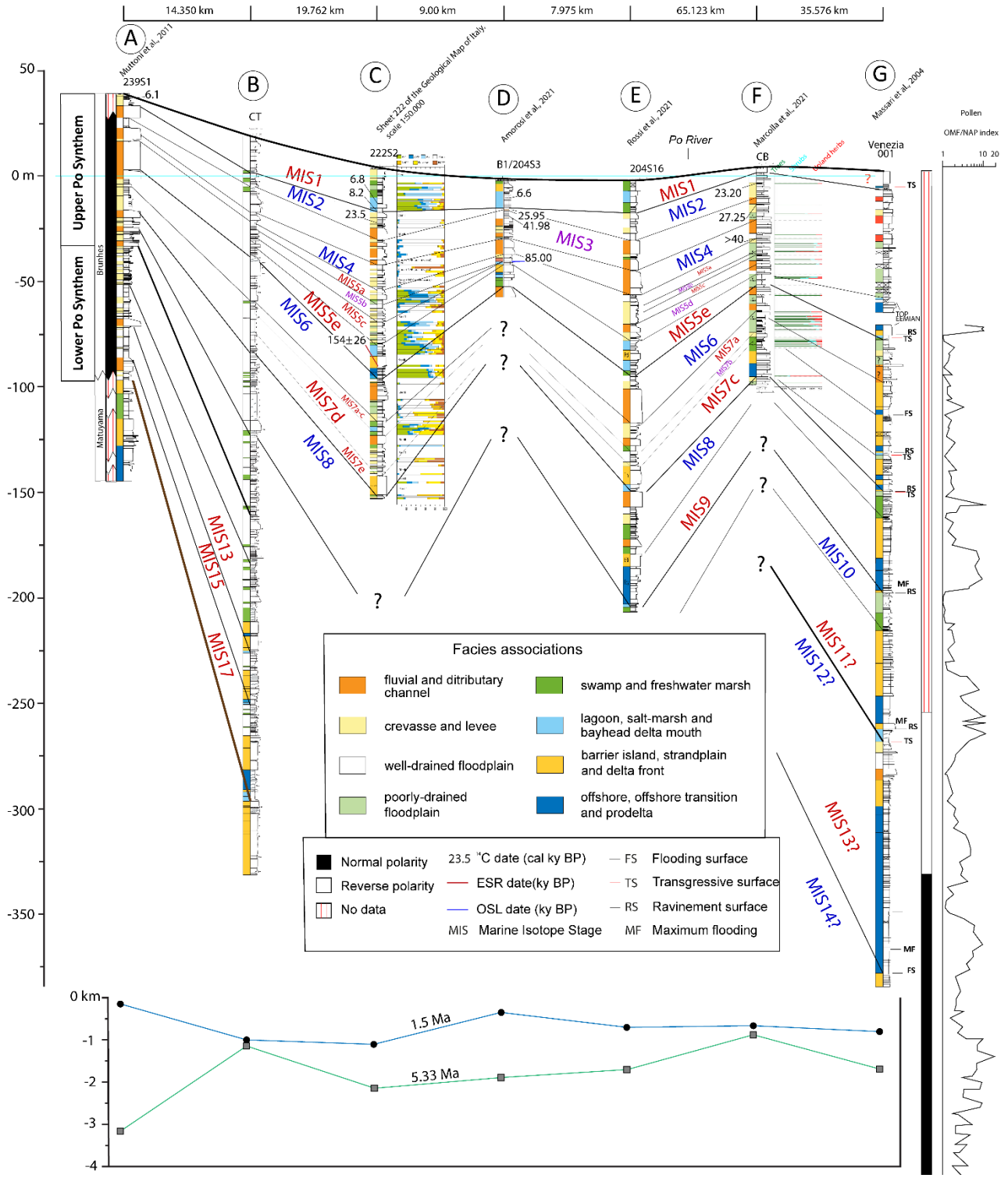

Figure 4. Stratigraphic correlation of cores from previous works which penetrated Middle and Late Pleistocene units of the Po coastal plain. See Fig. 1 for location.

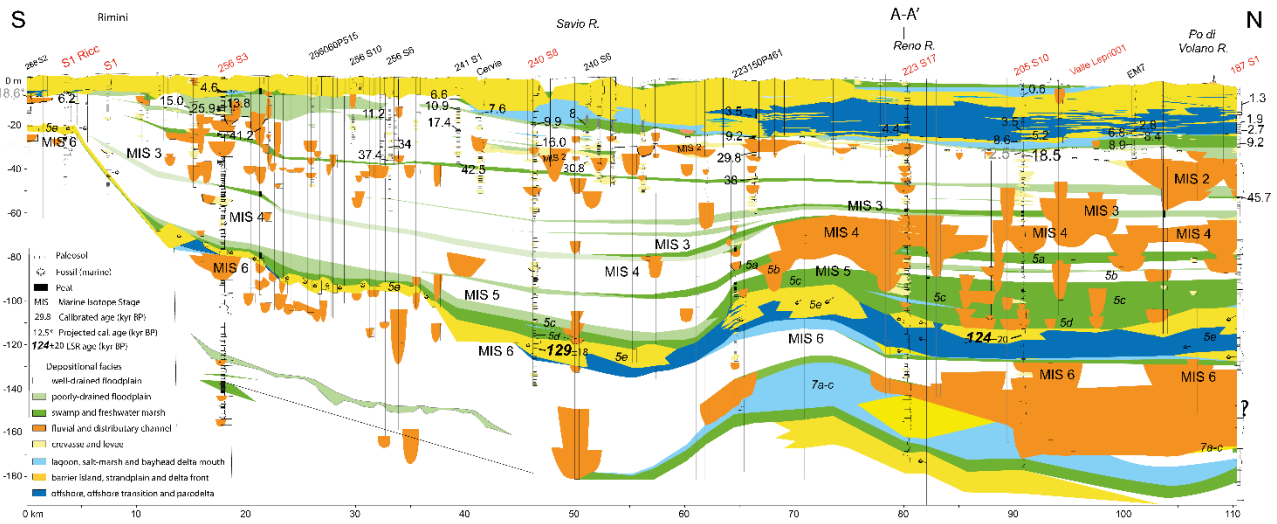

Figure 5. Mid-Late Pleistocene (from MIS 7 to Present) stratigraphy of the Po Basin depicted in a cross-section running along the Adriatic coast (modified after Campo et al., 2020).

3.3. METHODS

3.3.1. *Stratigraphic dataset*

In this work, the Middle-Late Pleistocene and Holocene stratigraphy of the central and eastern Po Plain was investigated over an area of ~3500 km^2 based on the correlation of 44 cores, 15 m to 220 m long (Fig. 1). Two cores (184S2 and 184S15), recently recovered for the realization of Sheet 184-Mirandola of the Geological Map of Italy at 1:50,000 scale (GMI), were used as a reference for facies analysis. They were split in two and described reporting: grain size, grain size trends, colour, consistency and accessory components, such as plant remains, peat horizons, carbonate nodules, and shell fragments. Thirty-nine core descriptions from published works (ENEL-DCO, 1984; Bruno et al., 2021; Demurtas et al., 2022; sheets 201, 202, 203, 204, 219, 222 and 223 of GMI), and from the Emilia-Romagna Geological, Soil and Seismic Survey database, were reinterpreted in terms of depositional facies associations and correlated into two stratigraphic sections. Seven out of these cores provide additional quantitative palynological and palaeontological (foraminifer and ostracod) data (Amorosi et al., 1999; Sheet 222 of GMI). Qualitative palynological and paleontological data derive from cores in ENEL-DCO (1984). Section A-A', 215 m deep, is elongated from land (WNW) to sea (ESE) for 117 km, along the Mirandola thrust system and its eastward prolongation (Fig. 1). Section B-B', 250 m deep, runs transversal to the main tectonic structures, from the Apennine margin (SSW) to the Po River (NNE), ~100 km inland of the Adriatic coast. A total of 132 water wells and 36 exploration wells were also projected in the stratigraphic sections. Water wells (depth 30-700 m) provide low-resolution data on grain size and colour, with local indication of fossils and peat,

and were mainly used to reconstruct the geometry and lateral extent of sand bodies. Exploration wells, which report paleontological data and information about older stratigraphic surfaces, helped to trace the base of the Po Supersynthem and to reconstruct the geometry of the buried anticlines. Well logs were projected within a distance of 3 km. In areas of intense tectonic deformation, core data were projected from a maximum distance of 1 km and following the trends of the buried thrusts and folds.

Stratigraphic correlations were based on facies relationships, the lateral tracking of stratigraphic markers (e.g. paleosols, peat horizons), and pollen data. Absolute ages from 42 radiocarbon dates (8 from this work and 34 from ENEL-DCO, 1984; Bruno et al., 2021; Amorosi et al., 2021; Demurtas et al, 2022 and from the Sheets 202, 203, 222, 223 of GMI), 3 ESR dates (Ferranti et al., 2006) and 3 new IRSL ages (see section 3.2 for details) supported and validated stratigraphic correlations.

3.3.2. *Absolute chronology*

Eight wood and soil samples were collected from cores 184S2, 184S5, 184S9 and 184S15 (see Tab. 1) and ^{14}C-dated at the KIGAM Laboratory (Korea Institute of Geoscience and Mineral Resources, Daejeon, Republic of Korea). All samples were cleaned through acid-alkali-acid pretreatment, to remove secondary calcite and humic acids. Radiocarbon ages were calibrated using OxCal 4.4 (Bronk Ramsey & Lee, 2013) with the IntCal 20 curve (Reimer et al., 2020).

Three sand samples were collected with a Shelby sampler from cores 184S2 and 184S15 (see Tab. 2) to be dated through the IRSL method. About 1 dm^3 of sediment from the innermost part of each sample was collected in the darkroom, as equivalent dose (D_E), whereas sediments below and above D_E were sampled for environmental Dose Rate (D_{Ra} and D_{Rb}). An additional sample was taken and stored in a waterproof container to measure the moisture of the sediment. All samples, packed in light-proof containers, were shipped to the Utah State University Luminescence Laboratory, where they were prepared and analyzed. The 0.075-0.150 mm fraction was selected from D_E samples through wet sieving and treated with hydrogen peroxide, to remove organic matter, and with 10% hydrochloric acid to remove carbonates. Sodium polytungstate was used to isolate feldspar grains from heavy minerals and quartz. Infrared measurements were performed on Risø TL/OSL Model DA-20 readers, following the Single-Aliquot Regenerative (SAR) protocol of Wallinga et al. (2000). DR was calculated by analyses performed with ICP-MS and ICP-AES.

3.3.3 *Subsidence-rates calculation*

Subsidence rates, averaged over different periods, were calculated in cores along section AA' using lagoon and beach deposits, which accumulated close to the coeval sea-levels, as reference horizons (Bruno et al., 2020). The calculation of subsidence rates (SR) for a selected time interval (Δt) between the time of deposition (t_d) and the Present (t_0) was based on Eq. (1):

$$SR(\Delta t) = (Z_{td} - Z_{t0})/\Delta t \quad (1)$$

where Z_{td} is the elevation of the stratigraphic marker at the time of deposition and Z_{t0} is the present elevation (see supplementary data). As sediment accumulation in back-barrier environments presumably took place in shallow water bodies (< 2 m in Amorosi et al., 2004), an error of ±1 m was considered in SR calculation. An error of ±2 m was considered for beach deposits (Rovere et al., 2016). For the estimation of sea-level at the time of deposition of lagoon and beach horizons, we referred to Ferranti et al. (2006), Kopp et al. (2009), Dutton et al. (2009), Bowen (2010), Rovere et al. (2011), Raymo & Mitrovica (2012), Zazo et al. (2012), and Rohling et al. (2014). Considering the highest and the lowest sea-level estimations, we obtained a maximum and a minimum value of subsidence. Then we calculated the mean value and the standard deviation.

Table 1. List of radiocarbon dates. Details on radiocarbon dates from cores 184S2, 184S5, 184S9 and 184S15.

Core	Lab	Material	depth (m)	^{14}C age	Calibrated age (mean ± 2σ)	Lab code
184S2	KIGAM	wood	19.2	8974±52	10130±200	KGM-OWd220087
184S2	KIGAM	wood	21.5	12034±65	13920±160	KGM-OWd220089
184S2	KIGAM	wood	28.2	NaN	>54364	KGM-Owd220091
184S5	KIGAM	wood	14.1	13370±66	16090±220	KGM-Owd220093
184S9	KIGAM	wood	19.1	23249±153	27500±260	KGM-Owd220103
184S9	KIGAM	bulk sediment	23.95	45850±782	48300±2100	KGM-OWd220105
184S15	KIGAM	bulk sediment	7.5	7299±52	8105±120	KGM-OSa220045
184S15	KIGAM	wood	18.1	27285±197	31320±320	KGM-OWd220119

Table 2. List of IRSL dates. Details on IRSL dates from cores 184S15 and 184S2.

Core	Location	Depth	# Disks	Dose Rate (Gy/Kyr)	De, Gy (2SE)	ISRL age, ka (1SE)	Fading Rate	USU code
184S15	Dogaro (MO)	87.45	9(10)	2.19 ± 0.10	795.81 ± 90.01	**363.9 ± 41.3**	1.75 ± 1.03, n =8	USU-4289 pIR250 DRC
184S15	Dogaro (MO)	110.25	10(11)	2.99 ± 0.15	1230.80 ± 168.64	**411.9 ± 49.5**	1.66 ± 0.90, n =3	USU-4290 pIR250 DRC
184S2	Poggio Rusco (MN)	76	9(10)	2.94 ± 0.14	467.33 ± 84.54	**158.9 ± 21.3**	1.48 ± 0.6, n =7	USU-4291 pIR250 DRC

3.4. RESULTS

3.4.1. *Depositional facies associations*

Based on the sedimentological analysis of cores 184S2 and 184S15 (Fig. 6), a brief description of depositional facies associations is presented here. The author is referred to Amorosi et al. (2021) for description of coastal and shallow marine facies.

3.4.1.1. Fluvial and distributary channel facies association

This facies association is composed of medium to coarse sand bodies with erosional lower boundary and fining-upward (FU) grain-size tendency. Towards the basin margin, sands are replaced by gravels, with imbricated cobbles or pebbles. Thickness is > 3 m. Fossils are rare and represented by freshwater specimens. Wood fragments are seldom encountered.

These coarse-grained deposits, with erosive base and FU grainsize trend are interpreted as fluvial-channel or distributary channel deposits (Allen, 1963; Miall, 1985, 1996; Bridge, 1993). These latter are distinguished by their lower lateral extent and slightly lower grain size and thus cannot be easily revealed by the analysis of a single core.

3.4.1.2. Crevasse and Levee facies association

This facies association includes sand bodies (fine to medium sand), with either FU or coarsening-upward (CU) trend, and sand-mud alternations. Thickness is < 3 m. Fossils are absent and wood fragments are seldom encountered.

Sand bodies with FU trend are interpreted as crevasse-channel deposit, whereas those with CU trend are referable to crevasse splays. Sand-mud alternations may reflect multiple episodes of

overbank sedimentation close to an active channel, and are interpreted as channel-levee deposits (Alexander & Prior, 1987).

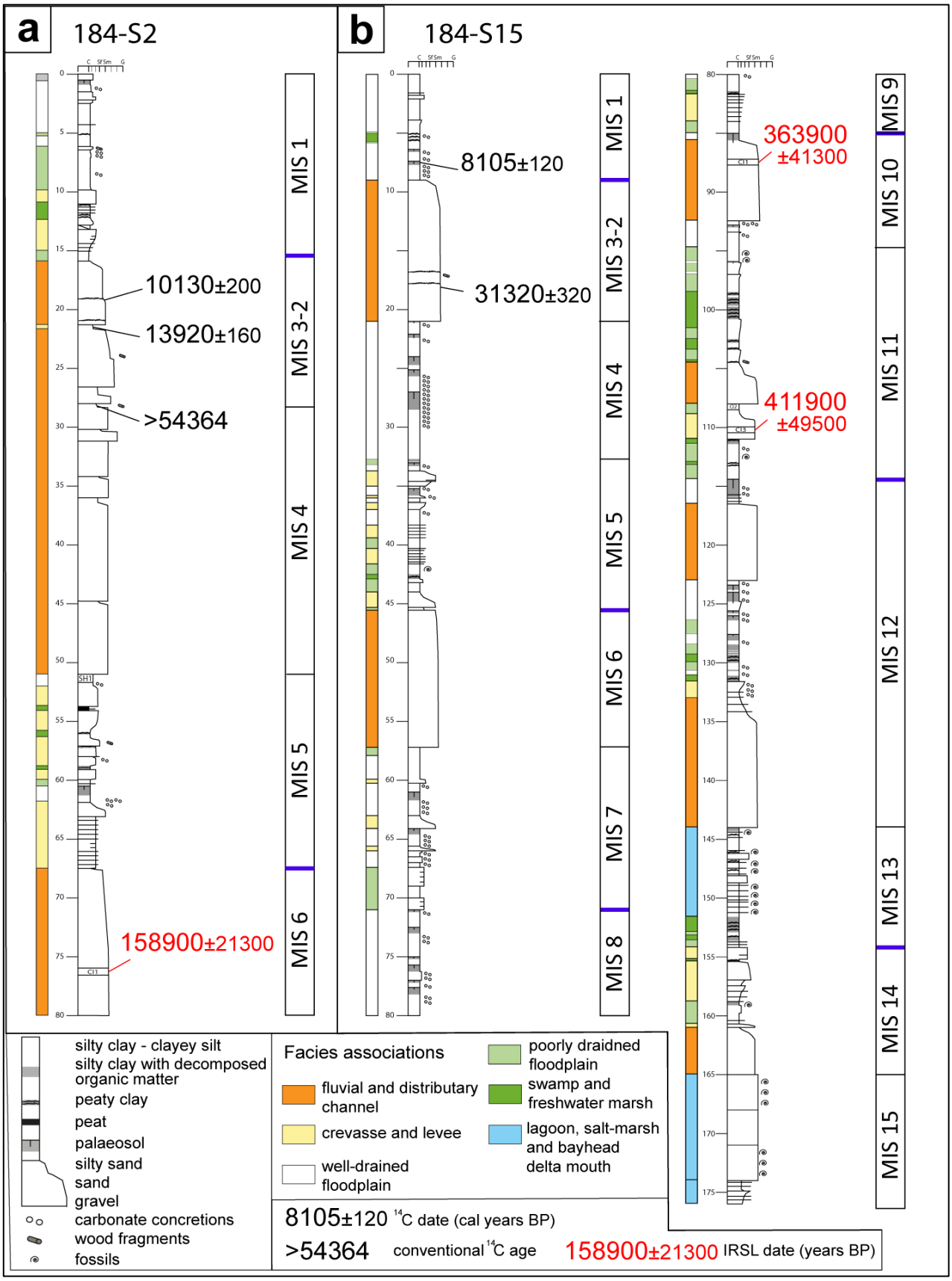

Figure 6. Facies interpretation and absolute ages of cores 184S2 and 184S15. Location in Figure 1.

3.4.1.3. Well-drained floodplain facies association

This facies association is dominated by varicolored silt and clay, with carbonate concretions and iron oxides, marked by the rhythmical alternation of dark brown and whitish horizons. Carbonate concretions are abundant in whitish horizons. Thickness may exceed 10 m.

The dominance of mud suggests deposition in a low-energy floodplain environment (Collinson, 1978). Couplets composed of dark and whitish horizons are interpreted as paleosols resulting from exposure periods of a few thousand years (Inceptisols, Buol et al., 2011; Bruno et al., 2022).

3.4.1.4. Poorly drained floodplain facies association

This facies association is composed of grey soft silt and clay, with faint horizontal lamination and rare carbonate concretions. Thickness is < 3 m.

Soft grey muds are interpreted as deposited in a low-energy floodplain environment with water table fluctuating close to the topographic surface (Tentori et al., 2022).

3.4.1.5. Swamp and freshwater marsh facies association

This facies association is composed of very soft and dark grey clays, rich in organic debris and marked by peat horizons. Freshwater fossils may be observed. Thickness ranges between a few dm and ca 5 m.

These deposits are interpreted as formed in submerged freshwater environments, such as swamps and marshes, where reducing conditions favoured the preservation of organic matter (Diessel, 1992; Richardson & Vepraskas, 2001; Stolt & Rabenhorst, 2011; Bruno et al., 2019). When these deposits are laterally continuous for tens of km, they have been interpreted as parts of wider bay-head- or upper-delta plain environments.

3.4.1.6. Lagoon, salt-marsh and bayhead delta mouth facies association

This facies association is composed of soft grey muds, with shells of brackish water fossils (e.g. *Abra segmentum* and *Cerastoderma glaucum*). Thin fine-sand intercalations are locally observed. Sand bodies with thickness ranging between 2 and 8 m, with brackish and freshwater fossils are seldom encountered.

Soft grey muds with faunal associations typical of brackish waters are interpreted as deposited in water bodies with partial communication with the open sea, such as lagoons, that can be part of lower delta plains or outer estuaries. Sand bodies in this facies associations are interpreted as lagoon channels or bay-head delta mouths.

3.4.1.7. Barrier Island, Strandplain and Delta Front facies association

This facies association has not been observed in the studied cores, but it has been reported in several core descriptions considered in this work (Amorosi et al., 1999; 2004; 2021). It consists mainly of well-sorted sands with fine to medium grain-size. The thickness is significantly variable, from a few meters to ~15 m. Reworked marine mollusks and plant debris can be observed.

These sandy deposits with salt-water fossils are interpreted as deposited in a high-energy coastal environment such as a barrier island, a strandplain or a delta front.

3.4.1.8. Prodelta, Offshore-Transition and Offshore facies association

For this facies association, not detected in the studied cores, we refer to core descriptions from Amorosi et al. (1999; 2004; 2021). It is composed of soft grey mud with thin intercalations of very-fine to silty sand. Fossils of marine specimens are often retrieved. Bioturbation, associated with highly diversified fossils assemblages, is locally observed.

This mud-dominated facies association includes the most distal facies recognized in this study. Muds with thin-bedded sand intercalations are interpreted as prodelta or offshore-transition deposits, with sand beds resulting from river floods or storm events, respectively. Bioturbated deposits with highly diversified faunal associations are typical of offshore conditions (Scarponi & Kowalewski, 2007). Prodelta facies, instead, include opportunistic species able to tolerate stressed marine conditions with freshwater and sediment input related to major river floods (Scarponi et al., 2014).

3.4.2. *Stratigraphy of cores 184S2 and 184S15*

3.4.2.1. Core 184S2

Core 184S2, 80-m long, is composed of two fluvial-channel sand bodies that alternate with finer-grained intervals (Fig. 6a). The lower sandy interval is 12.5 m thick (from 80 to 67.5 m depth), and is composed of coarse to medium sand, with FU grainsize tendency. This sand body, IRSL-dated to the

MIS 6, is overlain by a 16 m-thick horizon dominated by channel-related facies associations, with swamp peaty mud intercalations. A palaeosol was observed at 60.5 m depth. The interval between 51 and 16 m depth is composed of fluvial-channel sands. The uppermost ten metres encompass the Pleistocene-Holocene transition (10-13 ky BP), whereas a wood sample collected at 20.2 m yielded an age beyond the ^{14}C window (> 53364 y BP). The uppermost interval, attributed to the Holocene based on correlations with adjacent dated cores, is mainly composed of mud, with few sandy silt intercalations. Poorly drained floodplain and swamp facies associations are observed at depth > 5.7 m, whereas the overlying layers are composed of well-drained floodplain mud.

3.4.2.2. Core 184S15

Core 185S15, 176-m long, is composed of sand-mud alternations at the meter scale (Fig. 6b). Seven sand bodies were observed at distinct depths. The lowermost, from 174 to 161 m, containing rare brackish-water fossil, was interpreted as a bay-head-delta mouth deposit. The younger sand bodies, whose thickness varies between 3.5 and 12 m, are barren in fossils and were interpreted as fluvial or distributary channel deposits. The two shallowest fluvial-channel sand bodies, at depths of 57-45 and 21-9 m are the thickest and were assigned to MIS 6 and MIS 3-2, respectively.

Sand bodies are separated by mud-prone horizons, with thickness ranging between 5 and 28 m, which show an overall shallowing-upward trend. The oldest fine-grained horizon, from 161 to 144 m depth, is mainly composed of lagoon facies associations, with subordinate swamp, poorly drained floodplain and channel-related facies associations. The younger muddy horizons are composed of swamp, poorly drained floodplain and well-drained floodplain facies associations, with swamp and poorly drained floodplain intervals that thin upwards. Well-drained floodplain horizons exhibit an opposite trend and are characterized by the occurrence of pedogenized horizons. Paleosols are abundant between 34 and 21 m.

3.4.3. *Middle Pleistocene stratigraphy of the Po Basin*

The Middle Pleistocene stratigraphy of the Po Basin is depicted along two cross-sections: section AA' (Fig. 7), traced from land to sea for a total length of 117 km, and section B-B' (Fig. 7), N-S directed from the Apennine margin to the Po River, for 67 km (see Fig. 1 for location).

An overall shallowing-upward trend, from predominantly coastal deposits to exclusively alluvial facies, via paralic deposits of variable thickness, is observed in section AA'. Along individual cores

nearshore and paralic deposits thin upwards, whereas alluvial facies show an opposite trend (Fig. 6a).

In section AA', prominent wedge-shaped sediment bodies made up of coastal sands and shallow-marine muds occur at distinct stratigraphic levels, typically separated by alluvial sediments (Fig. 7). In the lower part of each wedge, coastal sands form relatively thin, poorly interconnected sediment bodies with a markedly retrogradational pattern. Upsection, sand bodies are more interconnected and stacked in an overall progradational trend. At the turnaround from retrogradation to progradation, sand bodies are thickest and typically amalgamated. Coastal sediments grade landwards into paralic (lagoon, marsh and swamp) and then alluvial sediments.

The uppermost coastal wedge in Fig. 7 was radiocarbon dated to the Holocene (MIS 1), whereas the coastal wedge encountered about 100 m below was ESR dated to the Last Interglacial (MIS 5e). Using the IRSL age of core 184S15 as a chronologic constraint for the MIS 9 coastal wedge, we tentatively assign the intervening wedges to MIS 7a-c and MIS 7e, respectively. This interpretation is consistent with pollen data from cores 222S2 (Fig. 4) and 223S17 (Amorosi et al., 1999). Based on the stratigraphic position of the 450 ky unconformity (Geomol Team, 2015; Martelli et al., 2017) and on IRSL ages from core 184S15, we tentatively assign the coastal wedges above and below this surface to MIS 11 and MIS 13, respectively. Chronologic attribution of the older coastal deposit is difficult, especially close to the culmination of the Mirandola anticline (Cores GLS5125 and MIR, Fig. 7), where the intense tectonic deformation hinders reliable stratigraphic correlations based uniquely on geometric criteria.

With the sole exception of the MIS 7a-c coastal wedge, progressively older coastal deposits are encountered at increasing distances from the modern coastline. Particularly, the MIS 1 wedge extends ca. 18 km landward of the modern coastline, whereas the innermost MIS 5 and MIS 7e coastal sands are recorded ca. 35 km from the present-day coastline (core 204S17). The innermost MIS 9 and MIS 11 coastal deposits were observed 60 km away from the modern coastline (core 203S9), whereas the most landward position of MIS 13 coastal sands is 90 km west of the present-day coastline, slightly seaward of correlative lagoon deposits in core 184S15. Paralic sediments show a trend similar to the one of coastal sands. Lagoon deposits are particularly abundant between MIS 11 and MIS 9 coastal sands (see cores 203S9 and 203S11).

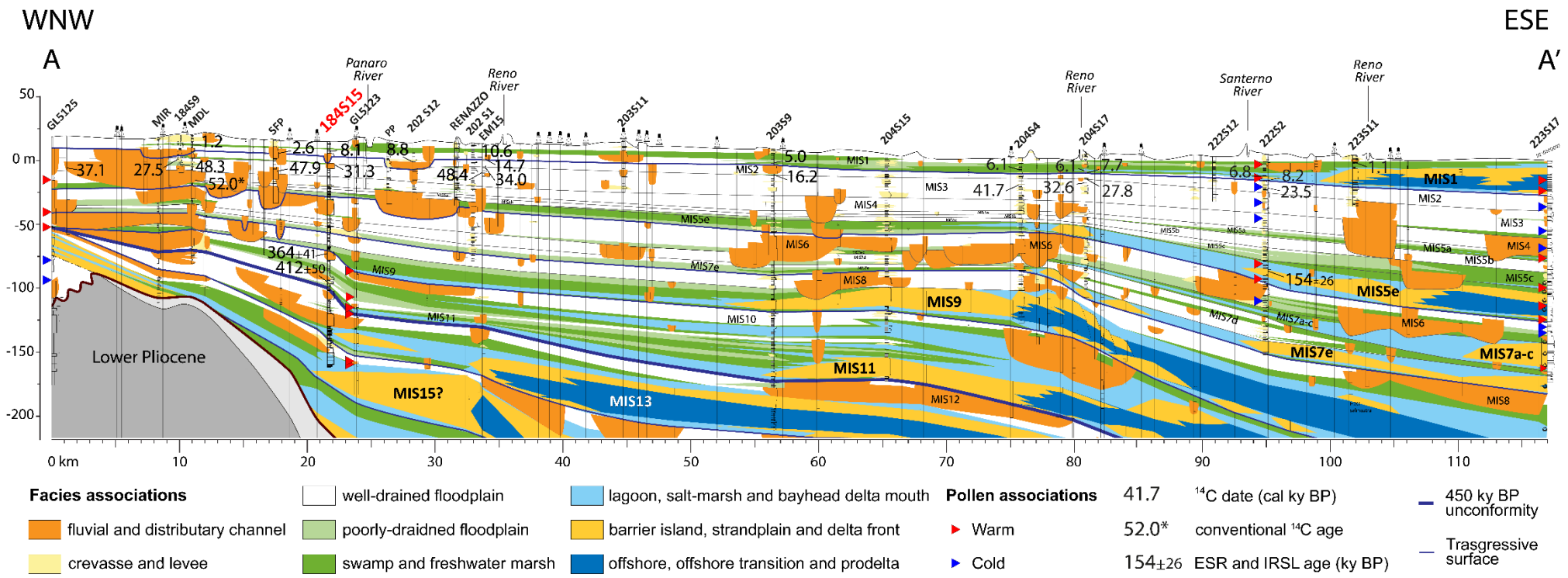

Figure 7. Mid-Late Pleistocene stratigraphy of the Po Basin depicted in a cross-section running along the Mirandola thrust system. Location in Figure 1. For details on new 14C and IRSL ages, see Tables 1 and 2.

Based on this cyclic organization of facies, the Mid-Late Pleistocene succession was subdivided into a set of transgressive-regressive (T-R) cycles. The bounding surfaces (transgressive surfaces or TS) were traced at the base of coastal wedges, where aggradationally stacked alluvial deposits are overlain by retrogradationally stacked paralic and coastal deposits. Landwards, the base of laterally extensive swamp or poorly drained-floodplain intervals represents the landward equivalent of the TS. Along single cores, the TSs invariably mark the base of sediment packages with deepening-upwards facies trends. Individual cycles are up to 55 m thick and thin out westward, toward the culmination of the Mirandola anticline.

In section BB' (Fig. 8), perpendicular to the main tectonic structures, the sedimentary succession is folded close the Apennine margin and above the Mirandola thrust-related anticline, with a degree of deformation that increases with depth. The thickness of Middle Pleistocene to Holocene deposits is about 100 m close to the Apennine margin and above the Mirandola anticline, whereas it may exceed 300 m in syncline areas. The stratigraphic succession, 85 km landward of the modern shoreline, consists almost exclusively of alluvial and paralic deposits, with highly subordinate coastal deposits in the older stratigraphic intervals (Fig. 8). The landward equivalents of the T-R cycles illustrated in section AA' (Fig. 5A) are composed, in their lower portions, by lagoon, marsh and swamp facies associations that are replaced upwards by alluvial facies associations. These latter are represented by thick fluvial channel-belts that are clustered close to the Apennine margin and in the axial portion of the plain, between the Mirandola thrust system and the modern Po River. Lateral to the fluvial channel-belt sand bodies, alluvial facies consist predominantly of floodplain muds. Lagoon and swamp intervals thin upwards, whereas the thickness and lateral extent of fluvial sand bodies increases upwards, with two 15-20 km-wide and 30-40 m-thick channel belts dated to MIS 6 (see IRSL age in core 184S2) and to the last glacial episode (MIS 4-MIS 2), respectively.

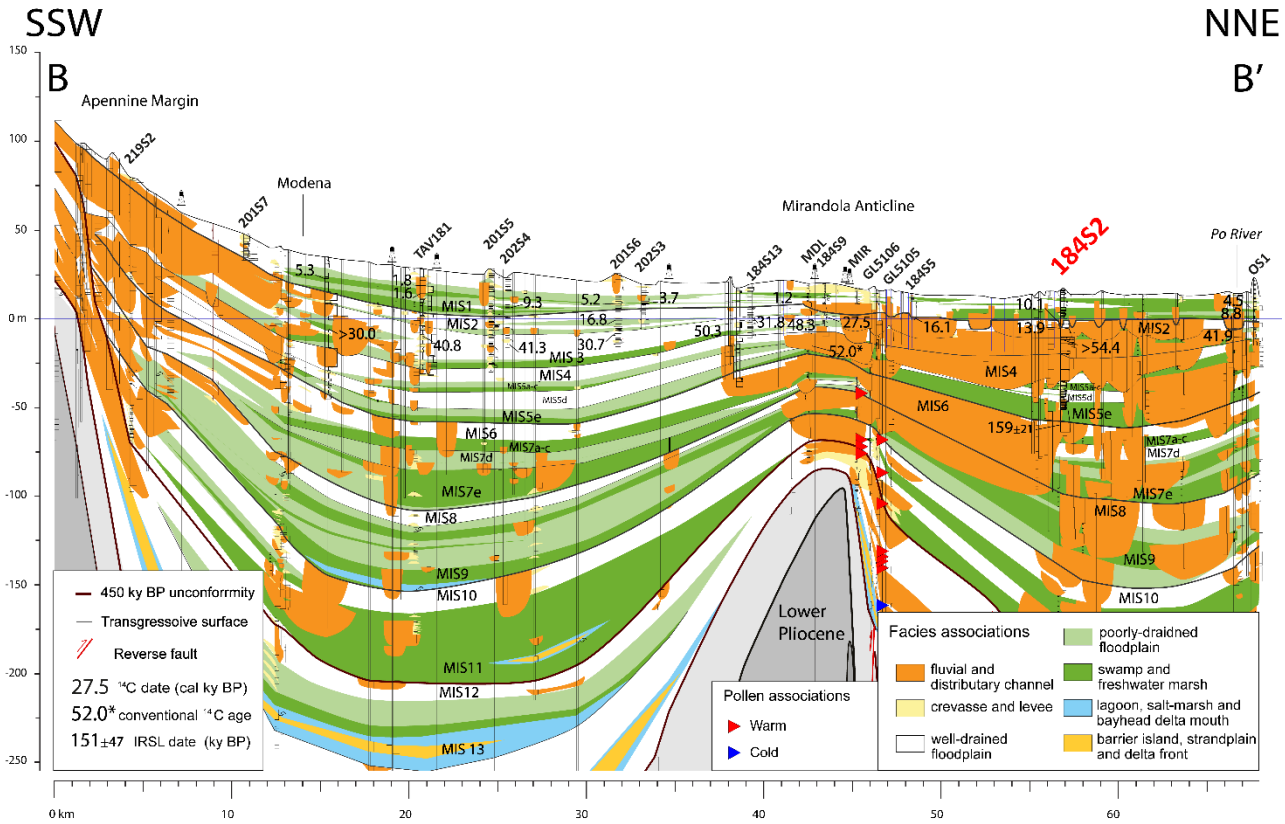

Figure 8. Mid-Late Pleistocene stratigraphy of the Po Basin depicted in a N-S oriented cross-section transversal to the Apennine Margin and to the Mirandola thrust system. Location in Figure 1. For details on new 14C and IRSL ages, see Tabs 1 and 2.

3.5. DISCUSSION

The Po Basin fill is characterized by an overall shallowing-upward trend, from Pliocene and Early Pleistocene turbidites to Mid-Late Pleistocene and Holocene shelf, coastal and alluvial deposits, which has been documented by a number of regional stratigraphic studies during the last decades (Ricci Lucchi et al., 1982; Ori, 1993; Massari et al., 2004; Ghielmi et al., 2013). This tendency reflects the progressive filling of the basin and the transition from the underfilled to the overfilled stage (*sensu* Catuneanu et al., 2017). Within this general trend, local studies carried in the central Po Plain (Amorosi et al., 2008) and beneath the modern coastal plain (Amorosi et al., 2004; Campo et al., 2020) documented the repeated alternation of fluvial/overbank and coastal/alluvial deposits in response to Milankovitch-scale 100 ky-cyclicity.

The stratigraphy of the late Quaternary succession of the Po Plain, reconstructed in this work on a basin scale along sections AA' (117 km long) and BB' (67 km long), highlights a similar trend of facies architecture, providing for the first time a detailed framework of Middle Pleistocene stratigraphy and of its relation with the underlying tectonic structures.

The overall shoaling-upward trend is punctuated at distal locations by a clearly detectable depositional cyclicity of coastal, paralic and alluvial systems (Fig. 7). More inland, depositional cycles include sharp swamp to alluvial or overbank to fluvial transitions (Fig. 8). Along-dip facies shifts for tens of km reflect the increased amplitude of glacio-eustatic oscillations after the Early/Middle Pleistocene Transition (Head and Gibbard, 2005; 2015), and were enhanced by the low gradients of the Po Plain and of the Adriatic shelf. The rhythmical occurrence of the T-R coastal wedges testifies to interglacial marine ingressions, followed by highstand deltaic and coastal progradation. The abundance of lagoon deposit at the top of MIS 11 deposits is likely related to the exceptional length of the MIS 11 highstand (Loutre & Berger, 2003; Siddall et al., 2007; Zazo et al., 2012).

The superposition of this glacio-eustatic signal to the structurally controlled basin fill resulted in the progradational stacking of T-R wedges, which migrated seawards through time (Figs. 7 and 9). The location of the MIS 7a-c coastal wedge, which does not comply to this trend, is possibly attributable to the relatively lower sea-level position during this interstadial, if compared to MIS 5e, MIS 7e and MIS 9 (Lea et al., 2002; Waelbroeck et al., 2002; Dutton et al., 2009; Rovere et al., 2011). On the other hand, MIS 13 coastal sands at the time of maximum marine ingression accumulated 30 km seaward of the MIS 11 shoreline, although maximum sea level during MIS 13 was lower than in MIS 11 (Rohling et al., 2014). The overall seaward shift of facies, thus, likely resulted from the high volumes of sediment supplied to the Po Basin from the two active orogens (Alps and Apennines), which overcame the rates of creation of accommodation space due to subsidence.

Subsidence rates calculated along section AA' vary from 0.2 mm/y, at the culmination of the Mirandola anticline, to ca. 1 mm/y close to the Adriatic coast (Fig. 10). This seaward increase in subsidence rates might be related to different growth rates of the Mirandola anticline, or to the relative abundance of highly compressible paralic and marine sediments at distal locations. Higher growth rates in the landward sector of the Mirandola anticline could have enhanced the progressive seaward migration of facies. However, the available data are insufficient to discriminate the relative role of sediment supply and differential subsidence. Sediment budget calculations based and specific structural studies of the Mirandola thrust system are required to this aim.

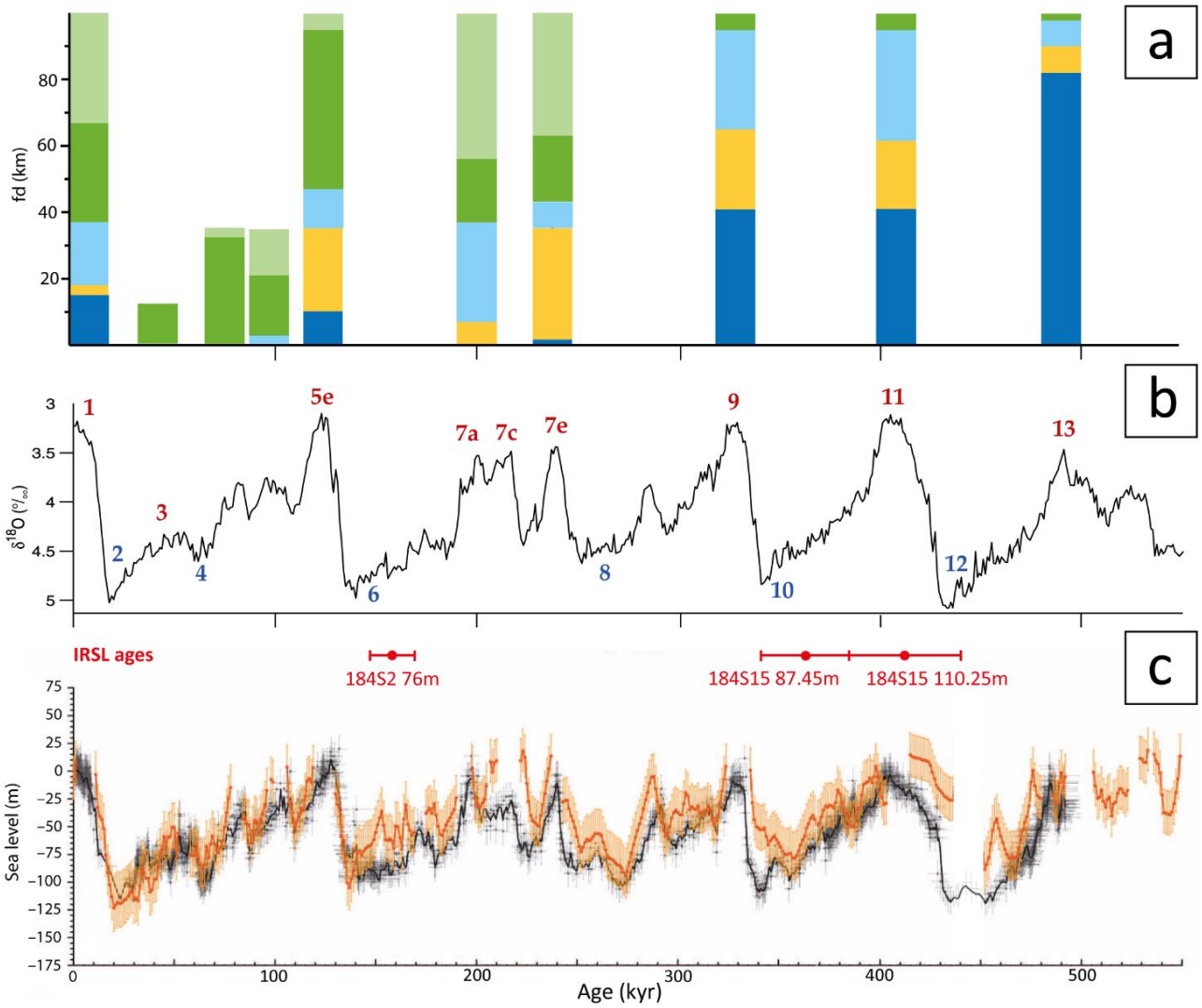

Figure 9. (a) maximum inland location of depositional facies associations during the Mid-Late Pleistocene and Holocene interglacials and interstadials, reported as distance from the modern coastline measured along section AA' (fd). Glacial and stadials are dominated by alluvial facies associations. See Figs. 7 and 8 for keys to facies associations. See text for details. (b) Global benthic stack in the last 550 ky (modified after Lisiecki and Raymo, 2005). (c) Sea-level oscillation in the Mediterranean (red) and in the Red Sea (from Rohling et al 2014).

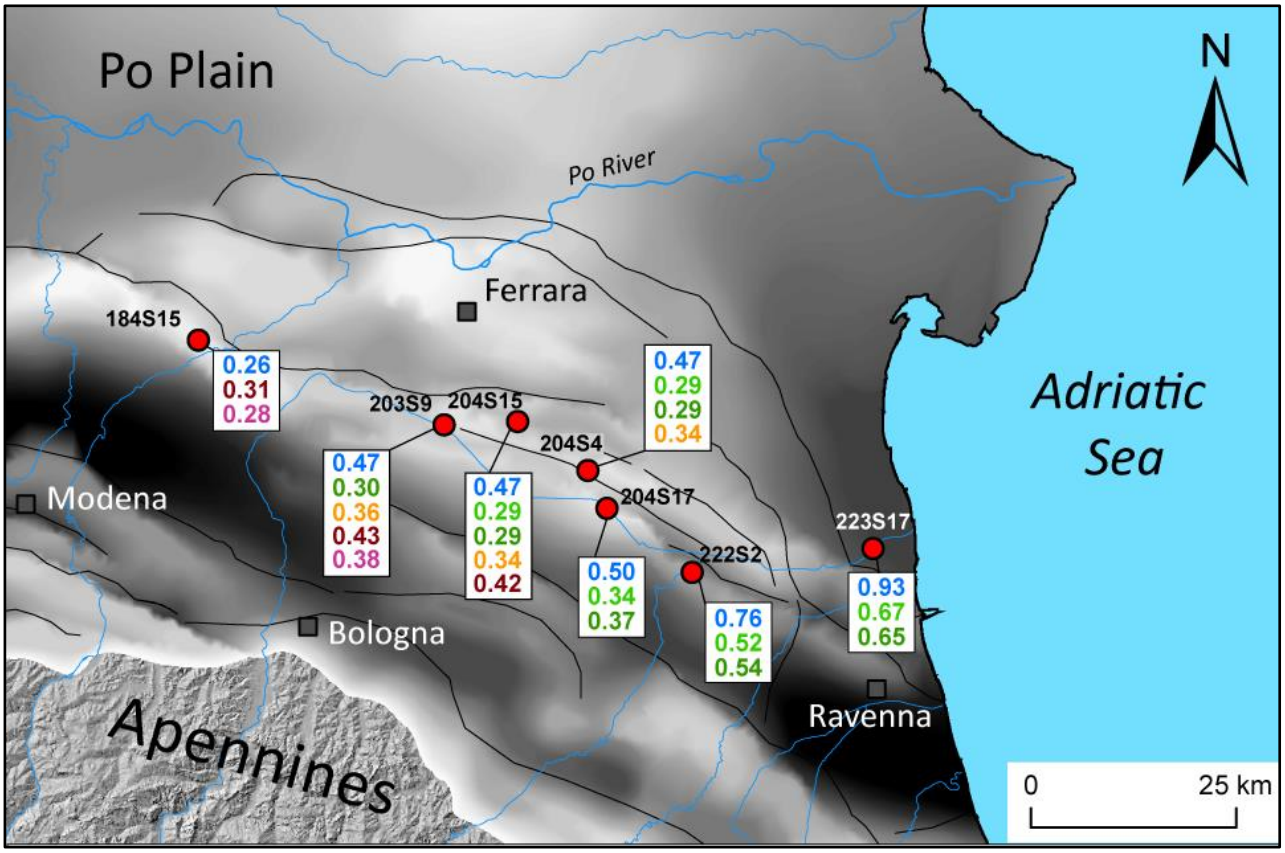

Figure 10. subsidence rates measured in cores along section AA' and averaged over the last 122 ky (blue), 196 ky (light green), 240 ky (green), 323 ky (orange), 404 ky (burgundy), and 494 ky (fuchsia).

3.6. CONCLUSIVE REMARKS

Through the correlation of 44 cores and 168 well data, we reconstructed the Mid-Late Pleistocene and Holocene stratigraphy of the Po Basin, with the aid of 42 ^{14}C dates, 3 ESR and 3 IRSL ages. The results of this research can be summarized as follows:

- The Mid-Late Pleistocene and Holocene sedimentary succession of the Po Basin is composed of alluvial, paralic, coastal and shallow marine facies associations stacked in an overall shallowing-upward trend.
- This general trend is punctuated by a cyclic organization of facies given by the rhythmical occurrence of transgressive-regressive (T-R) coastal wedges, separated by alluvial deposits. Landwards, where coastal facies are highly subordinate, the depositional cyclicity is marked by the alternation of paralic (mainly swamp and freshwater marshes) deposits with alluvial (fluvial channel and floodplain) facies associations.
- Superposition of the shoaling-upward trend with the higher-frequency depositional cyclicity resulted in an overall progradational stacking of (T-R) coastal wedges.

- The overall shallowing-upward trend reflects the progressive filling of the basin due to high sediment supply which overcame the rates of creation of accommodation induced by subsidence. Differential subsidence, with increasing values towards the sea, may have enhanced the seaward migration of coastal facies.
- The cyclic arrangement of facies reflects high-amplitude glacio-eustatic oscillations since the Early/Middle Pleistocene Transition. Along-dip facies shifts driven by sea-level changes were enhanced by the low gradients of the Po Plain and of the Adriatic shelf.

The results of this study provide clues on the sedimentary response of a low-gradient costal systems to sea-level oscillation in a period, the Mid-Late Pleistocene, characterized by dramatic climate changes. Therefore, the data presented here may help in predicting the response of depositional systems to near future climate and eustatic changes.

REFERENCES

Alexander, C. S., & Prior, J. C. (1971). Holocene sedimentation rates in overbank deposits in the Black Bottom of the lower Ohio River, southern Illinois. *American Journal of Science*, *270*(5), 361-372.

Allen J.R.L. (1963). The classification of cross-stratified units with notes on their origin. *Sedimentology*, **2**, 93-114.

Allen, G. P., & Posamentier, H. W. (1993). Sequence stratigraphy and facies model of an incised valley fill; the Gironde Estuary, France. *Journal of Sedimentary Research*, **63**(3), 378-391.

Amadori, C., Garcia-Castellanos, D., Toscani, G., Sternai, P., Fantoni, R., Ghielmi, M., & Di Giulio, A. (2018). Restored topography of the Po Plain-Northern Adriatic region during the Messinian base-level drop—Implications for the physiography and compartmentalization of the palaeo-Mediterranean basin. *Basin Research*, **30**(6), 1247-1263.

Amadori, C., Toscani, G., Di Giulio, A., Maesano, F.E., D'Ambrogi, C., Ghielmi, M. & Fantoni, R. (2019) From cylindrical to non-cylindrical foreland basin: Pliocene-Pleistocene evolution of the Po Plain-Northern Adriatic basin (Italy). *Basin Research*, **31**(5), 991–1015.

Amadori, C., Ghielmi, M., Mancin, N., & Toscani, G. (2020). The evolution of a coastal wedge in response to Plio-Pleistocene climate change: The Northern Adriatic case. *Marine and Petroleum Geology*, **122**, 104675.

Amorosi, A., Colalongo, M. L., Fusco, F., Pasini, G., & Fiorini, F. (1999). Glacio-eustatic control of continental–shallow marine cyclicity from late Quaternary deposits of the southeastern Po Plain, northern Italy. *Quaternary research*, **52**(1), 1-13.

Amorosi, A., Forlani, L., Fusco, F., & Severi, P. (2001). Cyclic patterns of facies and pollen associations from Late Quaternary deposits in the subsurface of Bologna. *GeoActa*, **1**, 83-94.

Amorosi, A., Colalongo, M. L., Fiorini, F., Fusco, F., Pasini, G., Vaiani, S. C., & Sarti, G. (2004). Palaeogeographic and palaeoclimatic evolution of the Po Plain from 150-ky core records. *Global and planetary Change*, **40**(1-2), 55-78.

Amorosi, A., Pavesi, M., Ricci Lucchi, M., Sarti, G. & Piccin, A. (2008). Climatic signature of cyclic fluvial architecture from the Quaternary of the central Po Plain, Italy. *Sedimentary Geology*, **209**, 58–68.

Amorosi, A., Bruno, L., Campo, B., Morelli, A., Rossi, V., Scarponi, D., Hong, W., Bohacs, K.M. & Drexler, T.M. (2017). Global sea-level control on local parasequence architecture from the Holocene record of the Po Plain, Italy. *Marine and Petroleum Geology*, **87**, 99–111.

Amorosi, A. & Sammartino, I. (2018). Shifts in sediment provenance across a hierarchy of bounding surfaces: A sequence-stratigraphic perspective from bulk-sediment geochemistry. Sedimentary Geology, **375**, 145–156.

Amorosi, A., Bruno, L., Campo, B., Costagli, B., Dinelli, E., Hong, W., Sammartino, I. & Vaiani, S.C. (2020). Tracing clinothem geometry and sediment pathways in the prograding Holocene Po Delta system through integrated core stratigraphy. *Basin Research*, **32**, 206–215.

Amorosi, A., Bruno, L., Campo, B., Costagli, B., Hong, W., Picotti, V., & Vaiani, S.C., (2021). Deformation patterns of upper Quaternary strata and their relation to active tectonics, Po Basin, Italy. *Sedimentology*, **68**, 402–424. https://doi.org/10.1111/ sed.12784.

Bassetti, M. (2001). Discussione dei risultati delle analisi palinologiche del sondaggio Cadelbosco-Reggio Emilia. in: M. Pizziolo, S. Segadelli, S.C. Vaiani: Note illustrative della Carta Geologica d'Italia alla scala 1:50.000, foglio 200 Reggio nell'Emilia, available online at https://www.isprambiente.gov.it/media/carg/note_illustrative/200_reggio_nellemilia.pdf. In Italian.

Blum, M.D. & Aslan, A. (2006). Signatures of climate vs. sea-level change within incised valley successions: quaternary examples from the Texas Coastal Plain and Shelf. *Sedimentary Geology*, **190**, 177–211.

Blum, M., Martin, J., Milliken, K., & Garvin, M. (2013). Paleovalley systems: insights from Quaternary analogs and experiments. *Earth-Science Reviews*, **116**, 128-169.

Boccaletti, M., Corti, G., & Martelli, L. (2011). Recent and active tectonics of the external zone of the Northern Apennines (Italy). *International Journal of Earth Sciences*, **100**(6), 1331-1348.

Bonini, L., Toscani, G. & Seno, S. (2014). Threedimensional segmentation and different rupture behaviour during the 2012 Emilia seismic sequence (Northern Italy). *Tectonophysics*, **630**, 33–42.

Bowen, D. Q. (2010). Sea level~ 400 000 years ago (MIS 11): analogue for present and future sea-level?. *Climate of the Past*, **6**(1), 19-29.

Bridge, J. S. (1993). The interaction between channel geometry, water flow, sediment transport and deposition in braided rivers. *Geological Society, London, Special Publications*, **75**(1), 13-71.

Bronk Ramsey, C. and Lee, S. (2013). Recent and planned developments of the program OxCal. *Radiocarbon*, **55**, 720–730.

Bruno, L., Amorosi, A., Severi, P., & Bartolomei, P. (2015). High-frequency depositional cycles within the late Quaternary alluvial succession of Reno River (northern Italy). *Italian Journal of Geosciences*, **134**(2), 339-354. https://doi.org/10.3301/IJG.2014.49.

Bruno, L., Bohacs, K.M., Campo, B., Drexler, T.M., Rossi, V., Sammartino, I., Scarponi, D., Hong, W. & Amorosi, A. (2017). Early Holocene transgressive paleogeography in the Po coastal plain (northern Italy). *Sedimentology*, **64**(7), 1792–1816.

Bruno, L., Campo, B., Di Martino, A., Hong, W., Amorosi, A., (2019). Peat layer accumulation and post-burial deformation during the mid-late Holocene in the Po coastal plain (Northern Italy). *Basin Research*, **31**, 621–639. https://doi.org/10.1111/ bre.12339.

Bruno, L., Campo, B., Costagli, B., Stouthamer, E., Teatini, P., Zoccarato, C., & Amorosi, A. (2020). Factors controlling natural subsidence in the Po Plain. *Proceedings of the International Association of Hydrological Sciences*, **382**, 285-290.

Bruno, L., Amorosi, A., Sammartino, I., Lugli, S., Fontana, D., (2021). Trunk river and tributary interactions recorded in the Pleistocene–Holocene stratigraphy of the Po Plain (northern Italy). *Sedimentology*, **68**, 2918-2943. https://doi.org/10.1111/sed.12880.

Bruno, L., Campo, B., Hajdas, I., Hong, W., & Amorosi, A. (2022). Timing and mechanisms of sediment accumulation and pedogenesis: Insights from the Po Plain (northern Italy). *Palaeogeography, Palaeoclimatology, Palaeoecology*, **591**, 110881.

Buol, S. W., Southard, R. J., Graham, R. C., & McDaniel, P. A. (2011). *Soil genesis and classification*. John Wiley & Sons. Chichester, 543 p. https://doi.org/10.1002/9780470960622.

Busschers, F. S., Weerts, H. J. T., Wallinga, J., Cleveringa, P., Kasse, C., De Wolf, H., & Cohen, K. M. (2005). Sedimentary architecture and optical dating of Middle and Late Pleistocene Rhine-Meuse deposits-fluvial response to climate change, sea-level fluctuation and glaciation. *Netherlands Journal of Geosciences*, **84**(1), 25-41.

Campo, B., Bruno, L., & Amorosi, A. (2020). Basin-scale stratigraphic correlation of late Pleistocene-Holocene (MIS 5e-MIS 1) strata across the rapidly subsiding Po Basin (northern Italy). *Quaternary Science Reviews*, **237**, 106300.

Carminati, E. & Doglioni, C. (2012). Alps vs. Apennines: the paradigm of a tectonically asymmetric Earth. *Earth-Science Reviews*, **112**, 67–96.

Catuneanu, O. (2017). Sequence stratigraphy: Guidelines for a standard methodology. In Stratigraphy & timescales (Vol. 2, pp. 1-57). Elsevier Inc. ISSN 2468-5178. http://dx.doi.org/10.1016/bs.sats.2017.07.003.

Changsong L., Herong Z., Jianye R., Jingyan, L. & Yigang, Q. (2004). The control of syndepositional faulting on the Eogene sedimentary basin fills of the Dongying and Zhanhua sags, Bohai Bay Basin. *Science in China Ser. D Earth Sciences*, **47** (9), 769—782.

Chaumillon, E., Bertin, X., Falchetto, H., Allard, J., Weber, N., Walker, P., ... & Woppelmann, G. (2008). Multi time-scale evolution of a wide estuary linear sandbank, the Longe de Boyard, on the French Atlantic coast. *Marine Geology*, **251**(3-4), 209-223.

Collinson, J.D. (1978). Alluvial sediments. In: Sedimentary Environments and Facies (Ed. Reading, H.G.), 2nd edn, pp. 20–67. Blackwell, Oxford.

Demurtas, L., Bruno, L., Lugli S., & Fontana, D. (2022). Evolution of the Po Alpine River System during the Last 45 Ky Inferred from Stratigraphic and Compositional Evidence (Ostiglia, Northern Italy). *Geosciences*, **12**, 342.

Diessel, C.F.K. (Ed.). (1992) Coal facies and depositional environment. In: Coal-Bearing Depositional Systems pp. 161–264. Springer, Berlin.

DISS Working Group. (2018). Database of individual seismogenic sources (DISS), version 3.2.0: A compilation of potential sources for earthquakes larger than M 5.5 in Italy and surrounding areas. Istituto Nazionale di Geofisica e Vulcanologia. https://doi.org/10.6092/INGV.IT-DISS3.2.0

Dutton, A., Bard, E., Antonioli, F., Esat, T. M., Lambeck, K., & McCulloch, M. T. (2009). Phasing and amplitude of sea-level and climate change during the penultimate interglacial. *Nature Geoscience*, **2**(5), 355-359.

ENEL-DCO (1984). Localizzazione di un impianto nucleare nella Regione Lombardia, completamento degli studi geologici e geomorfologici locali. Area di Viadana; Area di S. Benedetto Po; Dorsale Ferrarese: Rome, Ente Nazionale per L'Energia Elettrica– Direzione delle Costruzioni, 3 volumes.

Fantoni, R., & Franciosi, R. (2010). Tectono-sedimentary setting of the Po Plain and Adriatic foreland. *Rendiconti Lincei*, **21**, 197-209.

Ferranti, L., Antonioli, F., Mauz, B., Amorosi, A., Dai Pra, G., Mastronuzzi, G., ... & Verrubbi, V. (2006). Markers of the last interglacial sea-level high stand along the coast of Italy: tectonic implications. *Quaternary international*, **145**, 30-54.

Garzanti, E., Vezzoli, G. and Andò, S. (2011). Paleogeographic and paleodrainage changes during Pleistocene glaciations (Po Plain, Northern Italy). *Earth-Science Reviews*, **105**, 25–48.

GeoMol Team (2015) GeoMol, Assessing subsurface potentials of the Alpine Foreland Basins for sustainable planning and use of natural resources. Alpine Space Programme, Project Report, p. 188.

Ghielmi, M., Minervini, M., Nini, C., Rogledi, S., & Rossi, M. (2013). Late Miocene–Middle Pleistocene sequences in the Po Plain–Northern Adriatic Sea (Italy): the stratigraphic record of modification phases affecting a complex foreland basin. *Marine and Petroleum Geology*, **42**, 50-81.

Grant, K. M., Rohling, E. J., Ramsey, C. B., Cheng, H., Edwards, R. L., Florindo, F., ... & Williams, F. (2014). Sea-level variability over five glacial cycles. *Nature communications*, **5**(1), 5076. DOI: 10.1038/ncomms6076

Gunderson, K.L., Pazzaglia, F.J., Picotti, V., Anastasio, D.A., Kodama, K.P., Rittenou, R.T., Frankel, K.F., Ponza, A., Berti, C., Negri, A. & Sabbatini, A. (2014). Unraveling tectonic and climatic controls on synorogenic growth strata (Northern Appennines, Italy). *GSA Bulletin*, **126**-**3** (4), 532–552.

Head, M. J., & Gibbard, P. L. (2005). Early-Middle Pleistocene transitions: an overview and recommendation for the defining boundary. *Geological Society, London, Special Publications*, **247**(1), 1-18.

Head, M. J., & Gibbard, P. L. (2015). Early–Middle Pleistocene transitions: linking terrestrial and marine realms. *Quaternary International*, **389**, 7-46.

Krapez, B. (1996). Sequence stratigraphic concepts applied to the identification of basin-filling rhythms in Precambrian successions. *Australian Journal of Earth Sciences*; **43** (4); 355-380.

Kopp, R. E., Simons, F. J., Mitrovica, J. X., Maloof, A. C., & Oppenheimer, M. (2009). Probabilistic assessment of sea level during the last interglacial stage. *Nature*, **462**(7275), 863-867.

Lea, D. W., Martin, P. A., Pak, D. K., & Spero, H. J. (2002). Reconstructing a 350 ky history of sea level using planktonic Mg/Ca and oxygen isotope records from a Cocos Ridge core. *Quaternary Science Reviews*, **21**(1-3), 283-293.

Lisiecki, L. E., & Raymo, M. E. (2005). A Pliocene-Pleistocene stack of 57 globally distributed benthic δ18O records. *Paleoceanography*, **20**(1). https://doi.org/10.1029/2004PA001071PA1003

Liu, J., Cao, D., Tan, J., & Zhang, Y. (2023). Gzhelian cyclothem development in the western North China cratonic basin and its glacioeustatic, tectonic, climatic and autogenic implications. *Marine and Petroleum Geology*, **106355**. https://doi.org/10.1016/j.marpetgeo.2023.106355

Loutre, M. F., & Berger, A. (2003). Marine Isotope Stage 11 as an analogue for the present interglacial. *Global and planetary change*, **36**(3), 209-217.

Marcolla, A., Miola, A., Mozzi, P., Monegato, G., Asioli, A., Pini, R., & Stefani, C. (2021). Middle Pleistocene to Holocene palaeoenvironmental evolution of the south-eastern Alpine foreland basin from multi-proxy analysis. *Quaternary Science Reviews,* **259**, 106908. https://doi.org/10.1016/j.quascirev.2021.106908

Martelli, L., Bonini, M., Calabrese, L., Corti, G., Ercolessi, G., Molinari, F.C., Piccardi, L., Pondrelli, S., Sani, F. & Severi, P. (2017). Seismotectonic map of Emilia Romagna Region and surrounding areas to scale 1:250.000. D.R.E.Am. MAP, Pistoia, Italy.

Massari, F., Rio, D., Barbero, R. S., Asioli, A., Capraro, L., Fornaciari, E., & Vergerio, P. P. (2004). The environment of Venice area in the past two million years. Palaeogeography, *Palaeoclimatology, Palaeoecology*, **202**(3-4), 273-308.

Miall, A. D. (1985). Architectural-element analysis: a new method of facies analysis applied to fluvial deposits. *Earth-Science Reviews*, **22**(4), 261-308.

Miall, A.D. (1996) The Geology of Fluvial Deposits: Sedimentary Facies, Basin Analysis, and Petroleum Geology. Springer-Verlag, Berlin, 582 pp.

Muttoni, G., Carcano, C., Garzanti, E., Ghielmi, M., Piccin, A., Pini, R., Rogledi, S. & Sciunnach, D. (2003). Onset of major Pleistocene glaciations in the Alps. *Geology*, **31**, 989–992. https://doi.org/10.1130/G19445.1

Muttoni, G., Scardia, G., Kent, D.V., Morsiani, E., Tremolada, F., Cremaschi, M. & Peretto, C. (2011). First dated human occupation of Italy at ~0.85 Ma during the late Early Pleistocene climate transition. *Earth and Planetary Science Letters*, **307**, 241–252. https:// doi.org/10.1016/j.epsl.2011.05.025

Neal, J. & Abreu, V. (2009). Sequence stratigraphy hierarchy and the accommodation succession method. *Geology*, **37**, 779–782.

Ori, G.G. (1993). Continental depositional systems of the Quaternary of the Po Plain (northern Italy). *Sedimentary Geology*, **83**, 1-14.

Peeters, J., Busschers, F. S., Stouthamer, E., Bosch, J. H. A., Van den Berg, M. W., Wallinga, J., ... & Middelkoop, H. (2016). Sedimentary architecture and chronostratigraphy of a late Quaternary incised-valley fill: a case study of the late Middle and Late Pleistocene Rhine system in the Netherlands. *Quaternary Science Reviews*, **131**, 211-236.

Raymo, M. E., & Mitrovica, J. X. (2012). Collapse of polar ice sheets during the stage 11 interglacial. *Nature*, **483**(7390), 453-456.

Reimer, P. J., Austin, W. E., Bard, E., Bayliss, A., Blackwell, P. G., Ramsey, C. B., ... & Talamo, S. (2020). The IntCal20 Northern Hemisphere radiocarbon age calibration curve (0–55 cal kBP). *Radiocarbon*, **62**(4), 725-757.

Ricci Lucchi, F., Colalongo, M.L., Cremonini, G., Gasperi, G., Iaccarino, S., Papani, G., Raffi, S., Rio, D. (1982). Evoluzione sedimentaria e paleogeografica nel margine appenninico. In: Cremonini, G., Ricci Lucchi, F (Eds.), Guida alla Geologia del Margine Appenninico-Padano. *Guida Geol. Reg., Soc. Geol. It.*, 17-46.

Richardson, J.L. & Vepraskas, M.J. (2001). Wetland Soilsgenesis, Hydrology, Landscapes, and Classification. CRC Press, LLC, Boca Raton, FL, 417 pp.

Rohling, E. J., Grant, K., Bolshaw, M., Roberts, A. P., Siddall, M., Hemleben, C., & Kucera, M. (2009). Antarctic temperature and global sea level closely coupled over the past five glacial cycles. *Nature Geoscience*, **2**(7), 500-504.

Rohling, E. J., Grant, K. M., Roberts, A. P., & Larrasoana, J. C. (2013). Paleoclimate variability in the Mediterranean and Red Sea regions during the last 500,000 years: implications for hominin migrations. *Current Anthropology*, **54**(S8), S183-S201.

Rohling, E. J., Foster, G. L., Grant, K. M., Marino, G., Roberts, A. P., Tamisiea, M. E., & Williams, F. (2014). Sea-level and deep-sea-temperature variability over the past 5.3 million years. *Nature*, **508**(7497), 477-482.

Rossi, V., Amorosi, A., Barbieri, G., Vaiani, S. C., Germano, M., & Campo, B. (2021). A Long-Term Record of Quaternary Facies Patterns and Palaeonvironmental Trends from the Po Plain (NE Italy) as Revealed by Bio-Sedimentary Data. *Geosciences*, **11**(10), 401.

Rovere, A., Vacchi, M., Firpo, M., & Carobene, L. (2011). Underwater geomorphology of the rocky coastal tracts between Finale Ligure and Vado Ligure (western Liguria, NW Mediterranean Sea). *Quaternary International*, **232**(1-2), 187-200.

Rovere, A., Raymo, M. E., Vacchi, M., Lorscheid, T., Stocchi, P., Gomez-Pujol, L., ... & Hearty, P. J. (2016). The analysis of Last Interglacial (MIS 5e) relative sea-level indicators: Reconstructing sea-level in a warmer world. *Earth-Science Reviews*, **159**, 404-427.

Scarponi, D., & Kowalewski, M. (2007). Sequence stratigraphic anatomy of diversity patterns: Late Quaternary benthic mollusks of the Po Plain, Italy. *Palaios*, **22**(3), 296-305.

Scarponi, D., Huntley, J. W., Capraro, L., & Raffi, S. (2014). Stratigraphic paleoecology of the Valle di Manche section (Crotone Basin, Italy): a candidate GSSP of the Middle Pleistocene. *Palaeogeography*, *Palaeoclimatology, Palaeoecology*, **402**, 30-43.

Siddall, M., Chappell, J., & Potter, E. K. (2007). 7. Eustatic sea level during past interglacials. *In Developments in Quaternary Sciences* (Vol. **7**, pp. 75-92). *Elsevier*.

Stolt, M. H., & Rabenhorst, M. C. (2011). Introduction and historical development of subaqueous soil concepts. Handbook of Soil Sciences Properties and Processes; Huang, PM, Li, Y., Sumner, ML,

Eds. CRC Press, LLC, Boca Raton, FL. https://www.routledgehandbooks.com/doi/10.1201/b11267-71

Storms, J. E., Weltje, G. J., Terra, G. J., Cattaneo, A., & Trincardi, F. (2008). Coastal dynamics under conditions of rapid sea-level rise: Late Pleistocene to Early Holocene evolution of barrier–lagoon systems on the northern Adriatic shelf (Italy). *Quaternary Science Reviews*, **27**(11-12), 1107-1123. https://doi.org/10.1016/j.quascirev.2008.02.009.

Tentori, D., Mancini, M., Milli, S., Stigliano, F., Tancredi, S., & Moscatelli, M. (2022). Compositional, micromorphological and geotechnical characterization of Holocene Tiber floodplain deposits (Rome, Italy) and sequence stratigraphic implications. *Sedimentology*, **69**(4), 1705-1737. https://doi.org/10.1111/sed.12969.

Toscani, G., Burrato, P., Di Bucci, D., Seno, S., & Valensise, G. (2009). Plio-Quaternary tectonic evolution of the Northern Apennines thrust fronts (Bologna-Ferrara section, Italy): seismotectonic implications. *Italian Journal of Geosciences*, **128**(2), 605-613.

Turrini, C., Lacombe, O. & Roure, F. (2014). Present-day 3D structural model of the Po Valley basin, Northern Italy. *Marine and Petroleum Geology*, **56**, 266–289.

Vis, G. J., & Kasse, C. (2009). Late Quaternary valley-fill succession of the Lower Tagus Valley, Portugal. *Sedimentary Geology*, **221**(1-4), 19-39.

Waelbroeck, C., Labeyrie, L., Michel, E., Duplessy, J. C., Mcmanus, J. F., Lambeck, K., ... & Labracherie, M. (2002). Sea-level and deep water temperature changes derived from benthic foraminifera isotopic records. *Quaternary science reviews*, **21**(1-3), 295-305.

Wallinga, J., Murray, A., & Duller, G. (2000). Underestimation of equivalent dose in single-aliquot optical dating of feldspars caused by preheating. *Radiation measurements*, **32**(5-6), 691-695.

Yang, Y. (2011). Tectonically-driven underfilled–overfilled cycles, the middle Cretaceous in the northern Cordilleran foreland basin. *Sedimentary Geology*, **233**, 15–27.

Zazo, C., Goy, J. L., Dabrio, C. J., Lario, J., González-Delgado, J. A., Bardají, T., ... & Soler, V. (2013). Retracing the Quaternary history of sea-level changes in the Spanish Mediterranean–Atlantic coasts: Geomorphological and sedimentological approach. *Geomorphology*, **196**, 36-49.

CHAPTER 4. Multi-source detrital contributions in the Po alluvial basin (northern Italy) since the Middle Pleistocene. Insights into sediment accumulation in intermediate sinks

Luca Demurtas*[1], Daniela Fontana[1], Stefano Lugli[1] and Luigi Bruno[1]

[1] *Department of Chemical and Geological Sciences, University of Modena and Reggio Emilia, Via Campi 103, Modena, Italy*

Correspondence: luca.demurtas@unimore.it

Acknowledgments

The researched has been founded by FAR-Unimore 2022. We gratefully acknowledge L. Martelli and N. Ieva for access to core MDL and SBP. We are also indebted to the Reviewers D. Tentori and C. Stefani for the accurate revision that greatly improved the manuscript.

Abstract

Integrated stratigraphic-compositional studies on alluvial successions provide a valuable tool to investigate the provenance of detritus in multi-source systems. The Po Plain is an intermediate sink of the Po-Adriatic source-to-sink system, fed by rivers draining two orogens. The Alps are characterized by extensive outcrops of plutonic-metamorphic and ultramafic rocks to the north-west and of Mesozoic carbonates to the east (Southern Alps). The Northern Apennines, to the south, are dominated by sedimentary successions. The Po River flows from the Western Alps to the Adriatic Sea interacting with a dense network of transverse tributaries which drain the two orogens. Stratigraphic, sedimentological and compositional analyses of two 101 and 77.5 m-long cores, recovered from the Central Po Plain, reveal the stacking of three petrofacies, which reflects distinct provenance and configurations of the fluvial network. A South-Alpine sedimentary input between MIS 12 and MIS 10 is testified by petrofacies 1, characterized by carbonate- and volcanic-rich detritus from rocks exposed in the Southern Alps. A northward shift of the Po River of more than 30 km is marked by a quartz-feldspar and metamorphic-rich detritus (petrofacies 2), similar to modern Po River sands. This dramatic reorganization of the fluvial network likely occurred around MIS 9 - MIS 8 and is possibly structurally controlled. A further northward shift of the Po River and the onset of Apennine sedimentation in the Late Holocene is revealed by petrofacies 3, rich in sedimentary lithics from the Apennine successions. The results of this study document how compositional

analysis, if framed in a robust stratigraphic picture, may provide clues on the evolution of multi-source alluvial systems.

KEYWORDS: Middle Pleistocene, Po Plain, Sediment Provenance, intermediate sink

DOI: https://doi.org/10.1111/bre.12858

4.1. INTRODUCTION

Compositional studies represent a valuable tool to investigate the provenance of sediments accumulated in sedimentary basins. In alluvial successions, the primary compositional signal of sediments eroded from different source areas is generally preserved, whereas in transitional and marine depositional environments this could be contaminated by littoral transport, wave swash and tides (Caracciolo, 2020). Despite that, only few sand provenance studies focused on the sediment accumulation and residence time in intermediate alluvial sinks (Sinha et al., 2009; Garzanti et al., 2011). On the contrary, several researches investigated the provenance of detritus accumulated in deep marine (Critelli et al., 2003; Schroeder et al., 2015; Liu et al., 2016; Tentori et al., 2018; Van Grinsven et al., 2019; Li et al., 2021; Amorosi et al., 2022; Limonta et al., 2023) and coastal sinks (Goodbred & Kuehl, 2000; Xue et al., 2010; Palamenghi et al., 2011; Ji et al., 2022).

The Po-Adriatic source-to-sink system is composed of: (i) a source zone consisting of three mountain belts, the Alps to the north, the Apennines to the west, and the Dinarides to the east, ii) a transport and partial deposition zone represented by the Po Plain and the Adriatic shelf, and iii) a two main marine sink represented by the Mid-and Southern Adriatic Depressions (respectively MAD and SAD in Fig. 1a). The Po Plain represents the first important sink of the Po-Adriatic System. This alluvial plain is an ideal site to study the mechanisms of sediment accumulation in intermediate sinks, because it hosts a thick sedimentary succession with high preservation potential, due to high subsidence rates (Bruno et al., 2020). The definition of the relative contribution of different source area is favoured by the contrasting characteristics of the orogens that feed the plain. The Alps, with peaks exceeding 4000 m, are characterized by widespread outcrops of plutonic, metamorphic and ultramafic rocks, and of Mesozoic carbonates. This mountain chain was largely glaciated during the Pleistocene cold phases. The Northern Apennines, with highest peaks < 2220 m, is a thin-skinned orogen characterized by the outcrop of sedimentary rocks. Apennines river catchments were covered by glaciers only locally (Baroni et al., 2018). These differences influence the composition of sediments delivered to the Po Plain, as recorded in many coring sites (Stefani, 2002; Lugli et al.,

2004, Piovan et al., 2010, Garzanti et al., 2011; Norini et al., 2021; Marcolla et al., 2021; Demurtas et al., 2022). Vertical changes in sediment composition recorded in these sites reflect reorganizations of the fluvial network (Fontana et al., 2019; Amorosi & Sammartino, 2018; Tentori et al., 2021), responding to different controlling factors (Bruno et al., 2021). The availability of several works depicting the depositional architecture of the Po Basin (e.g. Amorosi et al., 2008; Bruno et al., 2021) permits a direct link between surface geology of the source areas and subsurface stratigraphy of the basin, allowing a detailed reconstruction of the history of sediments, from generation to accumulation. The characteristics that make the Po Basin suitable for source-to-sink studies are shared with only few other fluvial systems worldwide. An example, at a different scale, is the Ganga River, which receives sediments from tributaries draining two markedly different source areas, the Himalayan chain and the Indian Craton (Sinha et al., 2009).

In this study, sedimentological, stratigraphic and compositional analyses carried out on two cores, respectively 101 m (MDL) and 77.5 m (SBP) long, recovered from the central sector of the Po Plain (see Fig. 1b for location), with the aim of defining the contribution of the main sectors of the Alpine and Apennine amphitheatre to sediment accumulation and preservation in this area. The provenance of the Middle-Late Pleistocene and Holocene cored sands has been assessed by comparing composition with that of modern Alpine and Apennine rivers, displaying specific compositional signatures. The stratigraphic framework, largely based on Bruno et al. (2021), benefited of 11 radiocarbon dates, and of pollen data from ENI-DCO (1987) and Amorosi et al. (2008). The definition of the provenance of core sands is aimed at the reconstruction and temporal framing of the main changes in the hydrographic network of the central Po Plain and the consequent sedimentary evolution of this sector of the Po Basin.

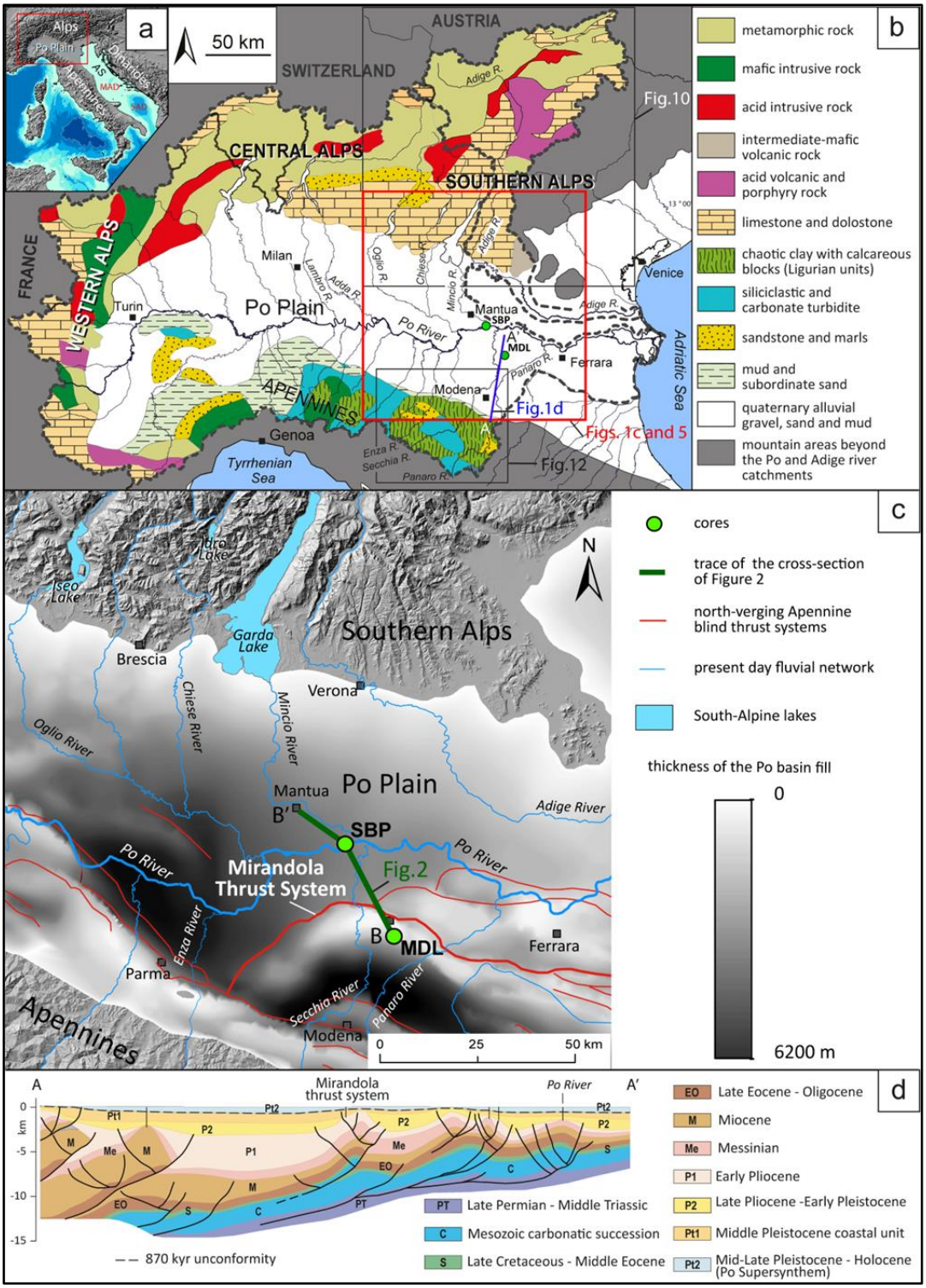

Figure 1. (a) The Po-Adriatic source-to-sink system with the three sediment source areas (the Alps, the Apennine and the Dinarides) and the two main marine sinks, the MAD (Mid Adriatic Depressions) and the SAD (Southern Adriatic Depressions). AS: Adriatic Sea. (b) Geolithogical map showing the main rock units cropping out in the Po and Adige drainage basins. The green dots indicate cores MDL and SBP; the red box indicates the extent of the area represented in Figs. 1c and 5, while the black boxes refer to Figs. 10 and 12. (c) Study area depicting the thickness of the Po Basin fill, the main north-verging Apennine thrust (red lines), and the configuration of the modern fluvial network. (d) Interpreted seismic profile showing the Po Basin fill (units P1 to Pt2) sealing the intensely folded and faulted Permian to Miocene substratum (from Martelli et al., 2017).

4.2. GEOLOGICAL SETTING

4.2.1. *Stratigraphy of the Po Basin*

The Po Basin represents the foreland of two mountain chains, the Southern Alps to the north and the Northern Apennines to the south (Fig. 1b). These thrust belts developed in response to the convergence between the African and European plates, starting from the Cretaceous (Carminati and Doglioni, 2012). The most external portion of the Northern Apennine accretionary wedge is buried beneath the Po Plain and is composed of arcuate systems of thrust-related folds (Figs. 1c and 1d; Turrini et al., 2014). The most important structure in the study area, affecting subsurface stratigraphy, is the Mirandola thrust system (Figs. 1c, 1d and 2). This structure is tectonically active as demonstrated by the 2012 seismic sequence (Bonini et al., 2014)The Po Basin fill, with thicknesses ranging between 6000-8000 m in the depocenters and 100-200 m at the top of the buried anticlines (Fig. 1c), is composed of Zanclean-Calabrian turbidites (Pliocene P1 and P2 in Fig. 1d, Martelli et al., 2017), overlained by Middle Pleistocene-Holocene coastal and continental units (Pt1 and Pt2, respectively, Fig. 1d). Unit Pt2 (the Po Supersynthem of Amorosi et al., 2008) is approximatively dated to the last 870 ka BP (Muttoni et al., 2003, 2011; Scardia et al., 2006; Gunderson et al., 2014). A regional unconformity, dated to 450 ka BP (Geomol Team, 2015; Martelli et al., 2017) divides the Po Supersynthem into two unconformity-bounded units: the Lower and the Upper Po Synthems (Fig. 2).

The stratigraphy of the Po Supersynthem in the study area (red rectangle in Fig. 1b) is depicted along the 78-km long cross-section of Fig. 2 (Bruno et al., 2021), running between the towns of Mirandola and Mantua (location in Fig. 1b). The Po Supersynthem is characterized by variable thickness, from ˜100 m above the culmination of the Mirandola Anticline, to ˜400 m in the depocentres (Fig. 2). The base of the Po Supersynthem, observed in deep exploration wells, is characterized by the upward transition from coastal to continental deposits (Fig. 1d).

The Lower Po Synthem, studied only along a few continuous cores (ENEL-DCO, 1984; Amorosi & Sammartino, 2018), is mainly composed of alluvial (fluvial-channel and channel-related sands, floodplain muds) and swamp facies associations, with subordinated paralic and coastal sediments (light blue horizon in Fig. 2). Numerous uncertainties exist on the geometry and lateral extent of the sediment bodies of this unit, being penetrated by few cores and wells (Fig. 2).

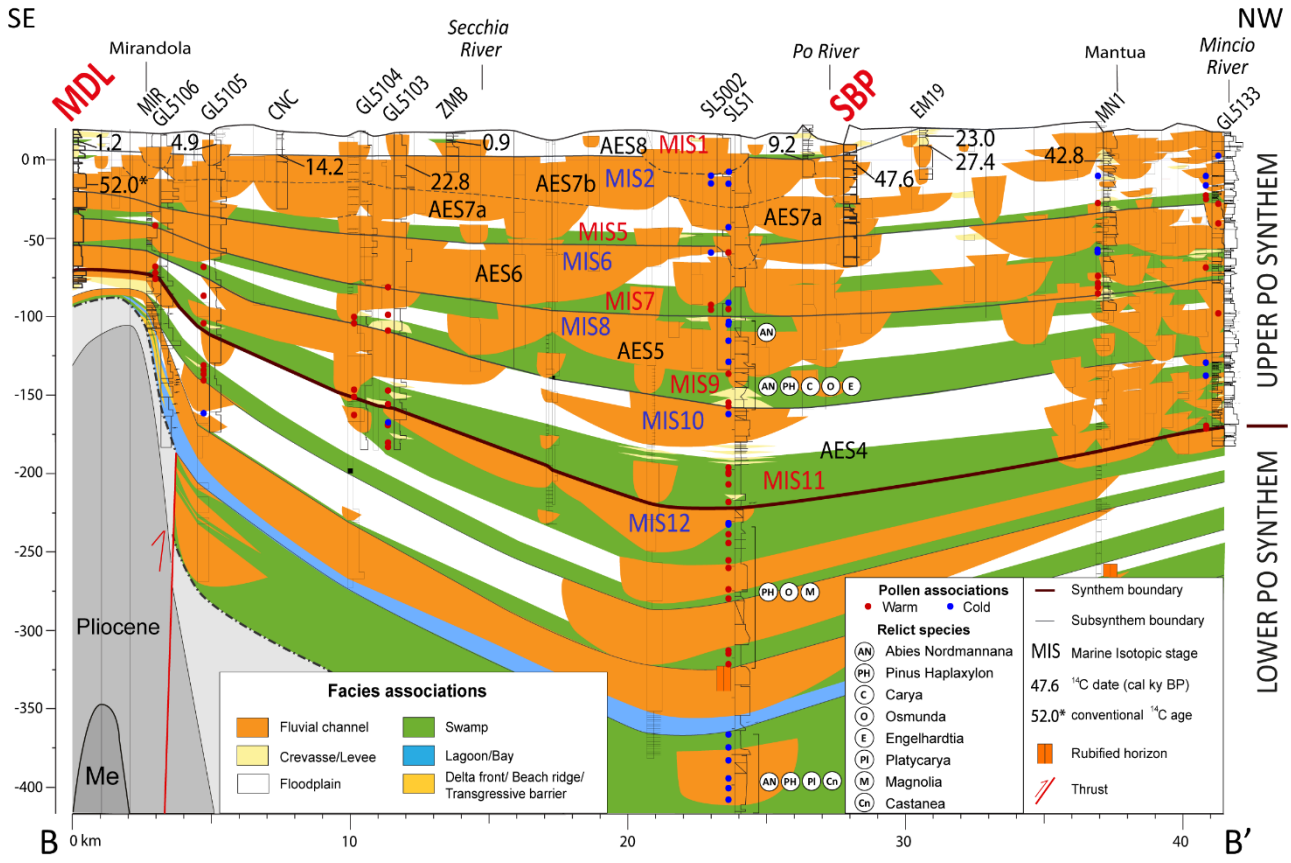

Figure 2. Stratigraphy of the Po Supersynthem along a SE-NW-oriented profile from core MDL to Mantua passing from core SBP (modified after Bruno et al., 2021). Location in Fig. 1b.

The stratigraphy of the Upper Po Synthem, on the contrary, is constrained by a considerably higher number of core and well data (Fig. 2). Four laterally extensive channel-belt sand bodies, up to 40 m-thick, are separated by relatively thin (ca. 5 m) swamp peaty muds and locally show lateral transition to floodplain muds (Bruno et al., 2021). A muddy horizon, dated to the Holocene, caps the whole succession (Fig. 2). This cyclic architecture, which reflects the onset of major glaciations since the Middle Pleistocene (Amorosi et al., 2008; Campo et al., 2020), permitted to subdivide the Upper Po Synthem into five lower-rank sedimentary units. Following the nomenclature of the Geological Map of Italy to scale 1:50,000, these are subsynthems AES4, AES5, AES6, AES7 and AES8 (Figs. 2 and 3). Subsynthem AES8 is exposed in large sectors of the Po Plain, whereas subsynthems AES4 to AES7 crop out only at the Apennine foothills and in intramontane valleys, in form of terraced fluvial-channel deposits. The base of each subsynthem, is characterized by pollens of warmth-loving species (i.e. broad-leaved trees, red circles in Fig. 2; ENEL-DCO, 1984; Amorosi et al., 2008) suggesting accumulation during interglacial periods. The upper part of each subsynthem, marked by pollen species pointing to cooler climatic conditions (*Pinus*, mountain trees and herbs, blue circles in Fig. 2; ENEL-DCO, 1984; Amorosi et al., 2008), accumulated during glacial periods. The AES7

channel-belt sand body results from the amalgamation of two channel complexes (AES7a and AES7b in Fig. 2). AES7a likely accumulated MIS 5 and 4, whereas AES7b is radiocarbon dated to MIS 2 and 3 (Campo et al., 2016; Bruno et al., 2018). An increasing percentage of old species (e.g. *Abien nordmanniana*, *Pinus haploxylon*, *Carya*, *Engelhardtia*, *Osmunda, Platycarya, Pterocarya, Magnolia, Castanea*), characterizes the Lower Po Synthem (ENEL-DCO, 1984).

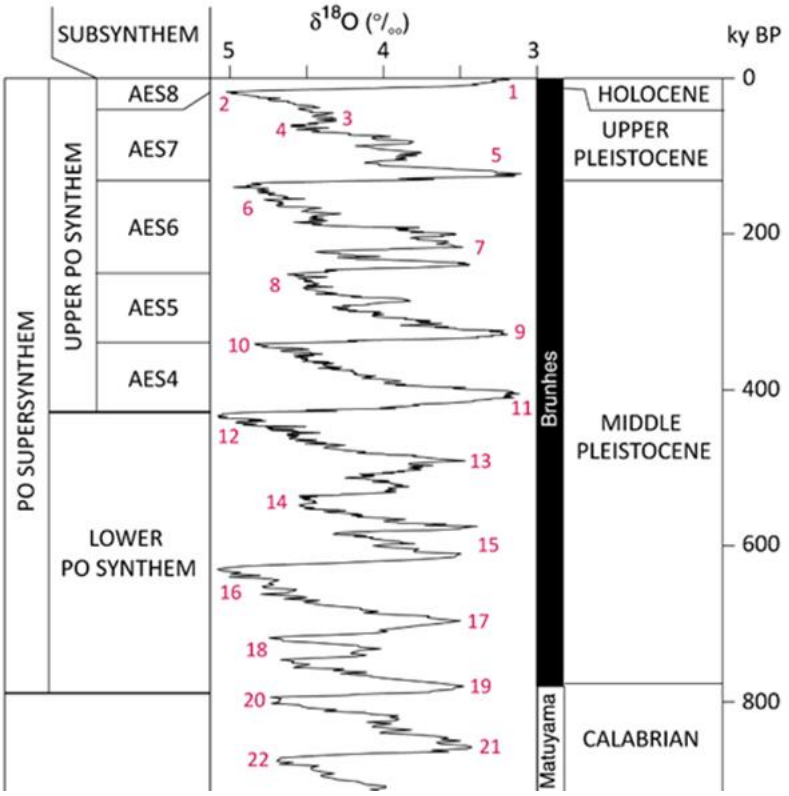

Figure 3. Correlation between the main stratigraphic unit composing the Po Supersynthem and the climatic oscillations during the last million years. The δ18O curve is from Lisiecki and Raymo (2005). Red numbers represent Marine Isotope Stages.

4.2.2. Surface geology of the drainage system

The cores analysed in this study are located in an area nowadays fed by the Po River and its southern tributary, the Secchia River. The analysis of the composition of sands from these rivers, and from those flowing close to the study area, is crucial to reconstruct the potential ancient drainages feeding this sector of the Po Plain. The Po River originates in the Western Alps and flows in west–east direction for 652 km (Fig. 1b). It is fed by 141 tributaries, which drain a cumulative area of about 75,000 km^2. The western part of the Po drainage basin, including large sectors of the

Western and Central Alps and of the western Apennines, is characterized by extensive outcrops of crystalline-metamorphic and ophiolite complexes (Fig. 1b).

Mesozoic carbonates and subordinately volcanic rocks are exposed in the Southern Alps (Fig. 1b) and their detritus is delivered by a number of rivers flowing toward the central Po Plain. The Oglio River and its tributary Chiese River, flowing in north-west tip of the study area, drain a cumulative area of about 6360 km^2. They are tributaries and emissaries of the Iseo and Idro periglacial lakes. The Sarca river flows into the Garda Lake after draining an area of about 1290 km^2. The Garda Lake emissary, the Mincio River, flows into the Po River close to core SBP (Figs. 1b and 1c), whereas the Adige River, passing close to the north-east corner of the study area, flows into the Adriatic Sea.

The Apennine tributaries, such as the Enza, Secchia and Panaro Rivers, which flow relatively close to cores MDL and SBP (Figs. 1b and 1c), have catchment areas < 2300 km^2, mainly composed of Cretaceous tectonically deformed clays with carbonate blocks (Ligurian units in Fig. 1b; Remitti et al., 2011) and of Paleocene to Neogene coastal-marine sandstones and marls (Epiligurian Units; Ricci Lucchi, 1987). Pliocene shallow-marine clays and subordinated Pleistocene coastal sands crop out at the Apennine margin (Post-Evaporitic units of Ricci Lucchi et al., 1982).

4.3. METHODS

This study relies upon sedimentological and petrographic analyses on two cores recovered in a sector of the central Po Plain located approximately at the same distance from the Southern Alps and the Northern Apennines (Figs. 1b and 1c). This area, therefore, could have been potentially fed by tributaries draining both chains and by the trunk river in the past. Core MDL, 101 m-long, has been recovered 20 km south of the Po River. Core SBP, 77.5m-long, has been recovered from the Po riverbed. Both cores were described in terms of lithology, grain-size, colour, consistency and accessory material (macrofossils, vegetal remains, peat, and carbonate concretions), and interpreted in terms of facies associations. Attribution to subsynthems is based on the stratigraphic scheme proposed by Bruno et al., 2021 (Fig. 2), constrained by pollen data from ENEL-DCO (1984) and Amorosi et al. (2008) and by 11 radiocarbon dates. Radiocarbon ages were calibrated using OxCal 4.4 (Bronk Ramsey & Lee, 2013) with the IntCal 20 curve (Reimer et al., 2020). One sample, providing an age close to the ^{14}C detection limit, was not calibrated due to insufficient resolution of the calibration curve (age with asterisk in Figs. 2 and 4).

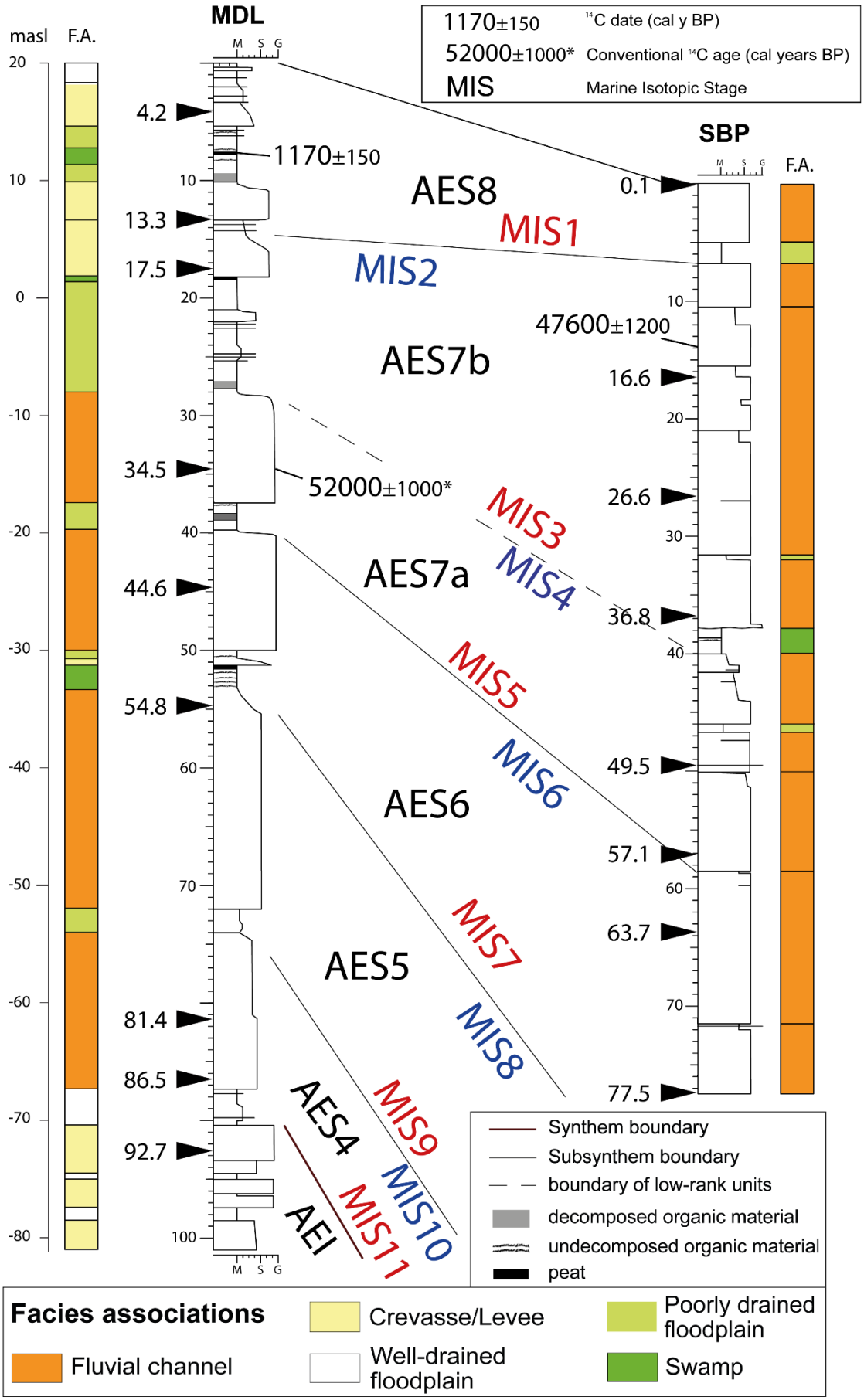

Figure 4. Stratigraphy and facies interpretation of cores MDL and SBP. Location in Fig. 1b.

Petrographic analyses were carried out on 17 sand and pebble samples (Fig. 4) collected from cores MDL and SBP. Recovery of core MDL between 72 and 55 m depth was poor and highly disturbed by methane emissions. Thus, sands from this interval were not sampled for compositional analysis. Bulk samples were used for qualitative petrographic observations, whereas point counting was carried out on the fine sand fraction (0.125–0.250 mm), separated by wet sieving. The modal analysis was performed according to the Gazzi-Dickinson method, designed to minimize the dependence of the analysis on the grainsize (Zuffa, 1985). At least 300 grains were point counted for each section. Components not related to the original sand composition, such as authigenic carbonate nodules, penecontemporaneous shell fragments and organic fragments were excluded from final calculations. Although all the grain components were analysed, only those with similar hydraulic behaviour (quartz, feldspars and volcanic, metamorphic and sedimentary lithics) were considered for provenance analyses (Fontana, 1991; Garzanti et al., 2008), as transport invariant components are essential for these type of studies (Weltje, 2004; Garzanti et al., 2008 and Razum et al., 2021). Along a single core, only one sample was collected from each sand body, assuming low compositional variations within each sediment body (Lugli et al., 2004, 2007; Fontana et al., 2019; and Bruno et al., 2021). Thin sections of core samples with significant carbonate content (≥ 20%) were stained with alizarin red in order to distinguish calcite from dolomite. The modal analyses of the core samples were compared with the detrital modes of the following modern rivers that could have supplied sands to the MDL and SBP areas since the Middle Pleistocene (Fig. 5): Po (from Bruno et al., 2021 and Demurtas et al., 2022), Oglio (samples O_1 and O_2, this work; sample O_3 from Demurtas et al., 2022), Chiese (Samples C_1, C_2, C_3, this work), Sarca-Mincio (Sr, this work; M from Demurtas et al, 2022), Adige (A_1 from Demurtas et al., 2022; A_2 this work), Enza (sample E, this work), Secchia and Panaro (samples S_1, S_2, S_3, P_1, P_2, P_3, P_4 from Lugli et al., 2004, 2007).

The results of the modal analysis were reported in the (Q+F)–L–C ternary diagrams (Q+F: quartz and feldspar; L: siliciclastic lithic; C: carbonate lithic) as well as in barcharts. The distribution of lithic fragments is shown in Lm-Lv-Ls and Lm-Lv-Lss ternary diagrams (Lm: metamorphic lithic; Lv: volcanic lithic; Ls: sedimentary lithic, carbonate included; Lss: siliciclastic sedimentary lithic). Instead of the classical Q-F-L diagram (Dickinson & Rich's, 1972), the Q+F-L-C diagram has been adopted, due to the key role of carbonates analysed in this work and to facilitate comparison with several compositional studies carried out in the central and southern Po Plain (Lugli et al., 2004; 2007, Fontana et al., 2015; 2019; Demurtas et al., 2022).

4.4. RESULTS

4.4.1. Stratigraphy of core MDL

Five facies associations were identified in core MDL (Fig. 4) based on grain-size, grain-size tendencies, thickness, upper and lower contacts of sediment bodies, colour, consistency and presence of vegetal remains and peat. The reader is referred to Bruno et al., 2015 and 2021 for detailed facies descriptions. Attribution to synthems (Lower vs Upper Po Synthems) and subsynthems (AES4 to AES8) is based on the stratigraphic section of Figure 2.

Three sand bodies, 2-4 m-thick, were observed at depth > 87 m, with heterolithic pebbles (diameter < 5 cm) at depth of 97.5 and 92.7 m. Sand bodies are interbedded with mud strata, up to 3.5 m-thick. Sand and mud colour is grey-peach (5YR 8/2). Fossils and vegetal remains are absent. Based on lithology, grain-size and on the lack of fossils, the three sand bodies at depth > 87 m have been interpreted as channel-related deposits. Although the lack of preserved sedimentary structures in cores do not permit unequivocal facies attribution, the limited thickness of these deposits suggests their interpretation as crevasse channels (Singh, 1972). Mud intervals are interpreted as floodplain deposits (Collinson, 1978). These deposits constitute the upper portion of the Lower Po Synthem (see Fig. 2).

Between 87 and 28 m depth, four sand bodies, more than 9 m-thick, are interbedded with thin (< 3 m) mud strata. The lower sand body, between 87 and 74 m depth is composed of grey, fine silty sand with sharp base, fining-upward grainsize trend and gradational upper contact. In the interval between 72 and 55 m, sands recovery is poor due to methane emissions during coring operations. The uppermost two sand bodies, at depths of 40-50 and 28.0-37.2 m are composed of grey (2.5YR 7/1), coarse sand, with erosional base and sharp top. A thinner sand body (less than 1 m thick), with erosional base and gradational top, has been observed between 51.15 and 50.50 m depth. Fossils were not encountered in sands, whereas a wood fragment collected at 34.5 m depth yielded an age of 52000±1200 years BP (conventional ^{14}C age). Mud horizons are composed of silty clay and clayey silt. Colour is grey (dark grey at 38.5 m depth). Abundant vegetal remains, with a 30 cm-thick peat layer on top, are recorded between 53.20 and 51.15 m depth. Thick, fossil-free sand bodies with sharp or erosional base are interpreted as fluvial channel deposits (Allen, 1963), whereas the thinner sand body at 50.50-51.15 has been interpreted as a crevasse-channel deposit. Grey muds are referable to a poorly drained floodplain, whereas muds with vegetal remains and peat are interpreted as deposited in a waterlogged environment (e.g. swamp, Diessel, 1992; Richardson et

al., 2001; Stolt & Rabenhorst, 2011). These deposits are referable to units AES4 to AES7a (see Figs. 2 and 4).

The uppermost 28 m are characterized by a considerably higher percentage of muds. Muds include silty clay and clayey silt, with local occurrence of vegetal remains and wood fragments. Subtle silty sand-mud intercalations are recorded at depths of 25.0-24.5 and 22.2-21.2- m. Colour is grey (dark grey between 27.8 and 27.0). Peaty muds are encountered at 18.35-18.10 m depth. A wood fragment of 8 cm diameter, collected at 7.65 m depth, yielded an age of 1170±150 years BP (calibrated age). Three sand bodies, with thickness of 3-5 m are encountered at depths of 18.1-13.4, 13.4-10.3 and 5.4-2.0 m. These are composed of fine to silty sand with sharp base, fining-upward trend and gradational top, marked by mm-scale clayey silt intercalations. Colour of the lowermost two sand bodies is grey with orange mottles of Fe oxides and-or hydroxides between 11.2 and 10.7 m depth. The uppermost sand body is grey (7.5YR 8/1) between 5.4 and 4.6 and pale brown (10YR 8/2) above 4.6 m. Grey muds with sparse vegetal remains and sand-silt intercalations are interpreted as deposited in a poorly drained floodplain, whereas peaty muds with abundant wood fragments are interpreted as deposited in a swamp environment. Given their limited thickness, sand bodies at depths < of 18 m are interpreted as crevasse channel deposits (Fig. 4).

4.4.2. *Stratigraphy of core SBP*

The 77.5 m-long core SPB, which penetrated only the Upper Po Synthem (Units AES 6 to AES8, Fig. 2), is dominated by grey (2.5YR 7/1), coarse-to medium sand with local thin fine-sand and mud intercalations (Fig. 4). Individual sand bodies, with sharp or erosional base and gradational top, are up to 12 m thick. Hetherolithic pebbles (diameter < 5 cm) have been recorded at 49.5 and 37.5 m depth. Between 46 and 40 m depth, coarse sand grade upwards into silty sand and clayey silt. A 2.2 m peaty mud horizon at 40-37.8 m depth separates AES7a and AES7b sand bodies. Three thin (< 2 m) horizons composed of grey (2.5YR 7/1) silty clay and clayey silt have been observed at depths of 31.5, 27.0 and 6 m. The uppermost fine-grained horizon marks the base of subsynthem AES8 (Figs. 2 and 4). Wood fragments have been recorded at 42.2 and 13.9 m depth. A wood fragment collected at 13.9 m depth yielded an age of 47600±1200 years BP (Figs. 2 and 4).

Based on grainsize, grainsize tendencies, upper and lower boundaries, and on the lack of fossils, sand bodies of core SBP, have been interpreted as fluvial-channel deposits. Peaty muds at 40-37.8 m depth are attributable to a swamp environment whereas grey muds intercalation have been interpreted as poorly drained floodplain deposits.

4.4.3. *Sand petrography*

The results of the modal analysis from modern rivers and core samples were reported in the bar chart of Figures 5 and 6 and plotted in the (Q+F)–L–C ternary diagrams of Figs. 7a and 7d. The distribution of lithic fragments is shown in the Lm-Lv-Ls and Lm-Lv-Lss ternary diagrams of Figs. 7b, 7c, 7e and 7f. The percentages reported in sections 4.3.1 and 4.3.2 refer, if not specified, to detrital components with similar hydraulic behaviour (see section 3 for details).

Section 4.3.1 reports the results of compositional analysis on 23 sand samples collected from rivers flowing across or close to the study area (see Fig. 1c), that could have potentially fed sites MDL and SBP since the Middle Pleistocene. All rivers were sampled upstream and downstream of lakes, to evaluate their potential selective sediment trapping, and of confluences with tributaries, to assess their sedimentary contribution. Particularly, five samples were collected from the Po River, in the sector across the study area, downstream of the confluence of each tributary to study the compositional variation induced by the sedimentary input of Alpine and Apennine sources. Section 4.3.2 reports the composition of 16 samples collected from sand bodies of cores MDL and SBP.

4.4.3.1. Modern River Sands

The composition of the Po River sands has been analysed in 5 samples collected along a 15 km-long sector of its riverbed: upstream the confluence with the Enza River (Po1); close to core SBP, between the confluences with Oglio and Mincio rivers (Po2); between the confluences of Secchia and Panaro Rivers (Po3); and downstream the Panaro confluence (Po4 and Po5). The Po River sands show in general high content in quartz and feldspars (up to ~59%, Figs. 5 and 7a). The distribution of sedimentary lithics changes downstream from Po1 to Po4, recording an overall decrease in metamorphic lithics (from 32.8% to 5.4%, Figs 5, 7b and 7c) and a parallel increase in sedimentary lithics (from 10.3% to ~28%, Figs 7b and 7c), particularly evident after the confluence of the Secchia and Panaro rivers (Fig. 5). The only sample out of this trend is Po5, which records a slight increase in metamorphic lithics (17.2%, Fig. 5). Volcanic grains are scarce in all samples (<3%). Heavy minerals are always present (mostly garnet), and their content is highly variable (up to 18% of the whole sandy fraction in Po1).

Sands of the Oglio River show a composition similar to samples Po1 and Po2, with high content of quartz and feldspar (up to 54.5% in O2, Figs. 5 and 7a), and metamorphic lithics, which constitute ~50% of the lithic component (Figs. 7b and 7c). A slight increase in quartz and feldspar (from 47.4% to 54.5%) and a parallel increase in lithics (from 52.6% to 45.5%) is recorded downstream from

sample O1 to O2; Sample O3, downstream of the confluence with the Chiese River, instead shows an increase in the lithic component (55.3%) and a slight decrease in quartz and feldspar (44.8%; Figs. 5 and 7a).

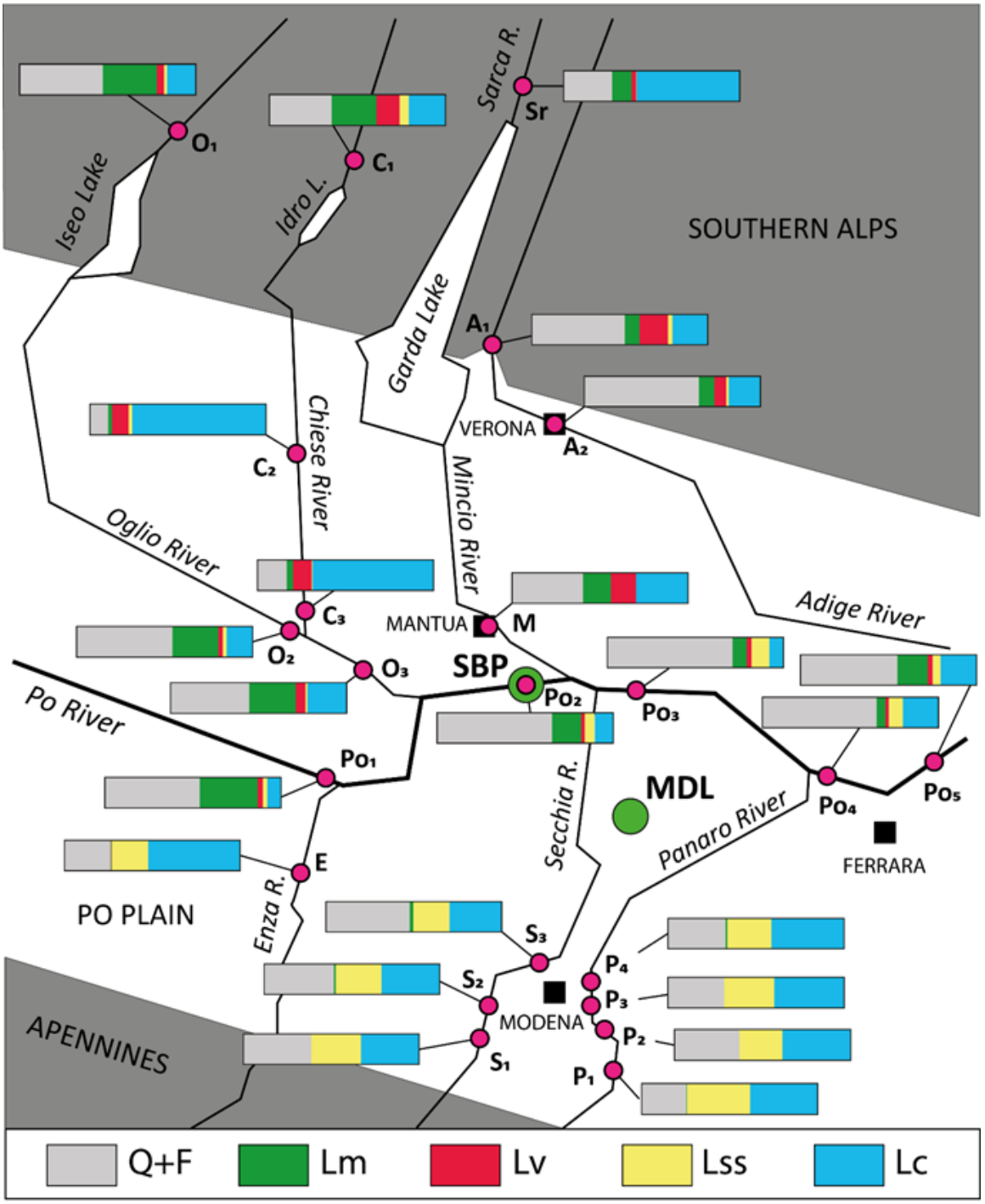

Figure 5. Modern Po and tributaries rivers composition collected at different locations along the middle Po drainage basin. The location of cores MDL and SBP is also indicated.

Compared to sands from Po and Oglio rivers, sands from the Chiese River show a relatively lower content in quartz and feldspar (from 35.3% in C1 to 10.5% in C2 to, Figs. 5 and 7a). Sample C1,

collected in the Alpine sector, upstream of the Idro Lake, is rich in carbonate lithics (20.9%) and shows relatively high percentage of metamorphic (25.4%) and volcanic (13.1%) lithics. Samples C2 and C3, collected in the Po Plain, downstream of the Idro Lake, have a very high content in carbonate (~70%), mainly sparitic grains; quartz, feldspar and siliciclastic lithics are subordinate. Volcanic lithics are the most common among the non-carbonate lithics (~10%).

Sands of the Sarca River consist mostly of sparitic and micritic carbonate grains (~58.5%, Figs. 5 and 7a). Quartz and feldspar constitute 27.6%. Non-carbonate lithics (14.0%) are mainly represented by metamorphic lithics (11.0%). The composition of the Mincio River sands, instead, is characterized by a comparatively lower amount of carbonate lithics (29.5%), associated with a higher percentage of quartz and feldspar (40.3%) as well as volcanic and metamorphic lithics (14.4 and 15.8% respectively; Figs 5, 7a, 7b and 7c). Siliciclastic lithics are almost absent in both Sarca and Mincio Rivers.

The Adige River sands are composed of quartz and feldspar for more than half of the sand fraction (Figs. 5 and 7a). Carbonate grains are the most common lithic component with values ranging from 17.9 to 20.1%; metamorphic lithics are comprised between 8.4 and 8.7%. Volcanic lithics are relatively abundant in A1 (16.1%, Fig. 7b) and decrease downstream in sample A2 (6.7 %). An opposite trend is observed for quartz and feldspar. The siliciclastic sedimentary lithic component is subordinate.

The sands from the Apennine rivers Enza, Secchia and Panaro show a quite homogeneous composition (Figs. 5, 7a, 7b and 7c). Carbonate and siliciclastic sedimentary lithics constitute more than 50% of the sand fraction. Carbonates are always more abundant than siliciclastic lithics, particularly the Lc/Lss is 2.53 in the Enza River sands, significantly higher than the Secchia and Panaro River (maximum value 1.58 recorded in P2). Quartz plus feldspar is less than 50% of the sand fraction, with highest values in the Secchia River sands (47.8% in S3) and comparatively lower in the Panaro (36.8%) and Enza (26.2%) rivers. Metamorphic and volcanic lithics are rare or absent.

4.4.3.2. Core Sands

Petrographic analyses on samples from cores MDL and SBP revealed changes in composition that allowed to distinguish 3 petrofacies.

In petrofacies 1, recognized in samples MDL 92.7, 86.5 and 81.4 (Lower Po Synthem and subsynthem AES4, Figs. 2, 3 and 6), is characterized by quartz and feldspar in the range of 42.0-48.4%, and carbonate lithics from 36.2 to 44.8% (Figs. 6, 7d, 8a and 8b). Among the non-carbonate lithics, volcanic lithics reach 15.2% in MDL 92.7 Figs. 6, 7e and 7f), metamorphic lithics range between 5.2 and 9.3% whereas siliciclastic sedimentary lithics are rare. Quartz is commonly found as single crystal and is slightly more abundant than feldspars (K-feldspar and plagioclase, Figs. 8a and 8b). Carbonate lithics are mudstones to grainstones with prevailing peloidal grains (Fig. 9b) and are equally represented by calcite and dolomite (Fig. 6). Oolitic grainstones have been observed in the fraction coarser than 0.250 mm (Fig. 9c). Volcanic grains have porphyritic and aphanitic texture and are referable to acidic and intermediate volcanites; few basaltic grains with microcrystalline groundmass and abundant plagioclase and opaque fenocrystals are also present, with similar features of basalt pebbles shown in Figure 9a.

Petrofacies 2 is the most common in both cores (samples MDL 54.8, 44.6, 34.5, 17.5, 13.3 and SBP 77.5, 63.7, 57.1, 49.5, 36.8, 26.6, 16.6) and has been recognized in sand bodies belonging to subsynthems AES5 to AES8. It shows a very high content of quartz and feldspar (from a minimum of 56.2% in MDL 34.5 to a maximum of 74.3% in MDL 17.5, see Figs. 6, 7d, 8c and 8d) and a high amount of metamorphic lithics (from 7.9% in MDL 13.3 to 23.0% in SBP 36.8, Figs. 6, 7e, 7f, 8c and 8d). The quartz/feldspar ranges from 1 to 2. Metamorphic lithics include phyllites, micascists, and metasiltstones (Figs. 8c and 8d). Serpentinite grains are occasionally found. The percentage of volcanic lithics is in general < 5%, with the exception of samples SBP 49.5 and MDL 34.5 (7.0 and 7.8% respectively, Fig. 6). Volcanic lithics are characterized by a microcrystalline to aphanitic groundmass with few feldspar and quartz fenocrystals (Fig. 9d). Carbonate lithics vary from 3.6% in MDL 17.5 to 20% in MDL 13.3, 34.5 and 44.6, with prevailing microspatitic and minor peloidal and oolitic grains. Among carbonates, dolostones are 43% (sample MDL 44.6, Fig. 6). Siliciclastic sedimentary lithics are scarce in all sample, with the exception of MDL 13.5 where they reach 8.2% (Figs. 6, 7e and 7f).

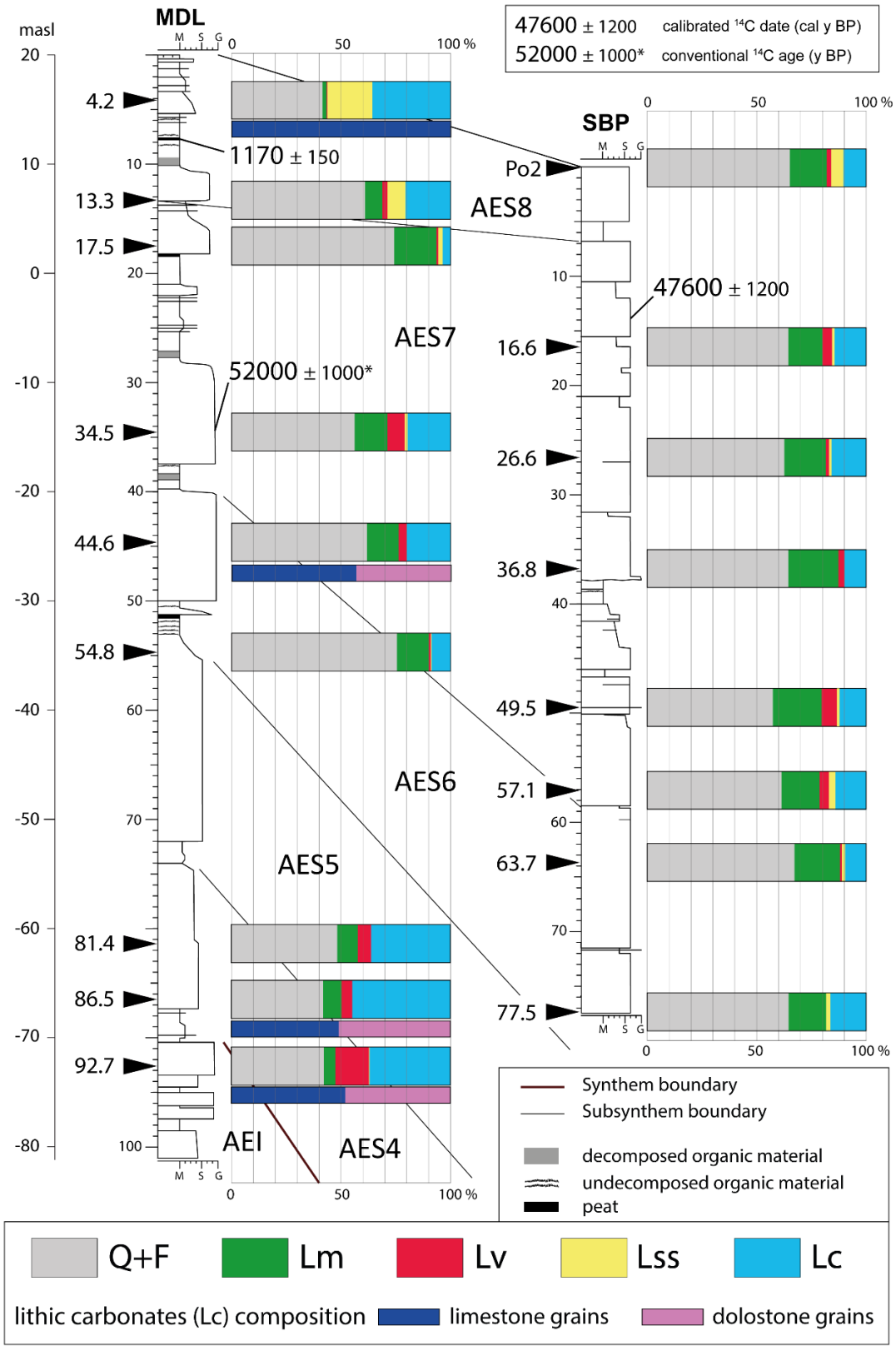

Figure 6. Composition of sands from cores MDL and SBP represented as bar charts. Q+F: quartz plus feldspar; Lm: metamorphic lithic; Lv: volcanic lithic; Lss: siliciclastic sedimentary lithic; Lc: carbonate lithic. Petrofacies 1 characterized by high content in limestones, dolostones and volcanic lithics corresponds to samples MDL 92.7, 86.5 and 81.4. Petrofacies 2 showing high content of quartz, feldspar and metamorphic lithics, is represented by samples MDL 54.8, 44.6, 34.5, 17.5, 13.3 and SBP 77.5, 63.7, 57.1, 49.5, 36.8, 26.6, 16.6. Petrofacies 3, rich in carbonate and siliciclastic sedimentary lithics, is observable only in sample MDL 4.2.

Petrofacies 3, recognized in the uppermost portion of core MDL, deposited after 1170±150 years BP (subsynthem AES8), is remarkably rich in sedimentary lithics (Fig. 6), represented by carbonate (35.7%) and siliciclastic lithics (20.6%; Lc/Lss=1.73). Quartz and feldspar represent the 41.6% (Figs. 6 and 7d); metamorphic and volcanic lithics are scarce (Figs. 6, 7e and 7f). Carbonates are composed exclusively of calcite (Fig. 6), as sparitic and micritic grains (Fig. 8e), whereas dolostones are no more present. Several detrital bioclasts mainly represented by not identifiable foraminifera are observed (Fig. 8e). Siliciclastic lithics consist of shales and subordinately of siltstones (Figs. 8e and 8f).

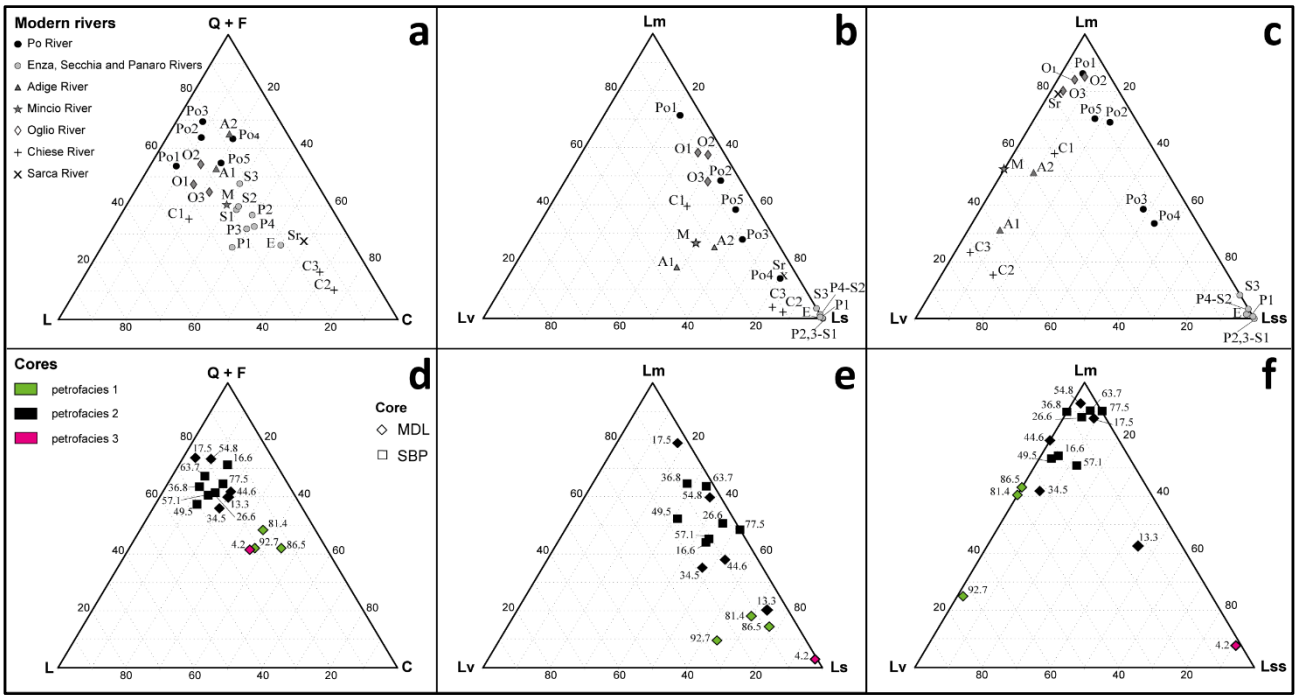

Figure 7. Ternary diagram showing the composition of sands from modern rivers flowing across the study area (panels a, b and c; location of samples in Fig. 5), compared with the composition of core samples (panels d, e and f, see Fig. 6 for a comparison with core logs and barcharts). (a) Q+F, L, C diagram showing the composition of modern rivers (Q: quartz; F: feldspar; L: fine grained siliciclastic lithic; C: carbonate lithic). (b) Lm-Lv-Ls ternary diagram depicting the distribution of lithic fragments in modern-river's sands (Lm: metamorphic lithic; Lv: volcanic lithic; Ls: sedimentary lithic, carbonate included). (c) Lm-Lv-Lss ternary diagram showing the distribution of lithic fragments in modern-river's sands, carbonate excluded (Lss: siliciclastic sedimentary lithic). (d) Q+F, L, C diagram showing the composition of core sands. (e) Lm-Lv-Ls ternary diagram depicting the distribution of lithic fragments in core sands. (f) Lm-Lv-Lss ternary diagram showing the distribution of lithic fragments in core sands, carbonate excluded.

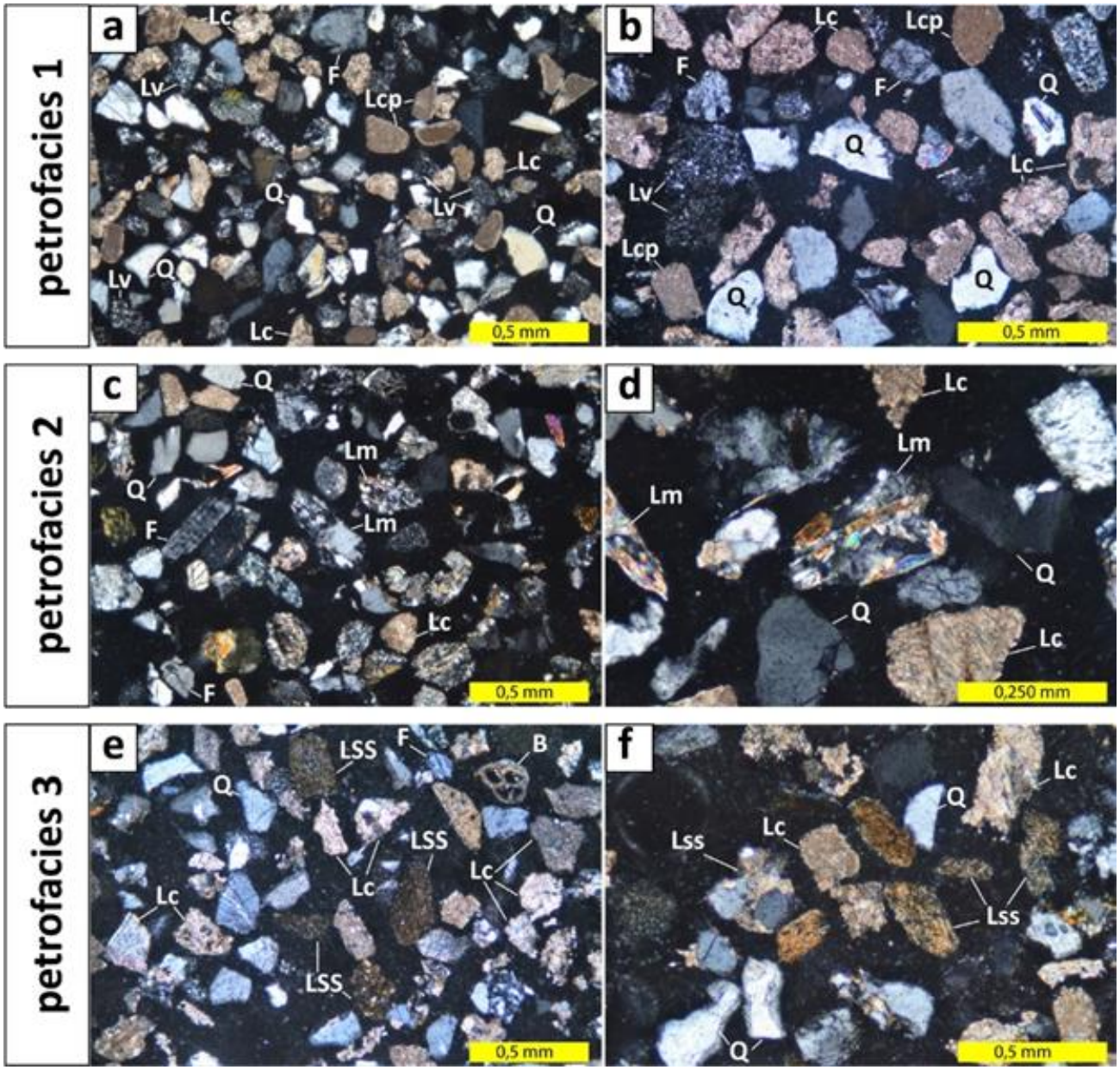

Figure 8. Photomicrographs of the three main petrofacies (1, 2 and 3) at different magnification. (a) Petrofacies 1 with abundant carbonate and volcanic lithics. (b) close-up on volcanic and carbonate grains. (c) Petrofacies 2 rich in quartz, feldspar and metamorphic lithics. (d) close-up on metamorphic lithics. (e) Petrofacies 3 characterized by abundant sedimentary lithics (including single bioclasts). (f) close-up on sedimentary lithics: siltite (Lss on the left) and shale (Lss, central right). Crossed polars. Q: quartz; F: feldspar; Lm: metamorphic lithic; Lv: volcanic lithic; Lc: carbonate lithic; Lcp: peloidal carbonate lithic; Lss: siliciclastic sedimentary lithic; B: bioclast.

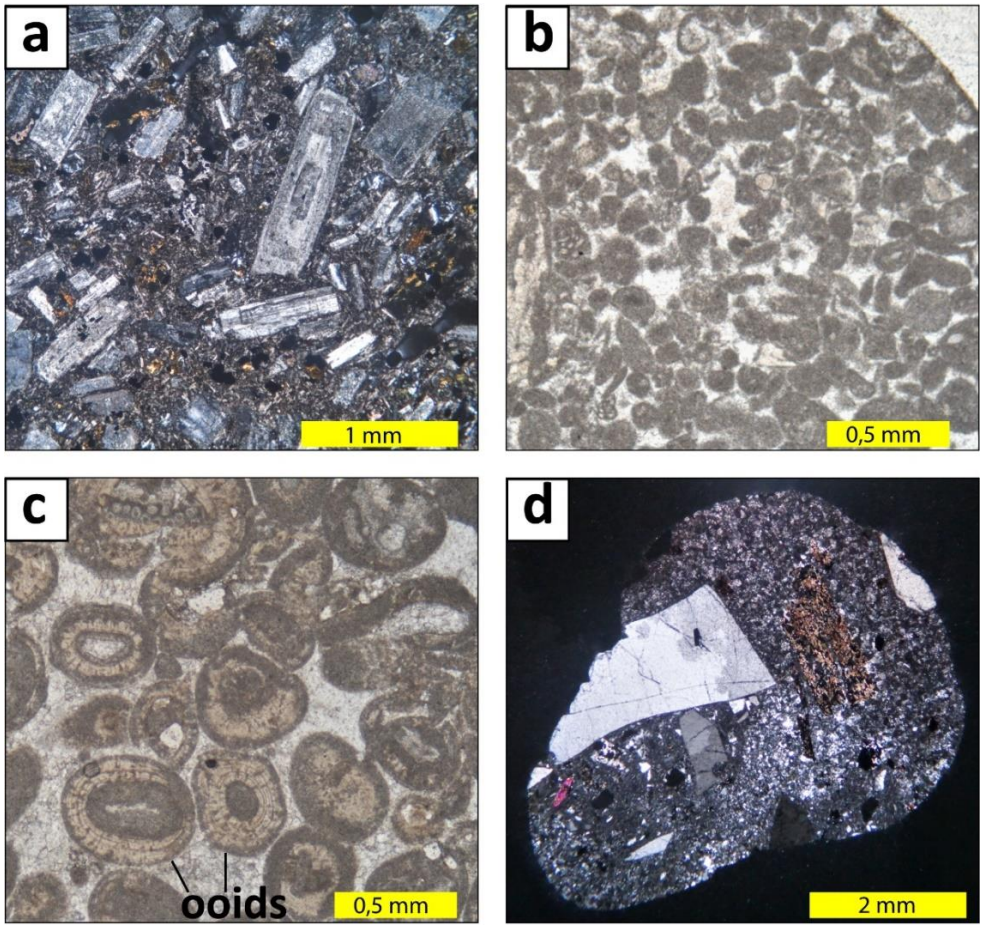

Figure 9. Photomicrographs of pebbles from petrofacies 1 and 2. (a) Femic hypoabissal volcanic rock with abundant plagioclase phenocrysts (crossed polars). (b) Peloidal grainstone (parallel polars). (c) Oolitic grainstone (parallel polars). (d) Acidic volcanic rock with phenocrysts of feldspar in a sialic microcrystalline groundmass (crossed polars).

4.5. DISCUSSION

4.5.1. *Geographic provenance of core sediments*

The provenance of core sands has been assessed through the comparison of their composition with that of sands from modern rivers and of rocks exposed in the Alpine and Apennine drainage basins. The presence of dolostones and the abundance of volcanites, indicate a South-Alpine provenance for petrofacies 1. Dolostones and limestones with peculiar peloidal and oolitic grains derive from Mesozoic formations exposed over wide areas of the Oglio, Chiese, Sarca and Adige drainage basins (Fig. 10). Permian rhyolites largely crop out in the Adige river catchment (*Gruppo Vulcanico Atesino*) and subordinately in the drainage areas of Sarca (*Gruppo di Tione*) and Chiese (*Gruppo delle Tre Valli Bresciane*) rivers. Basalts observed in these petrofacies may derive from the Mesozoic *Complesso Eruttivo Medio-Triassico* and from the Cenozoic *Basalto della Val Lagarina* (Fig. 10).

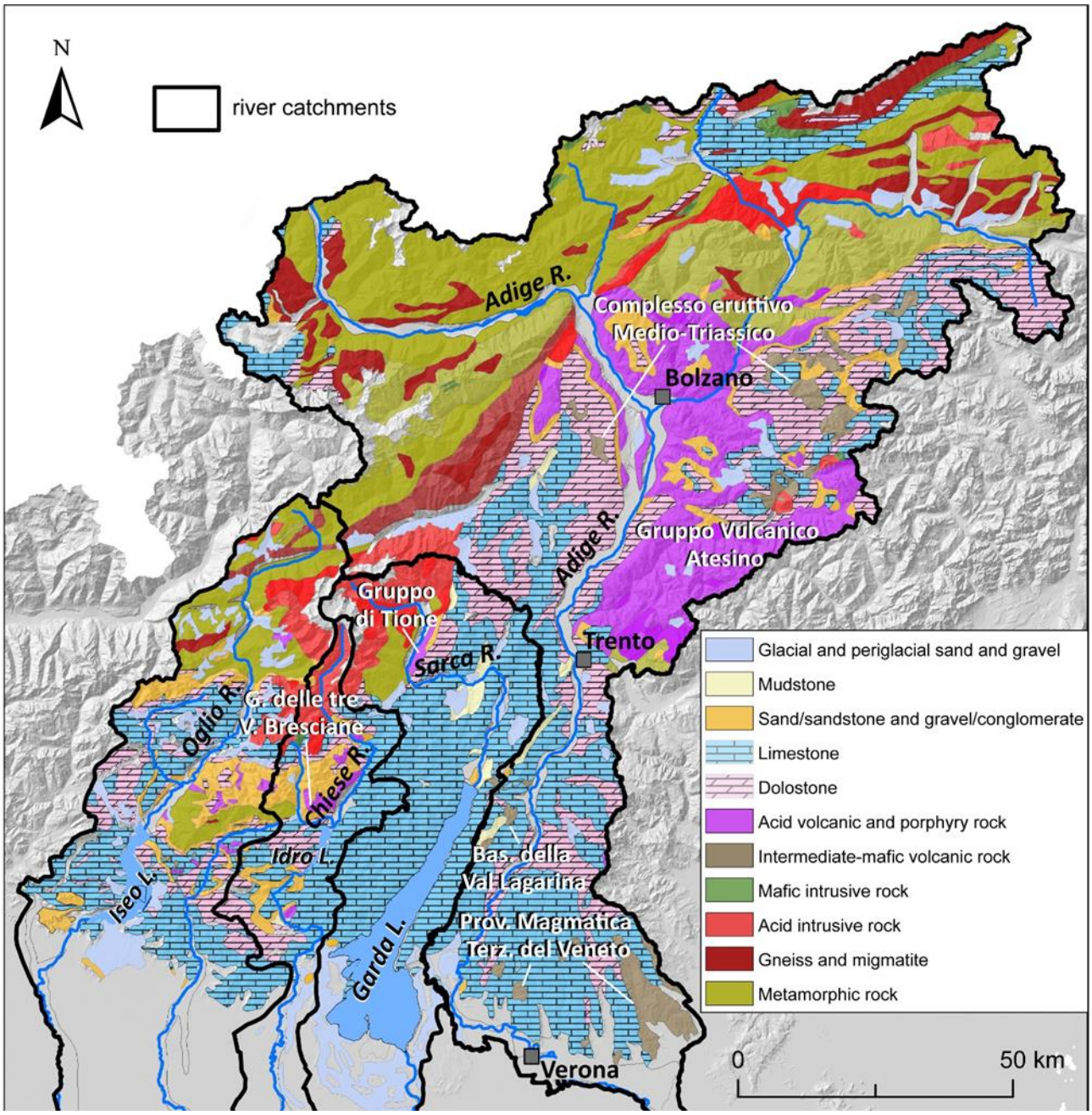

Figure 10. Geolithological map of the catchment areas of the Adige, Oglio, Chiese and Sarca rivers. The major volcanic groups are also shown in white. Location in Figure 1b.

The subtle difference in the amount of volcanic lithics among samples of petrofacies 1 may reflect the contribution from different volcanic complexes exposed in the South-Alpine area (Fig. 10). Sample MDL 92.7, for example, shows affinity with Chiese and Adige river sands (Figs. 5, 6 and 7), whereas samples MDL 86.5 and 81.4 match with the composition of Mincio sands (Fig. 7). However, the comparison with composition of sands from modern South-Alpine rivers should be considered with caution, especially for core sands deposited during glacial periods. Indeed, the watersheds of the Oglio, Chiese, Sarca and Adige catchments were breached during glacial culminations by several

transfluences. Particularly, the Adige glacier overstepped the Sarca watershed and fed the Garda glacier tongue (see arrow in Fig. 11a). Thus, sands from each sample of petrofacies 1 can hardly be referred to a specific present-day river catchment, but generically to the area of the Southern Alps around Oglio, Chiese, Mincio and Adige valleys.

Petrofacies 2, characterized by high quartz and feldspar content, with abundant metamorphic lithic fragments, shows a clear affinity with the composition of sands from the modern Po River (see Figs. 5, 6, 7). Quartz, Feldspars and metamorphic lithic fragments derive from the crystalline basement exposed in the central-western part of the Alps (Fig. 1b).

Petrofacies 3, characterised by abundant sedimentary lithics and a relatively low content in quartz and feldspar, shows a clear Apenninic affinity, in particular with the Enza, Secchia and Panaro rivers, (Figs. 5, 6, 7 and 12). Carbonates derive from carbonate-rich turbidites and from the calcareous blocks of the Ligurian Units (Fontana, 1991), whereas siliciclastic grains are sourced from the Ligurian, Epiligurian and Post-Evaporitic units (Ricci Lucchi et al., 1982; Ricci Lucchi, 1987). The attribution of petrofacies 3 (sample MDL 4.2, Fig. 6) to the Secchia River is constrained by geomorphological data (Castaldini et al., 2009), which depict a wide crevasse splay departing from the Secchia river course (Fig. 11e).

The subtle compositional variations within petrofacies 2 (Fig. 6) likely reflect the downstream or upstream shift of the confluences between the Po River and its transversal tributaries. As observed in modern samples (Fig. 5), the composition of Po River sands changes downstream, being influenced by the sedimentary input from the Apennine and South-Alpine tributaries (see also Tentori et al., 2021; Demurtas et al., 2022). Particularly, the Po River sands are enriched in volcanites and lithic fragments from Mesozoic carbonates after the confluence with Oglio, Chiese and Mincio rivers, and in carbonates and siliciclastic grains after the confluence with Enza, Secchia and Panaro rivers. These observations, permit to formulate hypothesis on palaeogeography at time of deposition of samples from petrofacies 2. For instance, sample SBP 49.5, including oolitic pebbles of South-Alpine provenance and a relatively high percentage of volcanic lithics (Fig. 6), has been interpreted as deposited by the Po River downstream of the confluence with a South-Alpine river (Fig. 11b). On the contrary, sample SBP 26.6, with a relatively lower content of volcanites and abundant metamorphites (Fig. 6), reflects confluences with South-Alpine rivers located downstream of site SBP (Fig. 11c). Sample MDL 13.3, dated to the Early Holocene and with a relatively high content of carbonate and siliciclastic lithics, has been interpreted as deposited by a Po River branch which collected the sedimentary input of Enza, Secchia, and possibly, Panaro rivers (Fig. 11d).

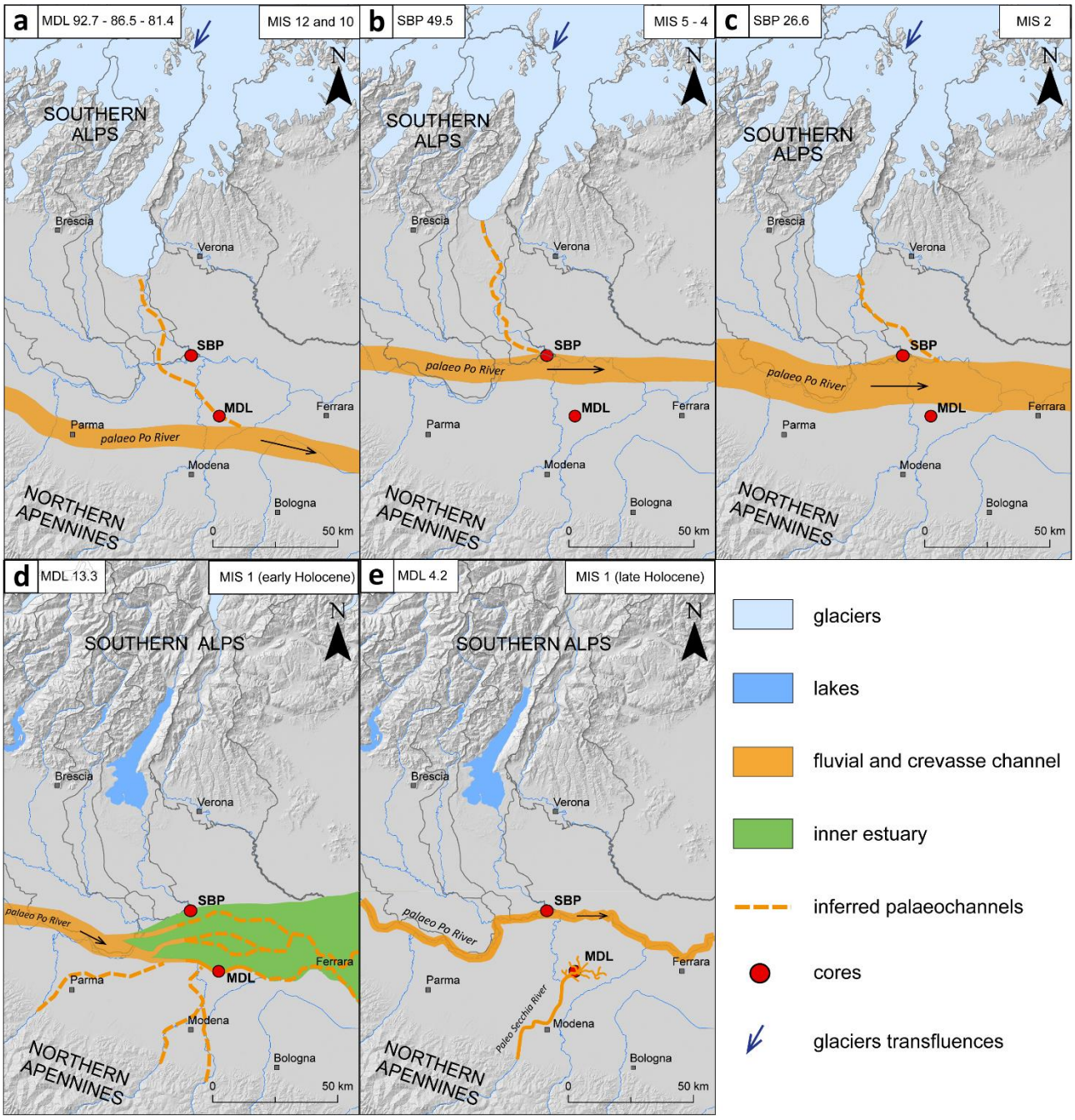

Figure 11. Palaeogeographic sketch maps showing the evolution of the Po River network during the last 500 ka and inferred palaeohydrography: (a) during MIS 12 and MIS 10 (samples MDL 92.7, 86.5, 81.4, petrofacies 1). (b) during MIS 5-4 (sample SBP 49.5, petrofacies 2). (c) during MIS 2 (sample SBP 26.6, petrofacies 2). (d) during the early Holocene (sample MDL 13.3, petrofacies 2). (e) during the late Holocene (sample MDL 4.2, petrofacies 3). The maximum extent of the Alpine glaciers during MIS 2 is from Ehlers, J. & Gibbard, P. (2011), whereas the extent of glaciers during older glacial events is hypothetical.

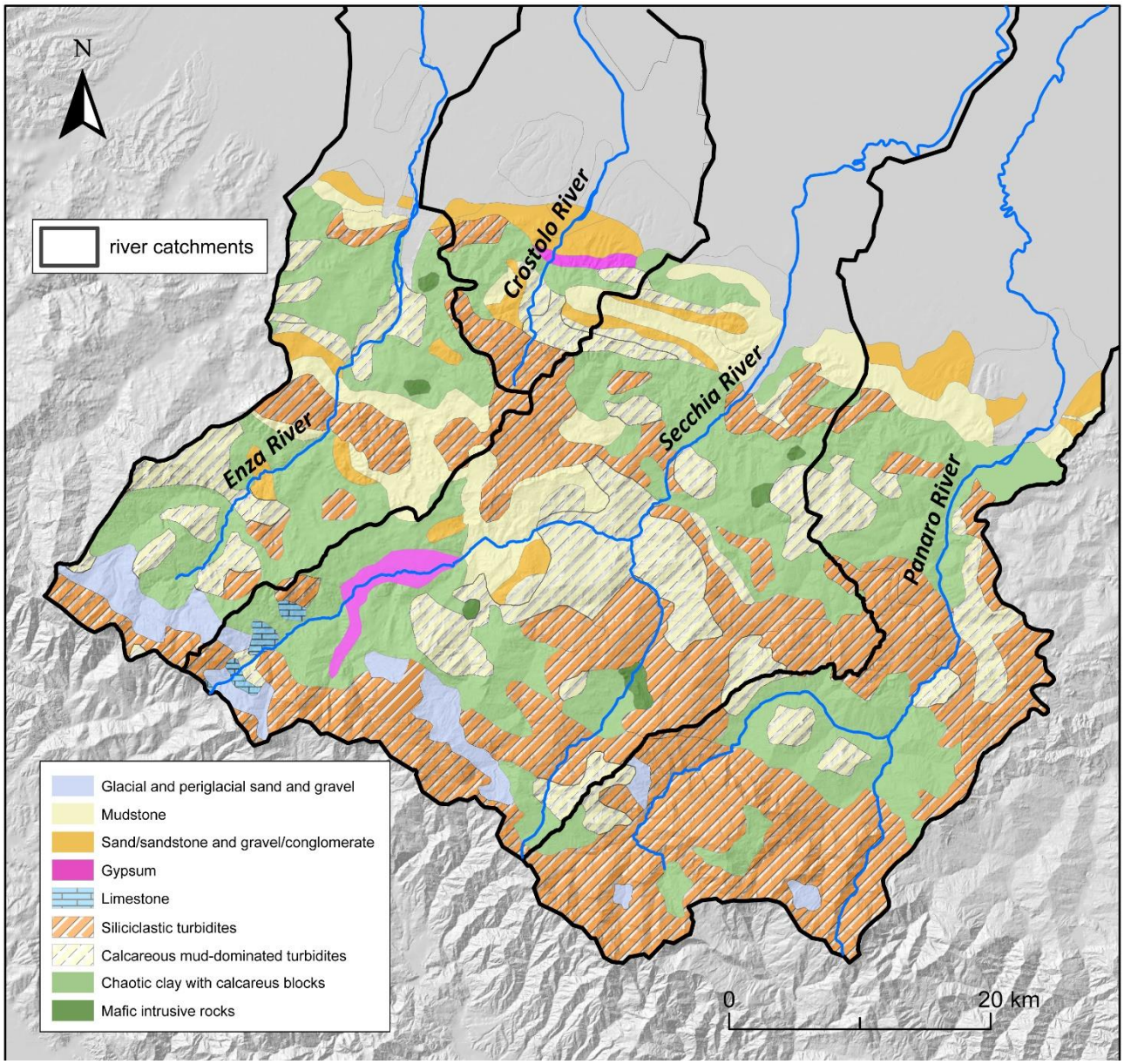

Figure 12. Geolithological map of the catchment areas of the Enza, Crostolo, Secchia and Panaro rivers. Location in Figure 1b.

4.5.2. *Evolution of the Po River network*

The hundreds meters-thick sedimentary succession deposited between cores SBP and MDL during the Middle Pleistocene (Figs. 2 and 3), testify to the efficiency of the Po Basin as an intermediate sink of the Po-Adriatic system. Sediments cored in sites SBP and MDL, derive from three source areas of the Alpine and Apennine amphitheatre: the Southern Alps, the Western Alps and the Apennines. The stacking of petrofacies 1 to 3 in core MDL records the transition from a Southern Alpine sediment delivery system to a fluvial system fed by the Apennines. This change in sediment provenance reflects the progressive northward migration of the Po River (see also

Amorosi and Sammartino, 2018; Bruno et al., 2021). The presence of sediments of South-Alpine provenance in site MDL places the Po River about 30 km south of its modern course during the deposition of the upper part of the Lower Po Synthem and of AES4 (Fig. 11a). According to pollen data, showing the presence of relict species for the Po Plain (ENEL-DCO, 1984; Fig. 2), and to basin-scale tracking of the 450 ka unconformity (Martelli et al., 2007; Geomol Team, 2015), these two units are tentatively assigned to the MIS 12 and 10 glacial stages (Fig. 3). The onset of the Po River sedimentation is marked by the development of 15-20 km-wide channel-belts during the following glacial stages (MIS 8, 6 and 2, units AES5, AES6 and AES7b in Fig. 2). During the MIS 2 (unit AES7b, Fig. 3), the southern boundary of the Po channel belt was located north of site MDL (Figs. 2, 11d), which was affected only by overbank and crevasse sedimentation (e.g. sample MDL 17.5, Fig. 6). During the Holocene, the study area became part of the inner Po estuary (11.5-7 ka BP, Bruno et al., 2017) and of the upper Po Delta Plain (last 7 ka, Amorosi et al., 2019). In the area between sites SBP and MDL, several river branches were active (Fig. 11d). During the late Holocene the Po River started to flow in the present-day position (Castaldini et al., 2009; Demurtas et al., 2022) leaving space for deposition of Apennine sediments in site MDL (AES8; Fig. 11e).

The progressive northward migration of the Po River may have occurred in response to the activity of the external Apennine thrust front (Figs. 1c and 1d), whose load may have increased subsidence rates in local sectors of the foreland (Ravazzi et al., 2013). However, additional structural data and a three-dimension reconstruction of the geometry of fluvial sand bodies are required to assess the influence of tectonics on channel-belts migration. Although, glacier advances and retreats since the Middle Pleistocene deeply influenced the amount of sediment delivered from both chains (see discussion in Garzanti et al., 2011, Simoni et al., 2013; Savi et al., 2014; Bruno et al. 2018; 2021), these cyclic events unlikely drove the northward migration of the Po River, which occurred in two main steps dated to ca. 350 ka BP and to the Late Holocene. Data from a single core (MDL) are insufficient to assess the role of the climate forcing and tectonics on the migration of Po channel belts. New core data could help to clarify the relationships with other sectors of the basin, upstream and downstream of the study area, and with the buried tectonic structures.

4.6. CONCLUSIONS

High subsidence rates allowed the accumulation and preservation in the Po Basin, of a thick alluvial succession since the Middle Pleistocene. Sedimentological, stratigraphic and petrographic analysis carried out on two cores (MDL and SBP) reveal the stacking of three petrofacies, which

reflect provenance of detritus from three distinct source areas. Petrofacies 1 is typified by a high content in limestones and dolostones, and by a relatively high percentage of volcanic lithics, which indicate provenance from the Southern Alps. Petrofacies 2, recognised in both cores, characterized by a high content of quartz, feldspar and metamorphic lithics, and scarce carbonate and volcanic lithics, is interpreted as deposited by the Po River, which carries detritus from the western part of the Alpine-Apennine amphitheatre. Petrofacies 3 is rich in sedimentary lithics (carbonate and siliciclastic) and poor in quartz and feldspar, showing affinity with the compositional signature of the modern Apennine rivers.

The changes in sediment provenance testify to the progressive northward migration of the Po River. Particularly the presence of alpine sediments at site MDL places the Po River about 30 km south of its current position during MIS 12 and 10. About 350 ka BP the Po River shifted northwards, forming 15-20 km-wide channel belts between MDL and SBP during MIS 8, 6 and 2. The Po River reached its current position during the late Holocene, leaving space for Apennine sedimentation at site MDL. The northward migration of the Po River may have occurred in response to the activity of the external Apennine thrust front, whose load may have increased subsidence rates in local sectors of the foreland. However, data presented in this work are insufficient to verify this hypothesis.

This work proves how integrated stratigraphic, sedimentological and compositional studies in key areas of Quaternary multi-sourced alluvial basins represent an efficient tool to reconstruct the evolution of fluvial networks through time. The recognition and quantification of distinct evolutionary trends in response to specific controlling factors could aid in the creation of long-term predictive models of basin evolution.

REFERENCES

Allen J.R.L. (1963). The classification of cross-stratified units with notes on their origin. *Sedimentology*, **2**, 93-114.

Amorosi, A., Pavesi, M., Ricci Lucchi, M., Sarti, G. & Piccin, A. (2008). Climatic signature of cyclic fluvial architecture from the Quaternary of the central Po Plain, Italy. *Sedimentary Geology*, **209**, 58–68.

Amorosi, A. & Sammartino, I. (2018). Shifts in sediment provenance across a hierarchy of bounding surfaces: A sequence-stratigraphic perspective from bulk-sediment geochemistry. *Sedimentary Geology*, **375**, 145–156.

Amorosi, A., Barbieri, G., Bruno, L., Campo, B., Drexler, T. M., Hong, W., ... & Bohacs, K. M. (2019). Three-fold nature of coastal progradation during the Holocene eustatic highstand, Po Plain, Italy‐close correspondence of stratal character with distribution patterns. *Sedimentology*, **66**(7), 3029-3052.

Amorosi, A., Sammartino, I., Dinelli, E., Campo, B., Guercia, T., Trincardi, F., & Pellegrini, C. (2022). Provenance and sediment dispersal in the Po-Adriatic source-to-sink system unraveled by bulk-sediment geochemistry and its linkage to catchment geology. *Earth-Science Reviews*, **104202**. https://doi.org/10.1016/j.earscirev.2022.104202.

Baroni, C., Guidobaldi, G., Salvatore, M. C., Christl, M., & Ivy-Ochs, S. (2018). Last glacial maximum glaciers in the Northern Apennines reflect primarily the influence of southerly storm-tracks in the western Mediterranean. *Quaternary Science Reviews*, **197**, 352-367.

Bonini, L., Toscani, G. & Seno, S. (2014). Three-dimensional segmentation and different rupture behavior during the 2012 Emilia seismic sequence (Northern Italy). *Tectonophysics*, **630**, 33–42.

Bronk Ramsey, C. & Lee, S. (2013). Recent and planned developments of the program OxCal. *Radiocarbon*, **55**, 720–730.

Bruno, L., Amorosi, A., Severi, P., & Bartolomei, P. (2015). High-frequency depositional cycles within the late Quaternary alluvial succession of Reno River (northern Italy). *Italian Journal of Geosciences*., **134** (2), 339–354.

Bruno, L., Bohacs, K. M., Campo, B., Drexler, T. M., Rossi, V., Sammartino, I., ... & Amorosi, A. (2017). Early Holocene transgressive palaeogeography in the Po coastal plain (northern Italy). *Sedimentology*, **64**(7), 1792-1816.

Bruno, L., Piccin, A., Sammartino, I. & Amorosi, A. (2018). Decoupled geomorphic and sedimentary response of Po River and its Alpine tributaries during the last glacial/post-glacial episode. *Geomorphology*, **317**, 184–198.

Bruno, L., Campo, B., Costagli, B., Stouthamer, E., Teatini, P., Zoccarato, C., & Amorosi, A. (2020). Factors controlling natural subsidence in the Po Plain. *Proceedings of the International Association of Hydrological Sciences*, **382**, 285-290.

Bruno, L., Amorosi, A., Lugli, S., Sammartino, I. & Fontana, D. (2021). Trunk river and tributary interactions recorded in the Pleistocene-Holocene stratigraphy of the Po Plain (northern Italy). *Sedimentology*, **68**, 2918-2943.

Campo, B., Amorosi, A. & Bruno, L. (2016). Contrasting alluvial architecture of late Pleistocene and Holocene deposits along a 120-km transect from the central Po Plain (northern Italy). *Sedimentary Geology*, **341**, 265–275.

Campo, B., Bruno, L. & Amorosi, A. (2020). Basin-scale stratigraphic correlation of late Pleistocene-Holocene (MIS 5e-MIS 1) strata across the rapidly subsiding Po Basin (northern Italy). *Quaternary Science Reviews*, **237**, 106300.

Caracciolo, L. (2020). Sediment generation and sediment routing systems from a quantitative provenance analysis perspective: Review, application and future development. *Earth-Science Reviews.*, **209**, 103226. https://doi.org/10.1016/j.earscirev.2020.103226.

Carminati, E. & Doglioni, C. (2012). Alps vs. Apennines: the paradigm of a tectonically asymmetric Earth. *Earth-Science Reviews*, **112**, 67–96.

Castaldini, D., Marchetti, M., & Cardarelli, A. (2009). Geomorphological and archaeological aspects in the central Po Plain (northern Italy). In *"Ol'man River". Geo-Archaeological Aspects Of Rivers And River Plains.* (pp. 21-22). Universiteit Gent.

Collinson, J.D. (1978). Alluvial sediments. In: H.G. Reading (Editor), Sedimentary Environments and Facies. Blackwell, Oxford.

Critelli, S., Arribas, J., Le Pera, E., Tortosa, A., Marsaglia, K. M., & Latter, K. K. (2003). The recycled orogenic sand provenance from an uplifted thrust belt, Betic Cordillera, southern Spain. *Journal of Sedimentary Research*, **73**(1), 72-81.

Demurtas, L., Bruno, L., Lugli S., & Fontana, D. (2022) Evolution of the Po Alpine River System during the Last 45 Ky Inferred from Stratigraphic and Compositional Evidence (Ostiglia, Northern Italy) *Geosciences*, **12**, 342.

Dickinson, W. R., & Rich, E. I. (1972). Petrologic intervals and petrofacies in the Great Valley sequence, Sacramento Valley, California. *Geological Society of America Bulletin*, **83**(10), 3007-3024.

Diessel, C.F.K. (1992). Coal facies and depositional environment, in: Coal-Bearing Depositional Systems. Springer, pp. 161–264.

Ehlers, J., & Gibbard, P. (2011). Quaternary glaciation. In V. P. Singh, P. Singh, & U. K. Haritashya (Eds.), *Encyclopedia of snow, ice and glaciers* (pp. 873–882).

ENEL-DCO (1984). Localizzazione di un impianto nucleare nella Regione Lombardia, completamento degli studi geologici e geomorfologici locali. Area di Viadana; Area di S. Benedetto Po; Dorsale Ferrarese: Rome, Ente Nazionale per L'Energia Elettrica– Direzione delle Costruzioni, 3 volumes.

Fontana, D. (1991)- Detrital carbonate grains as provenance indicators in the Upper Cretaceous Pietraforte Formation (northern Apennines): *Sedimentology*, **38**, p. 1085–1095.

Fontana, D., Lugli, S., Dori, S. M., Caputo, R., & Stefani, M. (2015). Sedimentology and composition of sands injected during the seismic crisis of May 2012 (Emilia, Italy): clues for source layer identification and liquefaction regime. *Sedimentary Geology*, **325**, 158-167.

Fontana, D., Amoroso, S., Minarelli, L. & Stefani, M. (2019). Sand liquefaction phenomena induced by a blast test: new insights from composition and texture of sands (late Quaternary, Emilia, Italy). *Journal of Sedimentary Research*, **89**(1), 13–27.

Garzanti, E., Ando, S., & Vezzoli, G. (2008). Settling equivalence of detrital minerals and grain-size dependence of sediment composition. *Earth and Planetary Science Letters*, **273**, 138–151.

Garzanti, E., Vezzoli, G. & Andò, S. (2011). Paleogeographic and paleodrainage changes during Pleistocene glaciations (Po Plain, Northern Italy). *Earth-Science Reviews*, **105**, 25–48.

GeoMol Team (2015). GeoMol, Assessing subsurface potentials of the Alpine Foreland Basins for sustainable planning and use of natural resources. Alpine Space Programme, Project Report, p. 188.

Goodbred Jr, S. L., & Kuehl, S. A. (2000). The significance of large sediment supply, active tectonism, and eustasy on margin sequence development: Late Quaternary stratigraphy and evolution of the Ganges–Brahmaputra delta. *Sedimentary Geology*, **133**(3-4), 227-248. https://doi.org/10.1016/S0037-0738(00)00041-5.

Gunderson, K.L., Pazzaglia, F.J., Picotti, V., Anastasio, D.A., Kodama, K.P., Rittenou, R.T., Frankel, K.F., Ponza, A., Berti, C., Negri, A. & Sabbatini, A. (2014). Unraveling tectonic and climatic controls on synorogenic growth strata (Northern Appennines, Italy). *GSA Bulletin*, ***126***-3 (4), 532–552.

Ji, H., Chen, S., Pan, S., Xu, C., Tian, Y., Li, P., ... & Chen, L. (2022). Fluvial sediment source to sink transfer at the Yellow River Delta: Quantifications, causes, and environmental impacts. *Journal of Hydrology*, **608**, 127622. https://doi.org/10.1016/j.jhydrol.2022.127622.

Li, J., Shi, X., Liu, S., Qiao, S., Zhang, H., Wu, K., ... & Kornkanitnan, N. (2021). Frequency of deep-sea turbidity as an important component of the response of a source-to-sink system to climate: A case study in the eastern middle Bengal Fan since 32 ka. *Marine Geology*, **441**, 106603. 3227, https://doi.org/10.1016/j.margeo.2021.106603.

Limonta, M., Garzanti, E., & Resentini, A. (2023). Petrology of Bengal Fan turbidites (IODP Expeditions 353 and 354): provenance versus diagenetic control. *Journal of Sedimentary Research*, **93**(4), 256-272. https://doi.org/10.2110/jsr.2022.071

Lisiecki, L. E., & Raymo, M. E. (2005). A Pliocene-Pleistocene stack of 57 globally distributed benthic δ18O records. *Paleoceanography*, **20**(1). https://doi.org/10. 1029/2004PA001071

Liu, Z., Zhao, Y., Colin, C., Stattegger, K., Wiesner, M. G., Huh, C. A., ... & Li, Y. (2016). Source-to-sink transport processes of fluvial sediments in the South China Sea. *Earth-Science Reviews*, **153**, 238-273. https://doi.org/10.1016/j.earscirev.2015.08.005.

Lugli, S., Marchetti Dori, S., Fontana, D., & Panini, F. (2004). Composition of sands in cores along the high-speed rail (TAV): preliminary indications on the sedimentary evolution of the Modena plain. *Alpine and Mediterranean Quaternary*, **17**, 379–389.

Lugli, S., Marchetti Dori, S. & Fontana, D. (2007). Alluvial sand composition as a tool to unravel the Late Quaternary sedimentation of the Modena plain, northern Italy, in Arribas, J., Critelli, S., and Johnsson, M.J., eds., Sedimentary Provenance and Petrogenesis: Perspectives from Petrography and Geochemistry. *Geological Society of America, Special Paper*, **420**, 57–72.

Marcolla, A., Monegato, G., Mozzi, P., Miola, A., & Stefani, C. (2021). Seesaw longitudinal–transverse drainage patterns driven by Middle and Late Pleistocene climate cycles in the foreland basin of the south-eastern European Alps. *Sedimentary Geology*, **421**, 105960. https://doi.org/10.1016/j.sedgeo.2021.105960.

Martelli, L., Bonini, M., Calabrese, L., Corti, G., Ercolessi, G., Molinari, F.C., Piccardi, L., Pondrelli, S., Sani, F. & Severi, P. (2017). Seismotectonic map of Emilia Romagna Region and surrounding areas to scale 1:250.000. D.R.E.Am. MAP, Pistoia, Italy.

Muttoni, G., Carcano, C., Garzanti, E., Ghielmi, M., Piccin, A., Pini, R., Rogledi, S. & Sciunnach, D. (2003). Onset of major Pleistocene glaciations in the Alps. *Geology*, **31**, 989–992.

Muttoni, G., Scardia, G., Kent, D.V., Morsiani, E., Tremolada, F., Cremaschi, M. & Peretto, C. (2011) First dated human occupation of Italy at ~0.85 Ma during the late Early Pleistocene climate transition. *Earth and Planetary Science Letters*, **307**, 241–252.

Norini, G., Aghib, F. S., Di Capua, A., Facciorusso, J., Castaldini, D., Marchetti, M., ... & Piccin, A. (2021). Assessment of liquefaction potential in the central Po plain from integrated geomorphological, stratigraphic and geotechnical analysis. *Engineering Geology*, **282**, 105997. https://doi.org/10.1016/j.enggeo.2021.105997.

Palamenghi, L., Schwenk, T., Spiess, V., & Kudrass, H. R. (2011). Seismostratigraphic analysis with centennial to decadal time resolution of the sediment sink in the Ganges–Brahmaputra subaqueous delta. *Continental Shelf Research*, **31**(6), 712-730. https://doi.org/10.1016/j.csr.2011.01.008.

Pellegrini, C., Maselli, V., Gamberi, F., Asioli, A., Bohacs, K. M., Drexler, T. M., & Trincardi, F. (2017). How to make a 350-m-thick lowstand systems tract in 17,000 years: The Late Pleistocene Po River (Italy) lowstand wedge. *Geology*, **45**(4), 327-330. https://doi.org/10.1130/G38848.1

Piovan, S., Mozzi, P., & Stefani, C., (2010). Bronze Age paleohydrography of the southern venetian Plain. *Geoarchaeology An Int. J.*, **25**, pp. 6-35.

Ravazzi, C., Marchetti, M., Zanon, M., Perego, R., Quirino, T., Deaddis, M., ... & Margaritora, D. (2013). Lake evolution and landscape history in the lower Mincio River valley, unravelling drainage changes in the central Po Plain (N-Italy) since the Bronze Age. *Quaternary international*, **288**, 195-205.

Razum, I., Lužar-Oberiter, B., Zaccarini, F., Babić, L., Miko, S., Hasan, O., ... & Pawlowsky-Glahn, V. (2021). New sediment provenance approach based on orthonormal log ratio transformation of geochemical and heavy mineral data: Sources of eolian sands from the southeastern Adriatic archipelago. *Chemical geology*, **583**, 120451.

Reimer, P. J., Austin, W. E., Bard, E., Bayliss, A., Blackwell, P. G., Ramsey, C. B., ... & Talamo, S. (2020). The IntCal20 Northern Hemisphere radiocarbon age calibration curve (0–55 cal kBP). *Radiocarbon*, **62**(4), 725-757.

Remitti, F., Vannucchi, P., Bettelli, G., Fantoni, L., Panini, F. & Vescovi, P. (2011). Tectonic and sedimentary evolution of the frontal part of an ancient subduction complex at the transition from accretion to erosion: The case of the Ligurian wedge of the northern Apennines, Italy. *Geological Society of America Bulletin*, **123**(1-2), 51–70.

Ricci Lucchi, F., Colalongo, M.L., Cremonini, G., Gasperi, G.F., Iaccarino, S., Papani G., Raffi, S. & Rio, D. (1982). Evoluzione sedimentaria e paleogeografica nel margine appenninico. In: Cremonini G. & Ricci Lucchi F. (eds.), Guida alla geologia del margine appenninico padano. Guide Geologiche Regionali S.G.I, Bologna, 17-46 *(in Italian)*.

Ricci Lucchi, F. (1987) Semi-allochtonous sedimentation in the Apenninic thrust belt. *Sedimentary Geology*, **50**, 119-134.

Richardson, J.L. & Vepraskas, M.J. (2001). Wetland soilsgenesis, hydrology, landscapes, and classification. CRC Press, LLC, 2000 N. W. Corporate Blvd., Boca Raton, FL 33431. Hardback, 417 pp.

Savi, S., Norton, K. P., Picotti, V., Akçar, N., Delunel, R., Brardinoni, F., ... & Schlunegger, F. (2014). Quantifying sediment supply at the end of the last glaciation: Dynamic reconstruction of an alpine debris-flow fan. *Geological Society of America Bulletin*, **126**(5-6), 773-790.

Scardia, G., Muttoni, G. & Sciunnach, D. (2006). Subsurface magnetostratigraphy of Pleistocene sediments from the Po Plain (Italy): Constraints on rates of sedimentation and rock uplift. *Geological Society of America Bulletin*, **118**, 1299–1312.

Schroeder, A., Wiesner, M. G., & Liu, Z. (2015). Fluxes of clay minerals in the South China Sea. *Earth and Planetary Science Letters*, **430**, 30-42. https://doi.org/10.1016/j.epsl.2015.08.001.

Simoni, A., Ponza, A., Picotti, V., & Berti, M. (2013). Landslide-related sediment yield rate in a large Apenninic catchment. In Margottini, C., Canuti, P., Sassa, K. (eds). *Landslide Science and Practice*: Volume 4: *Global Environmental Change*, **307**-313.

Singh, I.B. (1972). On the bedding in the natural-levee and point-bar deposits of the Gomti River, Uttar Pradesh, India. *Sedimentary Geology*, **7**, 309-317.

Sinha, R., Gibling, M.R., Kettanah, Y., Tandon, S.K., Bhattacharja, P.S., Dasgupta, A.S. & Ghazanfari, P. (2009) Craton-derived alluvium as a major sediment source in the Himalayan Foreland Basin of India. *GSA Bulletin*, **121**(11/12), 1596-1610.

Stefani C. (2002). Variation in terrigenous supplies in the Upper Pliocene to Recent deposits of the Venice area. *Sedimentary Geology*, **153**, Issues 1–2, Pages 43-55. ISSN 0037-0738, https://doi.org/10.1016/S0037-0738(02)00101-X.

Stolt, M.H. & Rabenhorst, M.C. (2011). Introduction and historical development of subaqueous soil concepts. In: Huang, P.M., et al. (Eds.), Handbook of Soil Science. CRC Press, LLC, Boca Raton, FL, ISBN 978-1-4398-0305-9.

Tentori, D., Milli, S., & Marsaglia, K. M. (2018). A source-to-sink compositional model of a present highstand: an example in the low-rank Tiber depositional sequence (Latium Tyrrhenian margin, Italy). *Journal of Sedimentary Research*, **88**(10), 1238-1259.

Tentori, D., Amorosi, A., Milli, S., & Marsaglia, K.M. (2021). Sediment dispersal pathways in the Po coastal plain since the Last Glacial Maximum: Provenance signals of autogenic and eustatic forcing. *Basin Research*, **33**, 1407–1428.

Turrini, C., Lacombe, O., & Roure, F. (2014). Present-day 3D structural model of the Po Valley basin, Northern Italy. *Marine and Petroleum Geology*, **56**, 266–289. https://doi.org/10.1016/j.marpetgeo.2014.02.006

Van Grinsven, M., Marsaglia, K. M., & Romans, B. W. (2019). Sand Provenance from Source to Sink in the Santa Monica Basin, California Borderlands: Significance of Calleguas Creek Input. https://doi.org/10.2110/sepmsp.110.06

Weltje, G.J. (2004). A quantitative approach to capturing the compositional variability of modern sands. *Sedimentary Geology*, **171**, 59–77.

Xue, Z., Liu, J. P., DeMaster, D., Van Nguyen, L., & Ta, T. (2010). Late Holocene evolution of the Mekong subaqueous delta, southern Vietnam. *Marine Geology*, **269**(1-2), 46-60. https://doi.org/10.1016/j.margeo.2009.12.005.

Zuffa, G.G. (1985). Optical analyses of arenites: influence of methodology on compositional results, in Zuffa, G., ed., Provenance of Arenites: Dordrecht, Netherlands, D. Reidel, NATO Advanced Study Institute, v. **148**, p. 165–189.

CHAPTER 5. Evolution of the Po–Alpine River System during the Last 45 Ky Inferred from Stratigraphic and Compositional Evidence (Ostiglia, Northern Italy)

Luca Demurtas *, Luigi Bruno*, Stefano Lugli and Daniela Fontana

Department of Chemical and Geological Sciences, University of Modena and Reggio Emilia, Via Campi 103, Modena, 41125, Italy; luigi.bruno@unimore,it (L.B.); stefano.lugli@unimore.it (S.L.); daniela.fontana@unimore.it (D.F.)

*Correspondence: luca.demurtas@unimore.it (L.D.); luigi.bruno@unimore.it (L.B.)

DOI: https://doi.org/10.3390/geosciences12090342

Abstract

The stratigraphic and compositional study of three sediment cores recovered close to the Po River near Ostiglia provides clues on changes in fluvial dynamics at the transition from the last glacial to the present interglacial. Upper Pleistocene units are dominated by sands with high content in volcanic lithics, denoting high sediment supply from the south-Alpine fluvio-glacial tributary system. The Early–Mid Holocene unit, peat-rich and barren in fluvial sands, results from low sediment supply and waterlogging, encompassing the maximum marine ingression. The Late Holocene unit, characterized by fluvial-channel sands with lower content in volcanics and relatively abundant metamorphic lithics, records the Po River sedimentation since the Late Bronze Age. Late Holocene sands show a lower content in siliciclastic lithic fragments (supplied mainly by Apennine tributaries) compared to modern Po River sands. This distinctive composition could reflect the diversion of Apennine sediments into a southern Po River branch during the Late Bronze Age and into an Apennine collector flowing south of Ostiglia during Roman times and the Middle Ages. The integrated stratigraphic-compositional methods used in this study permitted to recon-struct the major climate-related changes in sediment dispersal and may be potentially applied to other alluvial and coastal settings.

Keywords: Upper Pleistocene–Holocene stratigraphy; sand composition; Po River; Alpine–Apennine tributaries

5.1. INTRODUCTION

Alluvial and coastal plains store in their subsurface evidence of past environmental changes. In multi-sourced alluvial basins, compositional data, framed in a detailed stratigraphic picture, may provide clues on changes in sediment provenance that reflect past modifications of the river network (Singh et al., 2008; Sinha et al., 2009; Tentori et al., 2018; Marcolla et al., 2021). An integrated stratigraphic-compositional approach is particularly effective in late Quaternary studies for two main reasons: (i) drainage basins did not experience significant modifications during this relatively short time window, and the composition of preserved deposits is essentially comparable with composition of modern rivers (Garzanti et al., 2011; Tentori et al., 2021); (ii) the availability of high-resolution dating permits a chronological control on alluvial stratigraphy at the scale of the millennia/centuries (Rittenour, 2018; Molodkov, 2020; Reimer et al., 2020). In this perspective, every single sediment body can potentially be related to the activity of a specific watercourse during a precise time interval.

The Po Basin, in northern Italy, is a multi-sourced sedimentary basin fed by the Po River and a dense network of tributaries. Most of these rivers flow unconfined in the alluvial plain for large tracts of their courses (Castiglioni et al., 1997). This configuration resulted in frequent nodal avulsions before the construction of metre-high embankments (Correggiari et al., 2005; Morelli et al., 2017). As a consequence, different watercourses deposited their load in different areas through time (Garzanti et al., 2011; Fontana et al., 2019; Bruno et al., 2021; Tentori et al., 2021). The aim of

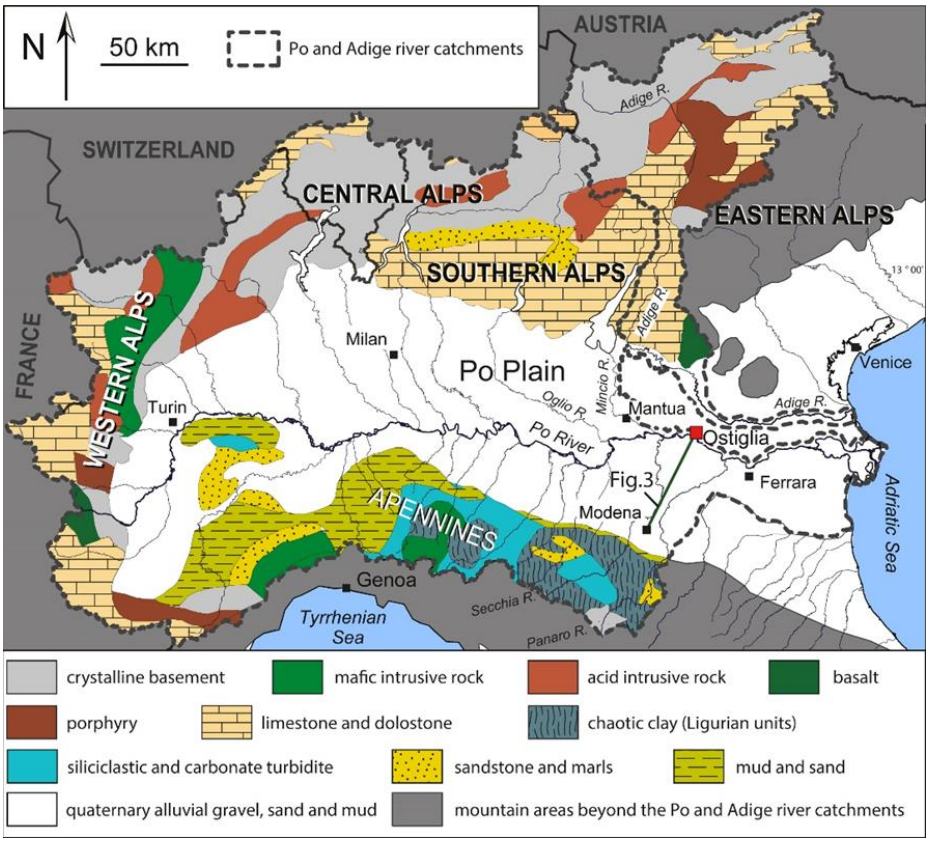

Figure 1. Lithological map of the Po and Adige river catchments. Lithological units cropping out in the drainage basin of the Po and Adige rivers (modified after Bruno et al., 2021).

this work is the reconstruction of the depositional history of the area around the town of Ostiglia, located on the eastern side of a Po meander (Figures 1 and 2). Historians Polybius and Plinius document that the Po River already flowed in the Ostiglia area in Roman times (*Naturalis Historia*, XXI-73). However, historical notes and archaeological data allow the stepping back in time for just a few millennia. In this work the major hydrographic changes in the Ostiglia area during the last 45 millennia were reconstructed through combined stratigraphic and petrographic analysis on three 30-m long cores recovered along the northern embankment of the Po River. The aims of this paper are: (i) to contribute to the reconstruction of the sedimentary evolution of the Po alluvial plain during the Late Pleistocene and Holocene; (ii) to highlight how the major changes in the Po River network are reflected in the sedimentary record of a relatively narrow 20 km^2 area; (iii) to discuss the main factors controlling fluvial architecture.

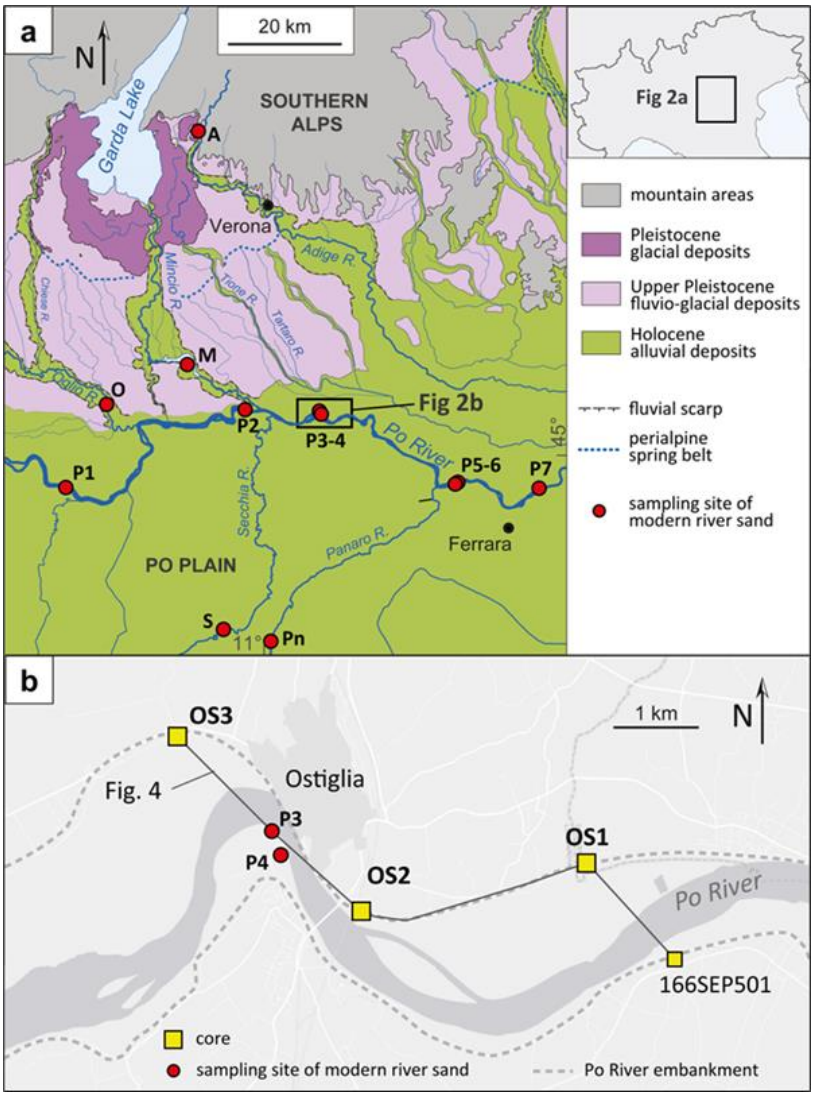

Figure 2. Location of study area. (a): Geological map of the Po Plain with location of the study area and of sampling sites of modern river sands (modified after Fontana et al., 2014). (b): close-up on the study area with the locations of the analysed cores.

5.2. BACKGROUND

5.2.1. *The Po Basin*

The Po Basin in Northern Italy (Figure 1) is a foreland basin bounded by two mountain chains, the south-verging Southern Alps to the north and the north-verging Northern Apennines to the south (Turrini et al., 2016). This structural setting originated in response to the collision between the Adria microplate and Eurasia, which began in the Cretaceous (Carminati & Doglioni, 2012 and references therein). High subsidence rates in the Po Plain were generated by the tectonic loading of the two chains (Carminati & Di Donato, 1999; Antonioli et al., 2009; Bruno et al., 2020).

The Po Basin records a complete foredeep cycle, from underfilled (deep marine) to overfilled (continental) stage (Amadori et al., 2019). The beginning of continental sedimentation is marked by a regional unconformity dated to ca. 870 ky BP (Muttoni e al., 2003, 2011; Scardia et al., 2006; Gunderson et al., 2014). Continental deposits are up to 400 m thick (Bruno et al., 2021).

Upper Pleistocene to Holocene continental deposits in the study area display a clear bipartition between a mud-dominated southern sector fed by Apennine rivers (Bruno et al., 2021), and a sand-dominated northern sector (Figure 3) fed by the Po River and its Alpine tributaries (Bruno et al., 2018, 2021; Fontana et al., 2019). The Po River deposited a 20-km wide channel-belt sand body during the Würmian glaciation (Figure 3; Bruno et al., 2021).

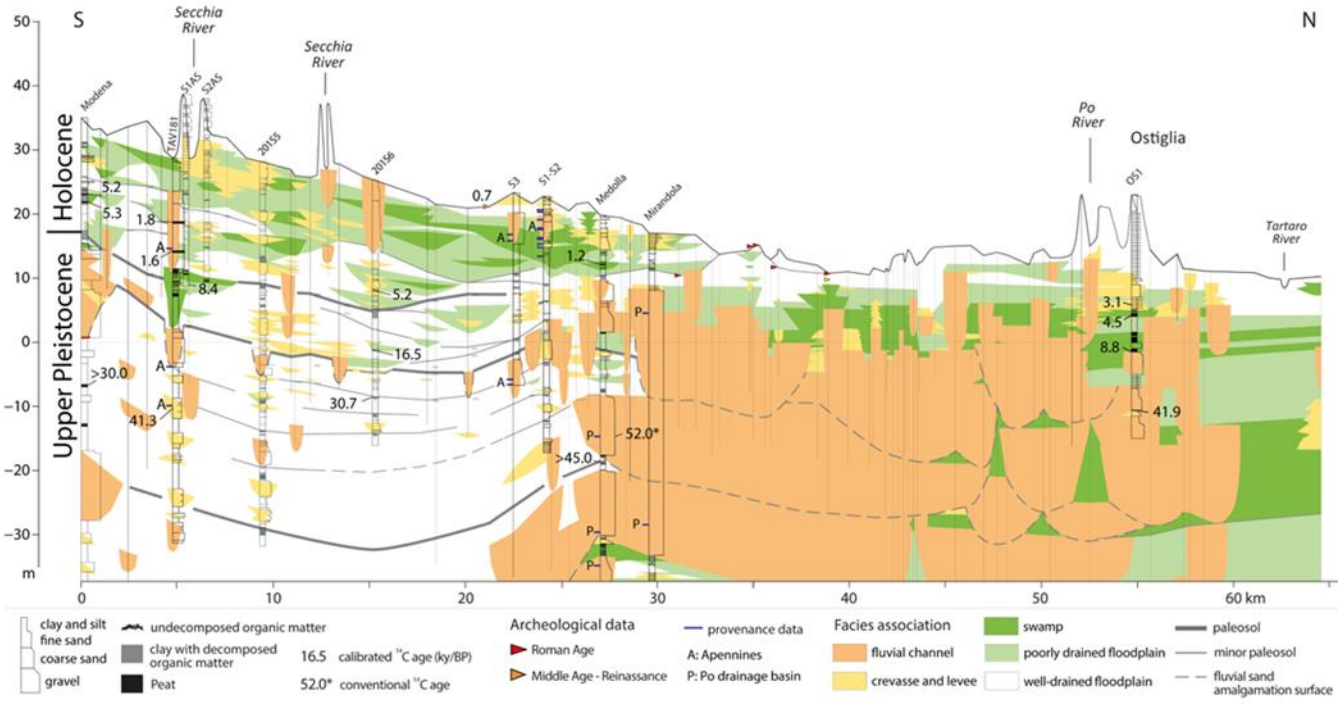

Figure 3. Late Quaternary stratigraphy of the Po Plain. Stratigraphic architecture of Upper Pleistocene and Holocene deposits along a south-north oriented stratigraphic cross section (modified after Bruno et al., 2021). Location in Figure 1.

Holocene deposits are instead characterized by ribbon-shaped fluvial channel bodies enclosed in abundant poorly drained floodplains and swamp muds (Campo et al., 2016). The boundary between the Po and the South-Alpine deposits has been locally reconstructed. West of the study area it corresponds to an erosional surface which separates Upper Pleistocene fluvio-glacial (South-Alpine) deposits to the north from Holocene fluvial deposits to the south (Bruno et al., 2018). East of the study area, in the coastal plain, stratigraphic and compositional data highlight a dynamic system fed by a distal paleo-Po River with episodic sediment input from the South Alpine and Apennine rivers (Tentori et la., 2021).

5.2.2. *The Po Drainage System*

The Po River, the longest watercourse in Italy, originates in the Western Alps, which are characterized by extensive outcrops of ultramafic and metamorphic rocks (Figure 1). Along its 652-km-long course towards the Adriatic Sea, the Po River interacts with a dense network of transverse tributaries draining catchments with distinct lithotypes. The northern tributaries from the Central and Southern Alps drain an area mainly characterized by carbonate (limestone and dolostone), plutonic-volcanic and metamorphic rocks (Figure 1). In the Po Plain sector, these rivers flow entrenched into Upper Pleistocene fluvio-glacial deposits, bordered by fluvial scarps, with maximum height of about 40 m close to the alpine margin. Based on sparse radiocarbon dates, Alpine rivers' entrenchment is dated to the end of Last Glacial Maximum (LGM, ca. 17–18 ky BP; Fontana et al., 2014; Campo et al., 2016; Bruno et al., 2018). Close to the Ostiglia area, the main tributaries of the Po River are the Oglio and Mincio rivers. Both rivers are effluent of peri-Alpine lakes (Iseo and Garda, respectively), which formed after the LGM in place of former glacial tongues (Fontana et al., 2014). The Adige River flows in north-south direction east of the Garda Lake, and then turns eastward, towards the Adriatic Sea (Figures 1 and 2). A set of minor rivers originated by a spring line located few kilometres south of the Alpine piedmont (Figure 2a); among these, the Tione and Tartaro rivers flow close to the Ostiglia area. The main southern tributaries of the Po River flowing through the study area are the Secchia and Panaro rivers. These rivers drain a sector of the northern Apennines dominated by sandstone, limestones, mudstone and flow in the Po Plain, bordered by anthropogenic levees. Whereas the South Alpine drainage system did not experience substantial modifications during the Holocene, the Apennine river system was characterized by a strong channel mobility, as highlighted by a dense network of abandoned fluvial ridges (Castiglioni et al., 1997).

5.3. MATERIALS AND METHODS

The village of Ostiglia is located on the north bank of a Po River meander (Figure 2b) close to the confluence of the Oglio (31 km), Mincio (11 km) and Secchia rivers (9 km) and 58 km south of the Adige valley outlet. The Tione and Tartaro rivers, and a set of minor watercourses originating from the perialpine spring-line, flow only 4 km north of Ostiglia. This particular location makes Ostiglia a key area for assessing Late Pleistocene and Holocene changes in sediment provenance through the analysis of core sediments.

Three cores (OS1, OS2 and OS3, locations in Figure 2b), 38-m-long, recovered along the Po River embankment, have been analysed and sampled for the characterisation of the depositional facies. Each core has been described in terms of lithology, grain-size, colour, consistency and accessory material (vegetal remains, peat and carbonate concretions). This study benefits from a well-known stratigraphy and from 15 radiocarbon dates from previous works (Campo et al., 2016; Bruno et al., 2021). The chronological framework has been improved with five new radiocarbon dates from wood, peat and soil samples collected from cores OS1 and OS3, carried out at the Geoanalysis center of the Korea Institute of Geoscience and Mineral Resources (KIGAM). Conventional ^{14}C ages were calibrated using OxCal 4.4 (Bronk Ramsey & Lee, 2013) with the IntCal 20 curve (see Table 1; Reimer et al., 2020). Facies associations, observed in the analysed cores, were correlated in a 7.3 km-long cross-section with the aid of available ^{14}C data. A nearby core from Campo et al. (2016) has also been considered. Stratigraphic units were defined, based on facies relationships and on the identification and lateral tracking of their bounding surfaces. The latter are marked by: (i) sharp facies change; (ii) erosional surfaces or (iii) amalgamation surfaces.

Table 1. List of radiocarbon dates. Details on radiocarbon dates from cores OS1 and OS3.

Core	Lab	Material	Depth (m)	^{14}C Age	Calibrated Age (mean ± 2σ)	Lab Code
OS3	KIGAM	soil	13.7	2442 ± 25	2520 ± 220	KGM-OSa200128
OS1	KIGAM	wood	17.2	2949 ± 25	3100 ± 50	KGM-OWd200614
OS1	KIGAM	peat	18.8	4030 ± 26	4490 ± 40	KGM-OWd200623
OS1	KIGAM	peat	24.5	7924 ± 34	8780 ± 220	KGM-OSa200130
OS1	KIGAM	peat	33.6	37111 ± 245	41900 ± 400	KGM-OSa200127

Petrographic analyses were carried out on 14 samples: 8 sand samples were collected from cores OS1 and OS2 and 6 from modern rivers. The modal analyses of cores were compared with detrital modes of samples collected from modern rivers: Po (3 samples, this work; 4 samples from Bruno et al., 2021), Oglio (sample O in Figure 2a), Mincio (sample M) and Adige (sample A). The composition of modern Secchia and Panaro rivers (Lugli et al., 2004, 2007) was also considered. Samples were treated with dilute H_2O_2 to remove organic matter and were dried and sieved to obtain fine-sand fraction (0.250–0.125 mm, 2–3 ϕ). The selected fraction was impregnated in epoxy resin under vacuum and processed to obtain thin sections. Point counting of 300 grains for each thin section, was performed under transmitted-light microscopy according to the Gazzi-Dickinson method, designed to minimize the dependence of the analysis on the grain-size (Zuffa, 1985). Although all grain components were analysed, only those with similar hydraulic behaviour (quartz, feldspars and lithic fragments—volcanic, metamorphic and sedimentary) were considered for provenance analyses (see Garzanti et al., 2008). Considering that the transport invariant components are essential for provenance analyses as demonstrated by Weltje (2004), Garzanti et al., (2008) and Razum et al., (2021). Along single core, one sample per stratigraphic unit was collected, based on the assumption of low intra-unit compositional variations, see Lugli et al., (2004, 2007), Fontana et al., (2019) and Bruno et al., (2021).

5.4. RESULTS

5.4.1. *Facies Associations*

This section provides a brief description of facies associations recognized through analysis of cores OS1, OS2 and OS3. Five facies associations have been identified based on lithology, grain-size, grain-size trends, colour, consistency and accessory material (wood, plant remains, peat, carbonate concretions, iron and manganese oxides, macrofossils).

5.4.1.1. Fluvial Channel (Fc)

This facies association is characterized by sand bodies more than 3.5 m thick (Figure 4). Sand is coarse to fine, with an overall fining-upward (FU) trend. Accessory materials, such as wood, vegetal remains and fragments of freshwater fossils, are rare.

Based on lithology, thickness and internal FU trend, this facies association could be interpreted as fluvial-channel deposits (Allen, 1963).

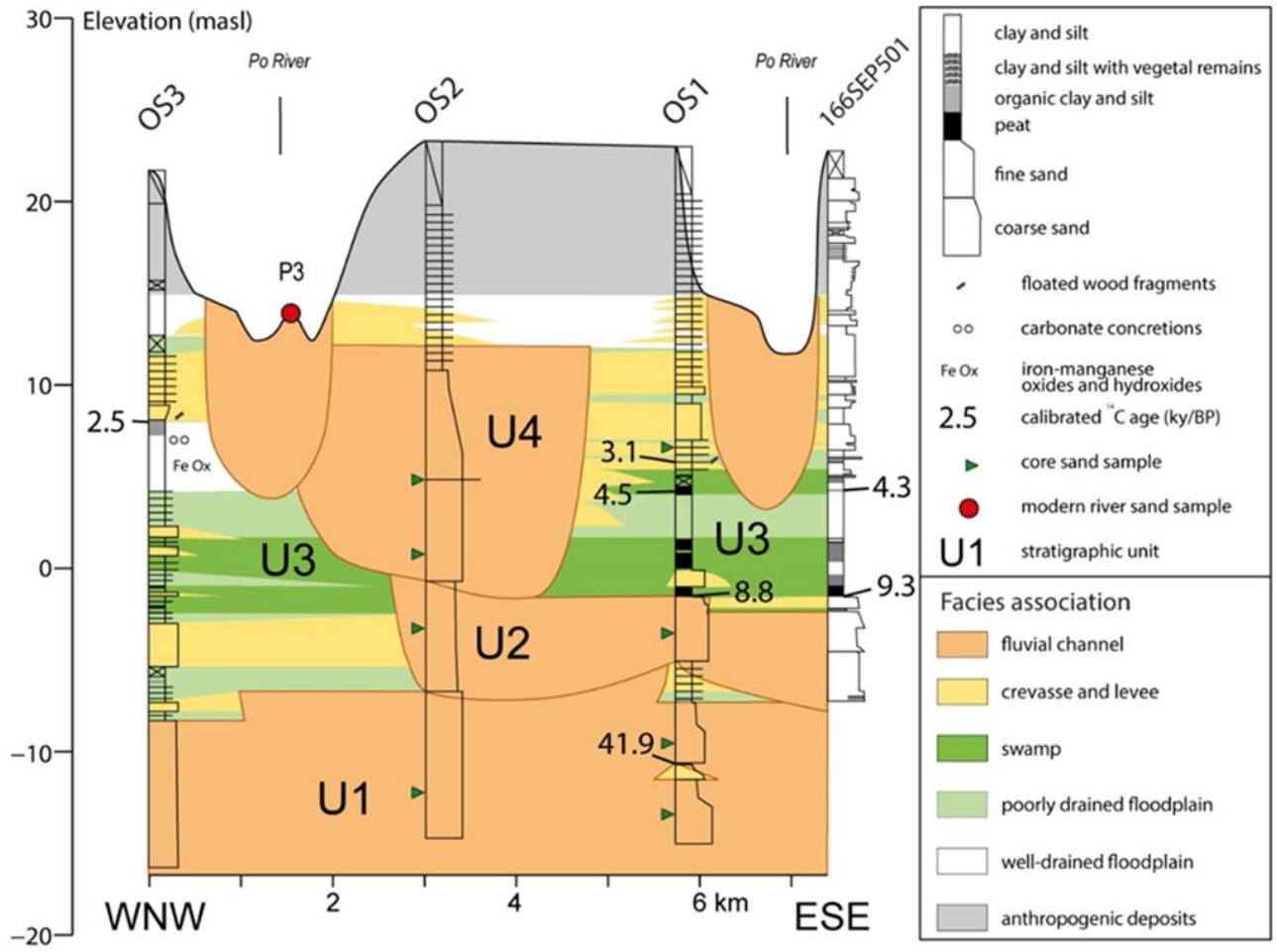

Figure 4. Stratigraphy of the Ostiglia area. Correlation panel showing facies distribution in the subsurface of the study area down to 38 m depth (location in Figure 2b). Details on radiocarbon dates from cores OS1 and OS3 are in Table 1. Stratigraphy and radiocarbon dates from core 166SEP501 are from Campo et al., (2016).

5.4.1.2. Crevasse and Levee (CL)

This facies association has a maximum thickness of 5 m and has been observed in cores OS1 and OS3; it consists of fine sand, silty sand and sandy silt, with both coarsening-upward (CU) and FU trend, locally arranged in rhythmic alternations at the decimetre scale. This facies association is laterally associated with fluvial-channel deposits (Figure 4). Floated wood fragments are rare.

Grain size, thickness and lateral relationships with fluvial channel facies permit to interpret these deposits as a channel-related facies association. Sand bodies with internal CU trends are interpreted as crevasse splays (the upward increase in grain size registers the progressive breach of the levee), whereas FU sands correspond to crevasse-channel deposits. Sand–clay alternations are interpreted as levee deposits, formed in response to repeated overflow events.

5.4.1.3. Swamp (SW)

This facies association, observed in cores OS1 and OS3, consists of plastic to very plastic clays and silty-clays, with occasional millimetre-scale sandy silt intercalations. Thickness ranges between 1.3 and 3 m. Colour is grey or dark grey. Organic matter is abundant in the form of sparse vegetal remains and of wood–peat layers. Rare fragments of freshwater fossils have been observed. Iron and manganese oxides are absent.

The grain size of these deposits suggests a low-energy interfluvial environment. The dark colour and the abundance of organic matter indicate reducing conditions, typical of swamp environments, that favoured the preservation of plants remains. (Diessel, 1992; Stolt & Rabenhorst 2011).

5.4.1.4. Poorly Drained Floodplain (PDF)

This facies association, up to 2 m-thick, includes light grey clay and silt with plastic consistency (Figure 4). Plant remains and wood fragments are rare, as well as freshwater mollusc fragments. Iron and manganese oxides and hydroxides are absent. Isolated millimetre-scale carbonate concretions have been observed.

The fine-grained size combined with the presence of carbonate nodules suggest sedimentation in an interfluvial environment. The grey colour, as well as the absence of oxidation-reduction features, indicates poor drainage conditions (poorly drained floodplain).

5.4.1.5. Well-Drained Floodplain (WDF)

This facies association is observed only in the core OS3 at about 15 m depth. It is about 4 m thick and consists of yellow-brownish clays with compact consistency. Carbonate concretions and iron-manganese oxides and hydroxides were observed. Undecomposed plant remains and body fossils are absent.

Grain-size indicates a low-energy interfluvial environment, while the compact texture, the colour and the presence of carbonate concretions and iron and manganese oxides suggest a low groundwater table. These features are ascribable to a well-drained floodplain environment.

5.4.1.6. Anthropogenic Deposits

This facies association, corresponding to the uppermost 9 m of the cored succession (Figure 4), is composed of a mixture of clay, silt and silty sand, including anthropogenic material (mainly concrete and brick fragments).

These deposits constitute the modern artificial levees of the Po River.

5.4.2. *Stratigraphy of Cores OS1, OS2 and OS3*

The correlation of facies associations recognized in cores OS1, OS2 and OS3, combined with those described in core 166SEP501 (Campo et al., 2016), led to the definition of four stratigraphic units (U1 to U4 in Figure 4).

The deepest unit U1 is dominated by fluvial channel sands, with a thin (~1 m) crevasse-levee lens observed in OS1 at about 34 m depth. This unit extends along the whole cross-section from bottom-cores to about 30 m depth (−7 m asl). The boundary with the overlying unit U2 is erosional in cores OS2 and 166SEP501 and marked by the upward transition to the poorly drained floodplain and crevasse-and-levee deposits in OS1 and OS3. The radiocarbon date of 41.9 ky BP from core OS1 indicates a Late Pleistocene age for this unit.

Unit U2 is characterized by the presence of less extensive fluvial channel deposits, 5–8 m thick, passing laterally to poorly drained floodplain and crevasse-and-levee deposits (Figure 4). The upper contact with U3 is marked by a peat layer in cores OS3, OS1 and 166SEP501 (Figure 4). In OS2, unit U2 is overlain by U4 with erosional contact, which was tentatively placed in correspondence of a subtle grain-size change at 24 m depth. Available radiocarbon dates from the underlying unit U1 and from peat layers of cores OS1 and 166SEP501 (8.7 and 9.3 ky BP, respectively), suggest deposition of this unit during the Late Pleistocene–Holocene transition.

Unit U3, about 7 m thick, is preserved in cores OS3, OS1 and 166SEP501 and is dominated by swamp and PDFP deposits (Figure 4). Crevasse-and-levee deposits are rare and rather thin (<1 m); fluvial channel sands are absent. Peat layers are abundant at the base and at the top of the unit. A paleosol marks the top of the unit in core OS3. Radiocarbon dates permit to assigning this unit to 9–2.5 ky BP.

U4 is characterized by a 11.5 m-thick fluvial-channel sand body in OS2 and by the associated crevasse-levee deposits in OS3, OS1 and 166SEP501 (Figure 4). The lower boundary of the unit is diachronous. Indeed, crevasse-levee deposits attributed to U4 are dated to 3.1 ky BP in OS1 and are younger than 2.5 ky BP in OS3.

Unit U4 is locally overlain by anthropogenic deposits, which represent the modern artificial levees of the Po River (Figure 4).

5.4.3. *Sand Petrography*

5.4.3.1. Core Sands

The results of the modal analysis were plotted in the Q + F (quartz and feldspar)– L (siliciclastic lithic)– C (carbonate lithic) ternary diagram (Figure 5a) and reported in the barchart of Figure 6a. The distribution of lithic fragments is shown in the diagram of Figure 5a: Lm (metamorphic lithic)– Lv (volcanic lithic)– Ls (sedimentary lithic, carbonate included). Samples were collected from units U1 (3 samples), U2 (2 samples) and U4 (3 samples). Sands suitable for petrographic analyses were not encountered in unit U3.

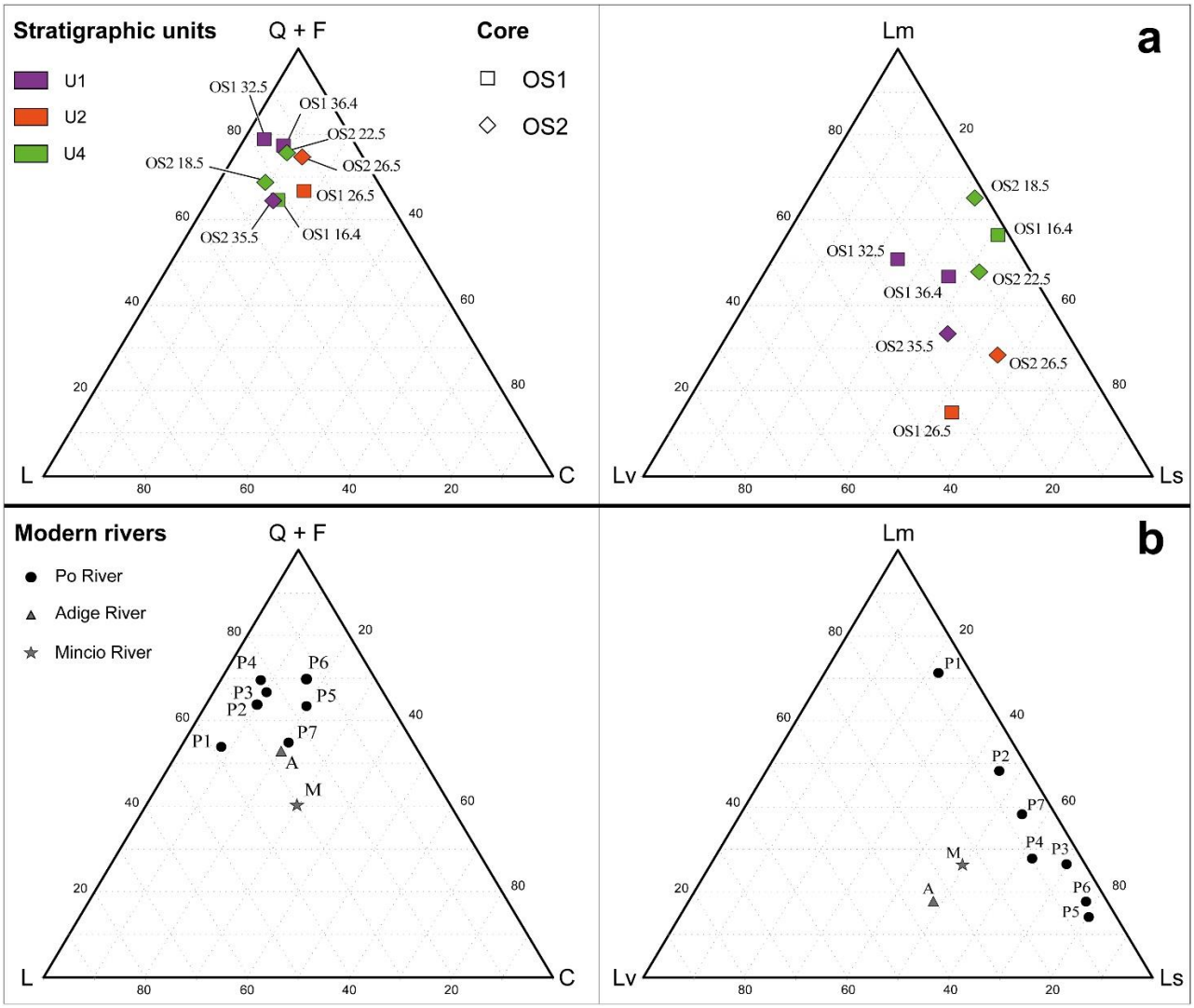

Figure 5. Composition of sands from Ostiglia cores and modern rivers. Ternary diagrams showing composition of sands from cores OS1 and OS2 (a) and from modern rivers (b). Q + F: quartz and feldspar; L: siliciclastic lithics; C: carbonate lithics; Lm: metamorphic lithic; Lv: volcanic lithic; Ls: sedimentary lithic.

The analysed sands exhibit an overall abundance of quartz and feldspars, with values ranging from 76% of the analysed sand fraction in the deepest unit U1 (OS1 32.5) to 57% in the shallowest

unit U4 (OS1 16.4). Quartz is generally more abundant than feldspars and is present mainly as single crystal; both fine- and coarse-grained polycrystalline quartz are subordinate. Feldspars include both plagioclase and k-feldspar, the latter represented mainly by orthoclase and microcline. Metamorphic lithics, consisting of low-grade phillades and micascists, are present in all samples and relatively more abundant in unit U4, reaching values close to 20% in samples OS1 16.4 and OS2 18.5. Volcanic lithics are relatively abundant in units U1 and U2, where they represent up to 10% of the sample, whereas unit U4 shows very low values, <1% (OS1 16.4 and OS2 18.5). Volcanics are mainly acidic aphanitic to microcrystalline, more rarely with porphyritic structure.

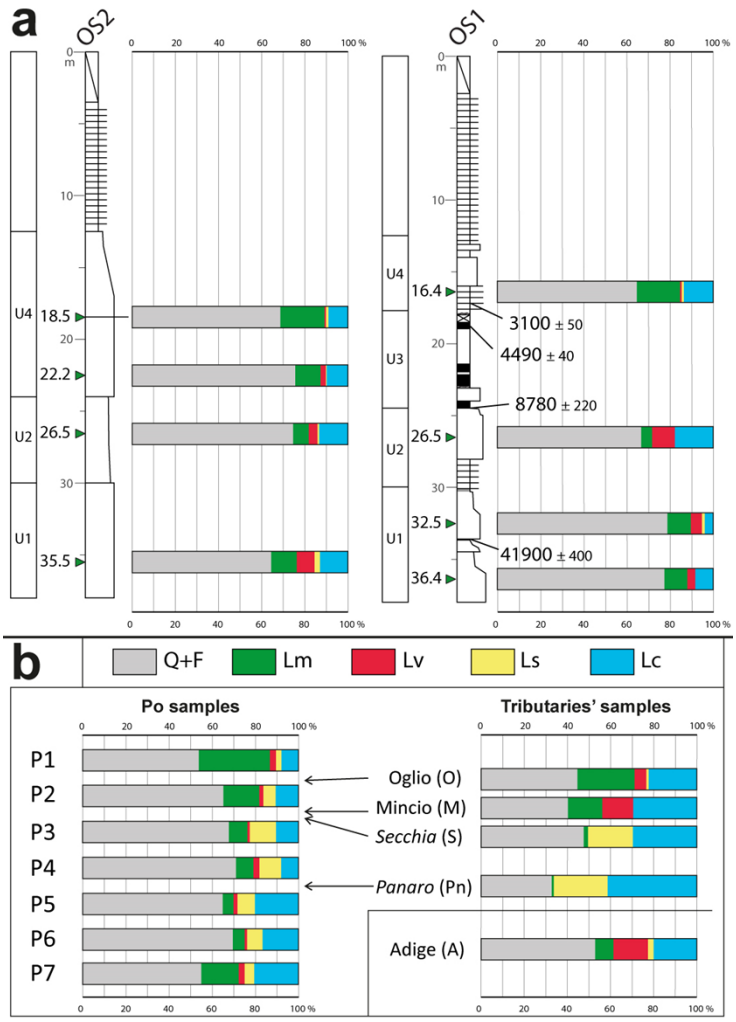

Figure 6. Composition of sand samples reported as barchart (a): composition of sands from OS2 and OS1 reported in the logs at the sampling level. (b): composition of sands from the modern Po, Oglio, Mincio, Secchia, Panaro and Adige rivers. The arrows indicate river confluences. The Adige River is shown in a separate box as it is not a Po tributary. Apennine rivers are in italics.

Sedimentary lithics consist almost exclusively of carbonate lithics that constitute 10–15% of the examined samples. Values lower than 10% are observed in samples OS1 32.5 and OS1 36.4 (unit U1). Only sample OS1 26.5 yielded a value higher than 15%. Sparitic and microsparitic carbonates

represent the most common carbonate grains; micritic carbonates are subordinate. Mesozoic carbonate grains made up of oolitic and peloidal packstones to grainstones, including local Cretaceous foraminifera, have been observed in samples from units U1 and U2. In samples OS2 35.5, OS2 26.5 and OS1 32.5 numerous carbonate grains show a characteristic oxidation as rim and along the cleavage planes. Siltstones, shales and serpentinites are subordinate lithic grains. Other minor components include micas (muscovite, biotite and chlorite) and heavy minerals (largely garnet), whose abundance is highly variable.

Significant differences in the distribution of lithic fragments between samples of units U1 and U2 and samples of unit U4 were observed (Figures 5a and 6a). The sands of units U1 and U2 are characterized by a significant content of volcanic lithics (in particular, samples OS2 35.5, OS2 26.5 and OS1 26.5, Figures 5a and 6a), while unit U4 is rich in metamorphic lithics and very poor in volcanics. The Q/Lsed ratio for all samples is comprised between 2.1 and 5.8. The Q/Lv ratio ranges between 3.5 and 12.8 in units U1 and U2 and between 22.7 and 64.5 in unit U4.

5.4.3.2. Modern River Sands

In the central Po Plain, the Po River collects water and sediment from Apennine and Alpine tributaries (Figures 1 and 2), which contribute to changing sand composition downstream (Figure 6b). In this work the fluvial-bar sands collected along a sector of the Po River, extending 125 km west of Ferrara (Figure 2), and from the Oglio, Mincio and Adige rivers, were analysed. Composition of Panaro and Secchia rivers (two representative samples, S and Pn, are reported in Figures 2a, 5b and 6b) have been calculated after Lugli et al., (2004, 2007).

The results show a marked difference in the Po sand composition from the westernmost (P1) to the easternmost sample (P7, Figure 5b). Sample P1 is rich in metamorphic lithics (>22% of the examined sand fraction), with a relative moderate content in quartz and feldspars (~37%). Downstream there is an overall increase in quartz + feldspar (up to ~59%) and sedimentary lithics (up to ~25), particularly evident after the confluence of the Secchia and Panaro rivers (Figure 6b), which supply siltstone, shale and carbonate grains, largely made up of micritic limestones of Ligurian affinity (Palombini and Helmintoid). The Q/Lsed ratio varies from 1.2 to 2.7 and Q/Lv from 9.5 to 41.3. The easternmost sample (P7) records a slight increase in metamorphic lithics. Volcanic grains are scarce in all samples (<3%). Heavy minerals are always present, and their content is highly variable (up to 18% in P1).

The Mincio and Adige rivers show a relative abundance of volcanics (~14% of the examined fraction) associated to metamorphic lithics (~15% Mincio and ~8% Adige). The Oglio River shows a higher percentage of metamorphic lithics (~23%) and a lower content in volcanics (~5%). Compared to the Po River, the Mincio, Adige and Oglio sands have a higher content in carbonate grains, and silicoclastic lithics are rare (Figures 5b and 6b) in agreement with the studies of (Garzanti et al., 2011; Tentori et al., 2021). The Q/Lsed and the Q/Lv ratios are lower than 1.4 and 4, respectively).

5.5. DISCUSSION

Stratigraphy, facies associations and the composition of sands from the Ostiglia cores, dating back to the Late Pleistocene (ca. 42 ky BP)–Late Holocene (ca. 3.1 ky BP), provide clues on past reorganizations of the Po Plain fluvial network.

Stratigraphic units U1, U2 and U4 show distinctive composition (Figure 6a). A markedly higher Q/Lv ratio is observable in unit U4, compared to units U1 and U2. The deepest units show Q/Lsed and Q/Lv values similar to those of the Adige and Mincio rivers sands. The South Alpine signature is also suggested by the occurrence of volcanics and Mesozoic carbonate rocks, which crop out extensively in the South Alpine river catchments and by a low content of siliciclastic sedimentary fragments. Alpine carbonate grains are clearly distinguishable from the those from the Apennine Ligurian units, based on their texture and fossils content. The affinity with modern Adige and Mincio rivers is compatible with the Last Glacial paleogeography, characterized by alpine glaciers extending down to the Po Plain margin and feeding their related fluvio-glacial system (Figure 7a; Fontana et al., 2014). While unit U1 is unequivocally attributable to the last glacial period, uncertainties exist for the age of unit U2, which is constrained by radiocarbon dates between ca. 41 and 9 ky BP (Figure 4). If unit U2 was deposited before glaciers retreat and entrenchment of the Alpine rivers (ca. 17 ky BP, Ravazzi et al., 2014), the composition of U2 would indicate the persistence of a direct sediment supply from the Mincio–Adige fluvio-glacial system (Figure 6b; Fontana et al., 2014). Otherwise, if unit U2 was deposited after 17 ky BP, the entrenchment of the south Alpine rivers would exclude a direct supply from the Adige River (see Figure 7b). In this case, the Mincio River or minor rivers, such as Tione, draining the Garda frontal moraine, and Tartaro, reworking Late Pleistocene fluvio-glacial sediments, would be the most suitable candidate for supplying the sediments of unit U2 (Figure 7b). Given the limited thickness of U2 sand bodies, their provenance from minor rivers catchments, with the partial reworking of morenic and fluvio-glacial deposits, seems the most likely hypothesis. This assumption is corroborated by the abundance of oxidized grains, probably derived from soil erosion,

and by the relatively high quartz and feldspar content in respect to the Mincio and Adige modern sands. Additional chronological and compositional data are required for an unequivocal definition of the paleogeographic setting.

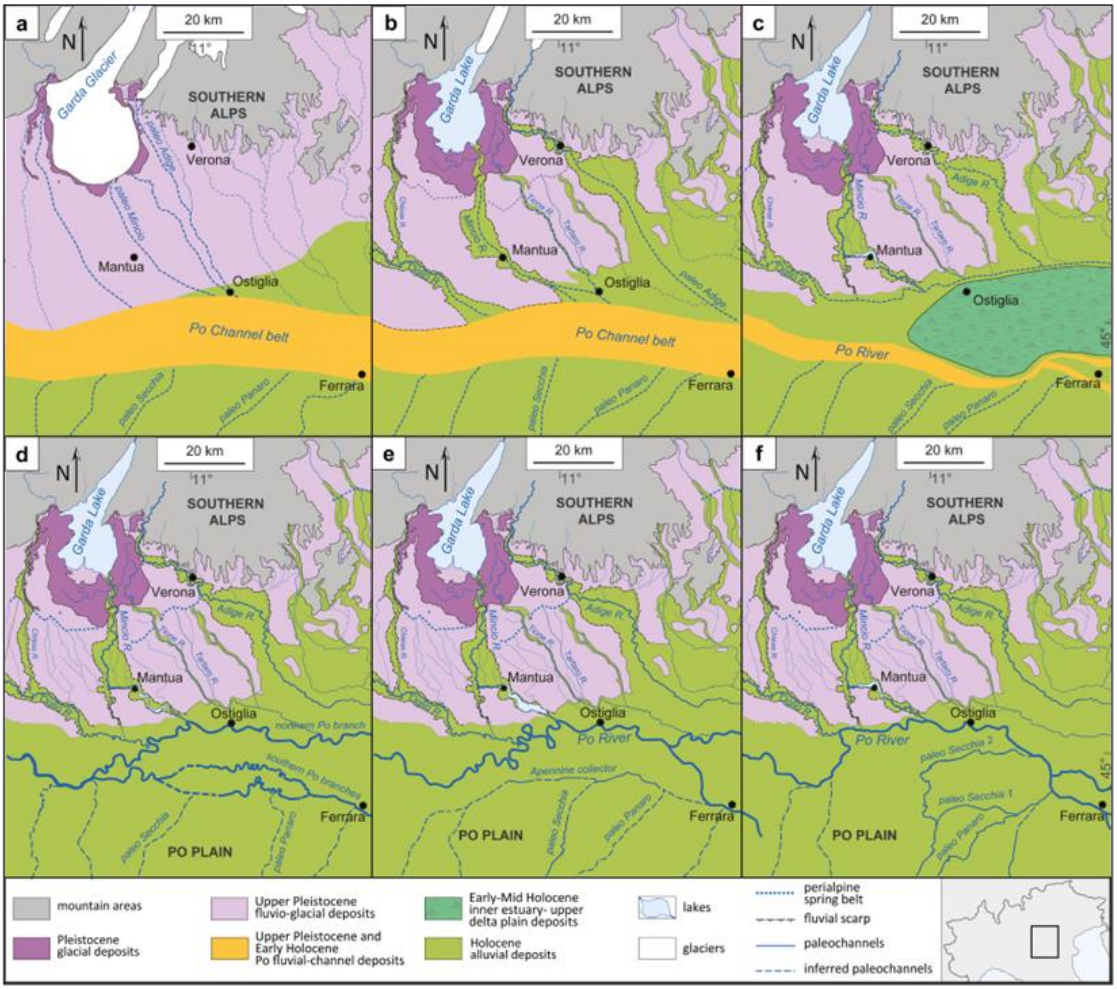

Figure 7. Main hydrographic changes of the Po Plain. Paleogeographic sketch maps showing the Po river network and depositional environment during (a): the Würmian glacial stage; (b): deglaciation; (c): maximum marine ingression; (d) Bronze Age–Iron Age; (e) Roman period; (f) Middle Ages. Extent of the Garda glacier during LGM is from Ravazzi et al., (2014). Extent of Upper Pleistocene fluvio-glacial deposits are from Fontana et al., (2014). Hydrography of the Mantua area during the Bronze Age and Roman period is from Ravazzi et al., (2013). Paleogeographic information from Cremonini, (1993); Castiglioni et al., (1997); Balista, (2003); Castaldini et al., (2003, 2009); Bruno et al., (2021) were also considered.

The peat-rich unit U3, barren in fluvial sand, resulted from scarce fluvial sediment supply. Peat formation indeed is favoured by waterlogging and low clastic input (Ishii et al., 2016; Bruno et al., 2019; Rossi et al., 2021). Widespread peat formation in the Po coastal plain between ca. 9 to 4 ky BP records the progressive flooding of the area during the last phases of post-glacial sea-level rise, with the consequent setting of estuarine and delta plain environments (Balista, 2003; Amorosi et

al., 2017; Bruno et al., 2017, 2021). In this phase the Ostiglia area was located at the western edge of the estuary-delta plain (Figure 7c; Bruno et al., 2021).

The Late Holocene unit (U4) shows affinity with samples P1 and P7 of the Po River, as indicated by the relative abundance of metamorphic detritus associated to a low carbonate content and by relatively high Q/Lv ratios; the Southern Alpine signature is no longer present. The relatively higher percentage of volcanic lithics in samples OS2 22.5 may indicate partial reworking of underlying unit U2. Thus, unit U4 records the onset of the Po River sedimentation in the Ostiglia area. This phase started during the Late Bronze Age (ca. 3 ky BP, Figure 4) and progressively expanded northward towards core OS3, where the first crevasse deposits attributable to the Po River postdate the Iron Age (ca. 2.8–2.4 ky BP). Low sediment input from the southern Alps may be attributable to sediment trapping by periglacial lakes (e.g., Garda Lake, Figure 2; Garzanti et al., 2011; Fontana et al., 2014), which formed after glacier retreat.

It should be noted that the composition of unit U4 is similar to the sand of the modern Po River far from the confluence with the Secchia and Panaro rivers. These two rivers supply large quantities of siliciclastic grains (shales and siltstones) and micritic carbonates of Ligurian affinity form the Apennine catchments (Figure 6b). Indeed, Ostiglia fluvial sand bars (samples P3 and P4, Figures 2 and 6b), located 10 km east of the Secchia confluence, present higher percentages of siliciclastic grains compared to samples of unit U4 (OS2 18.5 and OS1 16.4). This indicates that during the Bronze Age Secchia and Panaro rivers were not tributaries of the Po River at Ostiglia. This fact could be explained by the presence of a southern Po branch, which acted as a barrier to the Apennine sediment supply (Figure 7d). Alternatively, an Apennine river could have acted as a local collector flowing parallel to the Po River down to its confluence east of Ostiglia (Figure 7e,f). Both hypotheses are likely and could have occurred at different times. Indeed, several works have reported the existence of paleochannels of the Po River active south of Ostiglia during the Late Bronze and Iron Ages (see Figure 7d; Veggiani, 1985; Ravazzi et al., 2013; Amorosi et al., 2017; Bruno et al., 2019). The trace of several Apennine paleochannels is also observable south of the Po River (Castiglioni et al., 1997). These paleochannels, with a W–E orientation, were active in different periods between the Roman period (Figure 7e; Cremonini, 1993) and the Middle Ages (see paleo Secchia 1 and paleo Secchia 2 in Figure 7f; Castaldini et al., 2003) and merged with the Po River east of Ostiglia. The present confluence of the Secchia River west of Ostiglia dates back only to the 16th century AD (ca. 0.5 ky BP).

The integrated stratigraphy and sand composition from the Ostiglia area records an overall transition from a river system marked by a high south-Alpine sediment supply (units U1 and U2) to a fluvial system dominated by the Po sedimentary input, with a not negligible Apennine influence. This tendency reflects: (i) the deactivation of the south-Alpine fluvioglacial systems at the transition from the last glacial to the present interglacial; (ii) the progressive northward migration of the Po River during the Holocene (Burrato et al., 2003; Bruno et al., 2018); and (iii) an increase in sediment supply by Apennine rivers during the Late Holocene. Some authors argued that the northward migration of the Po River was forced by the growth of buried thrust-related folds (i.e., Mirandola Anticline; Burrato et al., 2003, 2012). Other authors inferred that the numerous avulsions of the Po River and its Apennine tributaries, detected through geomorphological studies (Veggiani, 1985; Castiglioni et al., 1997; Balista 2003; Castaldini et al., 2003, 2019; Cremonini, 2003), reflect a dominant autogenic control (Bruno et al., 2021). The Late Holocene increase in the sediment supply of Apennine rivers may have been enhanced by the widespread deforestation of mountain catchments, which took place during and after the Late Bronze Age (Cremaschi et al., 2016). Although the major reorganizations of the Po Plain fluvial systems are reflected in the composition of Ostiglia sands, the poor areal extent of the study area does not permit the unequivocally definition of the relative role of distinct controlling factors.

5.6. CONCLUSIONS

Stratigraphic and petrographic analyses on three cores collected in the Ostiglia area along the Po River allowed the reconstruction the main hydrographic changes that have occurred since the Late Pleistocene.

Four stratigraphic units (U1 to U4) were recognized based on facies distribution. Unit U1, deposited during the Late Pleistocene, is dominated by fluvial sands with high content in volcanic and carbonate lithics. Unit U2 (Pleistocene–Holocene transition), includes thinner and less extensive fluvial-channel bodies, with sand composition similar to U1. Unit U3 (Early–Mid Holocene) is dominated by peat-bearing muds and is barren in fluvial-channel sands. Unit U4 (Late Holocene), consists of fluvial channel-related deposits with abundant metamorphites and scarce volcanic and siliciclastic lithics.

Late Pleistocene deposits (U1) record high sedimentary input from the Garda fluvio-glacial system during the last glacial episode. Thinner sand bodies deposited after glacier retreat (U2) are instead likely attributable to minor rivers, which reworked morenic and fluvio-glacial sediments.

Early–Mid Holocene peaty muds (U3) record low fluvial input and waterlogging around the maximum marine ingression. Finally, the Late Bronze Age marks the onset of Po River sedimentation in the Ostiglia area (U4); the fluvial sands of this unit show a lower content in sedimentary grains, supplied by Secchia and Panaro rivers, compared to modern Po River sands. This difference is likely due to a local fluvial collector (Po branch or Apennine river), which impeded Apennine sediments from reaching Ostiglia from the Late Bronze Age to the Middle Ages.

Stratigraphic and compositional data from the Ostiglia cores testify to the transition from a river system characterized by a high south-Alpine clastic input to a fluvial system dominated by the Po sediment supply, with increasing Apennine contributions after the Middle Ages. This tendency reflects the deactivation of the south-Alpine fluvioglacial systems at the transition from the last glacial to the present interglacial, the northward migration of the Po River and an increased sediment supply from Apennine catchments. This study demonstrated that compositional data, framed into a detailed stratigraphic picture, can provide evidence of past changes in fluvial patterns and sediment supply. This multidisciplinary approach may be potentially applicable to other alluvial system worldwide.

Author Contributions: Conceptualization, L.D., L.B., D.F. and S.L.; methodology, L.D., L.B., D.F. and S.L.; validation, L.B., D.F. and S.L.; formal analysis, L.D.; investigation, L.D.; resources, L.D.; data curation, L.D.; writing—original draft preparation, L.D.; writing—review and editing, L.B., D.F and S.L.; visualization, L.D.; supervision, L.B.; project administration, L.B. and D.F; funding acquisition, L.B. and D.F. All authors have read and agreed to the published version of the manuscript.

Acknowledgments: We gratefully acknowledge Ing. Marcello Moretti and Arch. Lorella Togliani (Interregional Agency for the Po River) for access to Ostiglia cores. We acknowledge the three anonymous reviewers for their constructive suggestions.

REFERENCES

Allen, J.R.L. The classification of cross-stratified units with notes on their origin. Sedimentology 1963, 2, 93–114. https://doi.org/10.1111/j.1365-3091.1963.tb01204.x.

Amadori, C.; Toscani, G.; Di Giulio, A.; Maesano, F.E.; D'Ambrogi, C.; Ghielmi, M.; Fantoni, R. From Cylindrical to Non-Cylindrical Foreland Basin: Pliocene–Pleistocene Evolution of the Po Plain–Northern Adriatic Basin (Italy). Basin Res. 2019, 31, 991–1015. https://doi.org/10.1111/bre.12369.

Amorosi, A.; Bruno, L.; Campo, B.; Morelli, A.; Rossi, V.; Scarponi, D.; Hong, W.; Bohacs, K.M.; Drexler, T.M. Global sea-level control on local parasequence architecture from the Holocene record of the Po Plain, Italy. Mar. Pet. Geol. 2017, 87, 99–111. https://doi.org/10.1016/J.MARPETGEO.2017.01.020.

Antonioli, F.; Ferranti, L.; Fontana, A.; Amorosi, A.; Bondesan, A.; Braitenberg, C.; Dutton, A.; Fontolan, G.; Furlani, S.; Lambeck, K.; et al. Holocene relative sea-level changes and vertical movements along the Italian and Istrian coastlines. Quat. Int. 2009, 206, 102–133. https://doi.org/10.1016/j.quaint.2008.11.008.

Balista, C. Geoarcheologia dell'area terramaricola al confine fra le province di Modena, Mantova e Ferrara. In Atlante dei Beni Archeologici della Provincia di Modena; Cardarelli, A., Malnati, L., Eds.; Edizioni all'Insegna del Giglio s.a.s: Sesto Fiorentino (FI), Italy, 2003; Volume 1, pp 24–32, ISBN 88-7814-265-4.

Bronk Ramsey, C.; Lee, S. Recent and planned developments of the program OxCal. Radiocarbon 2013, 55, 720–730. https://doi.org/10.1017/S0033822200057878.

Bruno, L.; Bohacs, K.M.; Campo, B.; Drexler, T.M.; Rossi, V.; Sammartino, I.; Amorosi, A. Early Holocene transgressive paleogeography in the Po coastal plain (Northern Italy). Sedimentology 2017, 64, 1792–1816. https://doi.org/10.1111/sed.12374.

Bruno, L.; Piccin, A.; Sammartino, I.; Amorosi, A. Decoupled geomorphic and sedimentary response of Po River and its Alpine tributaries during the last glacial/post-glacial episode. Geomorphology 2018, 317, 184–198. https://doi.org/10.1016/j.geomorph.2018.05.027.

Bruno, L.; Campo, B.; Di Martino, A.; Hong, W.; Amorosi, A. Peat layer accumulation and post-burial deformation during the mid-late Holocene in the Po coastal plain (Northern Italy). Basin Res. 2019, 31, 621–639. https://doi.org/10.1111/bre.12339.

Bruno, L.; Campo, B.; Costagli, B.; Stouthamer, E.; Teatini, P.; Zoccarato, C.; Amorosi, A. Factors Controlling Natural Subsidence in the Po Plain. Proc. Int. Assoc. Hydrol. Sci. 2020, 382, 285–290. https://doi.org/10.5194/piahs-382-285-2020.

Bruno, L.; Amorosi, A.; Lugli, S.; Sammartino, I.; Fontana, D. Trunk river and tributary interactions recorded in the Pleistocene–Holocene stratigraphy of the Po Plain (northern Italy). Sedimentology 2021, 68, 2918–2943. https://doi.org/10.1111/sed.12880.

Burrato, P.; Ciucci, F.; Valensise, G. An inventory of river anomalies in the Po Plain, Northern Italy: Evidence for active blind thrust faulting. Ann. Geophys. 2003, 46, 865–882. https://doi.org/10.4401/ag-3459.

Burrato, P.; Vannoli, P.; Fracassi, U.; Basili, R.; Valensise, G. Is blind faulting truly invisible? Tectonic-controlled drainage evolution in the epicentral area of the May 2012, Emilia-Romagna earthquake sequence (northern Italy). Ann. Geophys. 2012, 55, 525–531. https://doi.org/10.4401/ag-6182.

Campo, B.; Amorosi, A.; Bruno, L. Contrasting alluvial architecture of late Pleistocene and Holocene deposits along a 120-km transect from the central Po Plain (northern Italy). Sediment. Geol. 2016, 341, 265–275. https://doi.org/10.1016/j.sedgeo.2016.04.013.

Carminati, E.; Doglioni, C. Alps vs. Apennines: The Paradigm of a Tectonically Asymmetric Earth. Earth Sci. Rev. 2012, 112, 67–96. https://doi.org/10.1016/j.earscirev.2012.02.004.

Carminati, E.; Di Donato, G. Separating natural and anthropogenic vertical movements in fast subsiding areas: The Po Plain (N. Italy) Case. Geophys. Res. Lett. 1999, 26, 2291–2294. https://doi.org/10.1029/1999GL900518.

Castaldini, D.; Giusti, C.; Marchetti, M. La Geomorfologia del corso del Po e del territorio nel tratto foce Enza-foce Oglio. In L'anima del Po. Terre acque e uomini tra Enza e Oglio; Venturi, S., Bacchi, N., Eds.; Battei: Parma, Italy, 2003; pp. 5–31.

Castaldini, D.; Marchetti, M.; Cardarelli, A. Some notes on geomorphological and archaeological aspects in the central Po Plain (northern Italy); In Ol'man River. Geo-Archaeological Aspects of Rivers and River Plains; De Dapper, M., Vermeulen, F., Deprez, S., Taelman, D., Eds.; Ghent University, Akademia Press: Ghent, Belgium, 2009, pp. 193–212, ISBN 9038214049

Castaldini, D.; Marchetti, M.; Norini, G.; Vandelli, V.; Vélez, M.C.Z. Geomorphology of the central Po Plain, Northern Italy. J. Maps 2019, 15, 780–787. https://doi.org/10.1080/17445647.2019.1673222.

Castiglioni, G.B.; Ajassa, R.; Baroni, C.; Biancotti, A.; Bondesan, A.; Brancucci, G.; Castaldini, D.; Castellaccio, E.; Cavallin, A.; Cortemiglia, F.; et al. Geomorphological Map of Po Plain, 3 Sheets, Scale 1:250,000; MURST–S.El.Ca: Firenze, Italy, 1997.

Correggiari, A.; Cattaneo, A.; Trincardi, F. The modern Po Delta system: Lobe switching and asymmetric prodelta growth. Mar. Geol. 2005, 222–223, 49–74. https://doi.org/10.1016/j.margeo.2005.06.039.

Cremaschi, M.; Mercuri, A.M.; Torri, P.; Florenzano, A.; Pizzi, C.; Marchesini, M.; Zerboni, A. Climate change versus land management in the Po Plain (Northern Italy) during the Bronze Age: New insights from the VP/VG sequence of the Terramara Santa Rosa di Poviglio. Quat. Sci. Rev. 2016, 136, 153–172. https://doi.org/10.1016/j.quascirev.2015.08.011.

Cremonini, S. Nuove osservazioni relative al "Dosso di Gavello" modenese. In Nuove ricerche sugli Etruschi; Gruppo studi Bassa Modenese: San Felice sul Panaro (Mo), Italy, 1993; pp. 149–159.

Diessel, C.F.K. Coal facies and depositional environment. In Coal-Bearing Depositional Systems; Springer: Berlin/Heidelberg, Germany, 1992; pp. 161–264. https://doi.org/10.1007/978-3-642-75668-9_5.

Fontana, A.; Mozzi, P.; Marchetti, M. Alluvial fans and megafans along the southern side of the Alps. Sediment. Geol. 2014, 301, 150–171. https://doi.org/10.1016/j.sedgeo.2013.09.003.

Fontana, D.; Amoroso, S.; Minarelli, L.; Stefani, M. Sand liquefaction phenomena induced by a blast test: New insights from composition and texture of sands (late Quaternary, Emilia, Italy). J. Sediment. Res. 2019, 89, 13–27. doi:10.2110/jsr.2019.1.

Garzanti, E.; Vezzoli, G.; Andò, S. Paleogeographic and paleodrainage changes during Pleistocene glaciations (Po Plain, Northern Italy). Earth Sci. Rev. 2011, 105, 25–48. https://doi.org/10.1016/j.earscirev.2010.11.004.

Garzanti, E.; Ando, S.; Vezzoli, G. Settling equivalence of detrital minerals and grain-size dependence of sediment composition. Earth Planet. Sci. Lett. 2008, 273, 138–151. https://doi.org/10.1016/j.epsl.2008.06.020.

Gunderson, K.L.; Pazzaglia, F.J.; Picotti, V.; Anastasio, D.A.; Kodama, K.P.; Rittenou, R.T.; Frankel, K.F.; Ponza, A.; Berti, C.; Negri, A.; et al. Unraveling tectonic and climatic controls on synorogenic growth strata (Northern Appennines, Italy). Geol. Soc Am. Bull. 2014, 126, 532–552. https://doi.org/10.1130/B30902.1.

Ishii, Y.; Hori, K.; Momohara, A.; Nakanishi, T.; Hong, W. Middle to late-Holocene decreased fluvial aggradation and wide-spread peat initiation in the Ishikari lowland (northern Japan). Holocene 2016, 26, 1924–1938. https://doi.org/10.1177/0959683616646189

Lugli, S.; Marchetti Dori, S.; Fontana, D.; Panini, F. Composition of sands in cores along the high-speed rail (TAV): Preliminary indications on the sedimentary evolution of the Modena plain. Alpine Mediterran. Quatern. 2004, 17, 379–390.

Lugli, S.; Marchetti Dori, S.; Fontana, D. Alluvial sand composition as a tool to unravel the Late Quaternary sedimentation of the Modena plain, northern Italy. In Sedimentary Provenance and Petrogenesis: Perspectives from Petrography and Geochemistry; Arribas, J., Critelli, S., Johnsson, M.J., Eds.; Geological Society of America, Special Paper: Boulder, CO, USA, 2007, 420, 57–72, ISBN-13 978-0-8137-2420-1. https://doi.org/10.1130/2006.2420(05).

Marcolla, A.; Monegato, G.; Mozzi, P.; Miola, A.; Stefani, C. Seesaw longitudinal–transverse drainage patterns driven by Middle and Late Pleistocene climate cycles in the foreland basin of the south-eastern European Alps. Sediment. Geol. 2021, 421, 105960. https://doi.org/10.1016/j.sedgeo.2021.105960.

Molodkov, A. The Late Pleistocene palaeoenvironmental evolution in Northern Eurasia through the prism of the mollusc shell-based ESR dating evidence. Quat. Int. 2020, 556, 180–197. https://doi.org/10.1016/j.quaint.2019.05.031.

Morelli, A.; Bruno, L.; Cleveland, D.M.; Drexler, T.M.; Amorosi, A. Reconstructing Last Glacial Maximum and Younger Dryas paleolandscapes through subsurface paleosol stratigraphy: An example from the Po coastal plain, Italy. Geomorphology 2017, 295, 790–800. https://doi.org/10.1016/j.geomorph.2017.08.013.

Muttoni, G.; Carcano, C.; Garzanti, E.; Ghielmi, M.; Piccin, A.; Pini, R.; Rogledi, S.; Sciunnach, D. Onset of major Pleistocene glaciations in the Alps. Geology 2003, 31, 989–992. https://doi.org/10.1130/G19445.1.

Muttoni, G.; Scardia, G.; Kent, D.V.; Morsiani, E.; Tremolada, F.; Cremaschi, M.; Peretto, C. First dated human occupation of Italy at ~0.85 Ma during the late Early Pleistocene climate transition. Earth Planet. Sci. Lett. 2011, 307, 241–252. https://doi.org/10.1016/j.epsl.2011.05.025.

Ravazzi, C.; Marchetti, M.; Zanon, M.; Perego, R.; Quirino, T.; Deaddis, M.; De Amicis, M.; Margaritora, D. Lake evolution and landscape history in the lower Mincio River valley, unravelling drainage changes in the central Po Plain (N-Italy) since the Bronze Age. Quat. Int. 2013, 288, 195–205. https://doi.org/10.1016/j.quaint.2011.11.031.

Ravazzi, C.; Pini, R.; Badino, F.; De Amicis, M.; Londeix, L.; Reimer, P.J. The latest LGM culmination of the Garda Glacier (Italian Alps) and the onset of glacial termination. Age of glacial collapse and vegetation chronosequence. Quat. Sci. Rev. 2014, 105, 26–47. https://doi.org/10.1016/j.quascirev.2014.09.014.

Razum, I.; Lužar-Oberiter, B.; Zaccarini, F.; Babić, L.; Miko, S.; Hasan, O.; Ilijanić, N.; Beqiraj, E.; Pawlowsky-Glahn, V. New sediment provenance approach based on orthonormal log ratio transformation of geochemical and heavy mineral data: Sources of eolian sands from the southeastern Adriatic archipelago. Chem. Geol. 2021, 583, 120451. https://doi.org/10.1016/j.chemgeo.2021.120451.

Reimer, P.; Austin, W.; Bard, E.; Bayliss, A.; Blackwell, P.; Bronk Ramsey, C.; Butzin, M.; Cheng, H.; Edwards, R.; Friedrich, M.; et al. The IntCal20 Northern Hemisphere radiocarbon age calibration curve (0–55 cal kBP). Radiocarbon 2020, 62, 725–757. https://doi.org/10.1017/RDC.2020.41.

Rittenour, T.M. Dates and Rates of Earth-Surface Processes Revealed using Luminescence Dating. Elements 2018, 14, 21–26. https://doi.org/10.2138/gselements.14.1.21.

Rossi, V.; Amorosi, A.; Barbieri, G.; Vaiani, S.C.; Germano, M.; Campo, B. A Long-Term Record of Quaternary Facies Patterns and Palaeonvironmental Trends from the Po Plain (NE Italy) as Revealed by Bio-Sedimentary Data. Geosciences 2021, 11, 401. https://doi.org/10.3390/geosciences11100401.

Scardia, G.; Muttoni, G.; Sciunnach, D. Subsurface magnetostratigraphy of Pleistocene sediments from the Po Plain (Italy): Constraints on rates of sedimentation and rock uplift. Geol. Soc. Am. Bull. 2006, 118, 1299–1312. https://doi.org/10.1130/B25869.1.

Singh, S.K.; Rai, S.K.; Krishnaswami, S. Sr and Nd isotopes in river sediments from the Ganga Basin: Sediment provenance and spatial variability in physical erosion. J. Geophys. Res. 2008, 113, F03006. https://doi.org/10.1029/2007JF000909.

Sinha, R.; Gibling, M.R.; Kettanah, Y.; Tandon, S.K.; Bhattacharja, P.S.; Dasgupta, A.S.; Ghazanfari, P. Craton-derived alluvium as a major sediment source in the Himalayan Foreland Basin of India. Geol. Soc. Am. Bull. 2009, 121, 1596–1610. https://doi.org/10.1130/B26431.1.

Stolt, M.H. and Rabenhorst, M.C. Introduction and historical development of subaqueous soil concepts. In Handbook of Soil Sciences Properties and Processes; Huang, P.M., Li, Y., Sumner, M.L., Eds.; CRC Press, LLC: Boca Raton, FL, USA, 2011; ISBN 978-1-4398-0305-9. https://doi.org/10.1201/b11267-71.

Tentori, D.; Milli, S.; Marsaglia, K.M. A source-to-sink compositional model of a present highstand: An example in the low-rank Tiber depositional sequence (Latium tyrrhenian margin, Italy). J. Sediment. Res. 2018, 88, 1238–1259. https://doi.org/10.2110/jsr.2018.60.

Tentori, D.; Amorosi, A.; Milli, S.; Marsaglia, K.M. Sediment dispersal pathways in the Po coastal plain since the Last Glacial Maximum: Provenance signals of autogenic and eustatic forcing. Basin Res. 2021, 33, 1407–1428. https://doi.org/10.1111/bre.12519.

Turrini, C.; Toscani, G.; Lacombe, O.; Roure, F. Influence of structural inheritance on foreland-foredeep system evolution: An example from the Po valley region (northern Italy). Mar. Pet. Geol. 2016, 77, 376–398. https://doi.org/10.1016/j.marpetgeo.2016.06.022.

Veggiani, A. Il delta del Po e l'evoluzione della rete idrografica padana in epoca storica. In Atti della Tavola Rotonda su: Il delta del Po; Bologna 24 novembre 1982; Accademia delle Scienze dell'Istituto di Bologna: Bologna, Italy, 1985; pp. 37–68.

Weltje, G.J. A quantitative approach to capturing the compositional variability of modern sands. Sed. Geol. 2004, 171, 59–77. https://doi.org/10.1016/j.sedgeo.2004.05.010.

Zuffa, G.G. (Ed.) Optical analyses of arenites: Influence of methodology on compositional results. In Provenance of Arenites; D. Reidel, NATO Advanced Study Institute: Dordrecht, Nederland, 1985; Volume 148, pp. 165–189.

CHAPTER 6. CONCLUSIONS

The integrated stratigraphic-compositional study of the Middle-Late Pleistocene and Holocene deposits of the Po Plain provide clues on the sedimentary evolution of the Po Basin in response to different controlling factors.

Firstly, this thesis provides a basin-scale reconstruction of the stratigraphic architecture of the Mid-Late Pleistocene and Holocene deposits of the central-eastern Po Plain, based on new core data and on the reinterpretation of data from the previous studies. This stratigraphic framework, constrained by 14C, ESR and IRSL dates, is depicted along two stratigraphic sections, exhibiting two prominent features:

- a cyclic organization of facies over the whole study area. Seaward each cycle is represented by coastal wedges, deposited during interglacial marine ingressions, passing upward to alluvial deposits deposited during glacial stages. Landward, paralic deposits alternate with alluvial facies associations, mostly represented by laterally extensive fluvial-channel bodies. This rhythmic organization of facies, reflecting Middle Pleistocene-to-Holocene glacio-eustatic oscillations, has been documented in previously published local studies. In this work, for the first time, we provide a comprehensive picture of basin scale facies distribution, with particular focus on lateral facies changes and along-dip sedimentary patterns and shoreline trajectories.
- an overall shallowing-upward trend within the Middle-Upper Pleistocene succession is recorded in the whole basin and an overall progradational stacking of coastal wedges is observable along dip. This feature reflects the progressive filling of the basin, resulting from of high sediment supply to subsidence ratio. A seaward increase in subsidence rates may have enhanced the progressive seaward migration of facies. A similar trend has been detected in studies at the seismic scale which documented the transition from Pliocene deep-sea to Quaternary coastal sediments. Due to the poor resolution of industrial seismic profiles in the uppermost 300 metres, these studies were not able to identify trends within Quaternary deposits. This study, carried out at a finer scale, provide clues on the depositional trends within Mid-Late Pleistocene and Holocene deposits.

The integration of these stratigraphic information with compositional analyses on core sands, outlined the sedimentary dynamics of the Po River system in the last 500 ka. Particularly, a sharp changes in composition detected along a 101 m-long core, recovered in the central sector of the plain testifies to a dramatic reorganization of the Po River network occurred around 350 ka BP, with a northward shift of the Po River of more than 30 km. Sediments supplied from the Southern Alps

during MIS 12 and MIS 10, are overlain by sands deposited by the Po River during MIS 8, 6 and 2 glacial periods. Another change in composition, consisting in the upward transition from sediment deposited by the Po River to sands supplied by the Norther Apennines, denotes a further northward shift of the Po River, occurred during the Late Holocene. The progressive northward shift of the Po River documented in this study, may reflect the activity of Apennine blind thrusts. However, data presented in this work do not permit to verify this assumption.

The upward transition from sediment supplied from the Southern Alps to sediment deposited by the Po River is recorded also along three cores collected close to the modern Po River course. This change is recorded at this coring location at the transition between the last glacial and the Holocene. Sands with south-alpine affinity, dated to the Late Pleistocene, testify to a high sedimentary input from the Garda fluvio-glacial system. Glacier retreat after the Last Glacial Maximum and the formation of the Garda Lake, which acted as a sediment trap, likely favoured the progressive formation of wetlands during the early Holocene and the activation of a norther branch of the Po delta system during Late Bronze Age. This northward branch did not receive the sediment contribution from Apennine Rivers Secchia and Panaro at least until the Middle Ages.

This work provides a comprehensive stratigraphic picture of the Middle Pleistocene-to-Holocene deposits of the central and eastern Po Basin and discusses the influence of the main controlling factors on the stratigraphic record. Compositional studies portrayed a highly dynamic fluvial network at different spatial and temporal scales.